

## 4.6. Reciprocal-space images of aperiodic crystals

BY W. STEURER AND T. HAIBACH

### 4.6.1. Introduction

The discovery of materials with icosahedral diffraction symmetry (Shechtman *et al.*, 1984) was the main reason for the reassessment of the definition of *crystallinity* and for the introduction of the concept of *aperiodic crystals*. The first aperiodic crystal, *i.e.* a material with Bragg reflections not located only at reciprocal-lattice nodes, was identified long before (Dehlinger, 1927). In the following decades a wealth of incommensurately modulated phases and composite crystals were discovered. Nevertheless, only a few attempts have been made to develop a crystallography of aperiodic crystals; the most powerful of these was the higher-dimensional approach (see de Wolff, 1974, 1977; Janner & Janssen, 1979, 1980*a,b*; de Wolff *et al.*, 1981). In fact, incommensurate structures can be easily described using the higher-dimensional approach and also, fully equivalently, in a dual way: as a three-dimensional (3D) combination of one or more periodic basic structures and one or several modulation waves (de Wolff, 1984). However, with the discovery of quasicrystals and their noncrystalline symmetries, the latter approach failed and geometrical crystallography including the higher-dimensional approach received new attention. For more recent reviews of the crystallography of all three types of aperiodic crystals see van Smaalen (1995), of incommensurately modulated structures see Cummins (1990), of quasicrystals see Steurer (1990, 1996), of quasicrystals and their crystalline approximants see Goldman & Kelton (1993) and Kelton (1995). Textbooks on quasicrystals have been written by Janot (1994) and Senechal (1995).

According to the traditional crystallographic definition, an *ideal crystal* corresponds to an infinite 3D periodic arrangement of identical structure motifs. Its symmetry can be described by one of the 230 3D space groups. Mathematically, a periodic structure can be generated by the convolution of a function representing the structure motif with a lattice function. The structure motif can be given, for instance, by the electron-density distribution  $\rho(\mathbf{r})$  of one primitive unit cell of the structure. The lattice function  $g(\mathbf{r})$  is represented by a set of  $\delta$  functions at the nodes  $\mathbf{r} = \sum_{i=1}^3 k_i \mathbf{a}_i$  of a 3D lattice  $\Lambda$  with basis  $\mathbf{a}_i$ ,  $i = 1, \dots, 3$ , and  $k_i \in \mathbb{Z}$  ( $\mathbb{Z}$  is the set of integer numbers). In reciprocal space, this convolution corresponds to the product of the Fourier transform  $G(\mathbf{H})$  of the lattice function  $g(\mathbf{r})$  and the Fourier transform  $F(\mathbf{H}) = \int_V \rho(\mathbf{r}) \exp(2\pi i \mathbf{H} \cdot \mathbf{r}) \, d\mathbf{r}$  of the structure motif  $\rho(\mathbf{r})$ .  $G(\mathbf{H})$  is represented by the reciprocal lattice  $\Lambda^*$  decorated with  $\delta$  functions on the reciprocal-lattice nodes  $\mathbf{H} = \sum_{i=1}^3 h_i \mathbf{a}_i^*$ , with the reciprocal-basis vectors  $\mathbf{a}_i^*$ ,  $i = 1, \dots, 3$ , defined by  $\mathbf{a}_i \cdot \mathbf{a}_j^* = \delta_{ij}$  and  $h_i \in \mathbb{Z}$ . The product  $G(\mathbf{H}) \times F(\mathbf{H})$  is called the weighted reciprocal lattice; the weights are given by the structure factors  $F(\mathbf{H})$ . Thus, the characteristic feature of an ideal crystal in direct and reciprocal space is the existence of a lattice. In direct space, this lattice is decorated with identical structure motifs preserving translational and point symmetry in the framework of *space-group symmetry*. In reciprocal space, only the point symmetry between structure factors is maintained. The *Fourier spectrum* (or *Fourier image*, *i.e.* the Fourier transform) of the electron-density distribution of an ideal crystal consists of a countably infinite set of discrete Bragg peaks with a strictly defined minimum distance.

This crystal definition can be generalized to  $n > 3$  dimensions. A  $d$ -dimensional ( $d$ D) *ideal aperiodic crystal* can be defined as a  $d$ D irrational section of an  $n$ -dimensional ( $n$ D,  $n > d$ ) crystal with  $n$ D lattice symmetry. The intersection of the  $n$ D *hypercrystal* with the  $d$ D physical space is equivalent to a projection of the weighted  $n$ D reciprocal lattice  $\Sigma^* = \{\mathbf{H} = \sum_{i=1}^n h_i \mathbf{d}_i^* | h_i \in \mathbb{Z}\}$  onto the  $d$ D physical space. The resulting set (Fourier module)  $M^* =$

$\{\mathbf{H}^\parallel = \sum_{i=1}^n h_i \mathbf{a}_i^* | h_i \in \mathbb{Z}\}$  is countably dense. *Countably dense* means that the dense set of Bragg peaks can be mapped one-to-one onto the set of natural numbers. Hence, the Bragg reflections can be indexed with integer indices on an appropriate basis. The Fourier module of the projected reciprocal-lattice vectors  $\mathbf{H}^\parallel$  has the structure of a  $\mathbb{Z}$  module of rank  $n$ . A  $\mathbb{Z}$  module is a free Abelian group, its rank  $n$  is given by the number of free generators (rationally independent vectors). The dimension of a  $\mathbb{Z}$  module is that of the vector space spanned by it. The vectors  $\mathbf{a}_i^*$  are the images of the vectors  $\mathbf{d}_i^*$  projected onto the physical space  $\mathbb{V}^\parallel$ . Thus, by definition, the 3D reciprocal space of an ideal *aperiodic crystal* consists of a countably dense set of Bragg reflections only. Contrary to an ideal *crystal*, a minimum distance between Bragg reflections does not exist in an aperiodic one. In summary, it may be stressed that the terms *aperiodic* and *periodic* refer to properties of crystal structures in  $d$ D space. In  $n$ D space, as considered here, lattice symmetry is always present and, therefore, the term *crystal* is used.

Besides the *aperiodic crystals* mentioned above, other classes of *aperiodic structures* with strictly defined construction rules exist (see Axel & Gratias, 1995). Contrary to the kind of aperiodic crystals dealt with in this chapter, the Fourier spectra of aperiodic structures considered in the latter reference are continuous and contain only in a few cases additional sharp Bragg reflections ( $\delta$  peaks).

Experimentally, the borderline between aperiodic crystals and their periodic approximations (*crystalline approximants*) is not sharply defined. Finite crystal size, static and dynamic disorder, chemical impurities and defects broaden Bragg peaks and cause diffuse diffraction phenomena. Furthermore, the resolution function of the diffraction equipment is limited.

However, the concept of describing an aperiodic structure as a  $d$ D physical-space section of an  $n$ D crystal (see Section 4.6.2) is only useful if it significantly simplifies the description of its structural order. Thus, depending on the shape of the *atomic surfaces*, which gives information on the atomic ordering, incommensurately modulated structures (IMs, Sections 4.6.2.2 and 4.6.3.1), composite structures (CSs, Sections 4.6.2.3 and 4.6.3.2), or quasiperiodic structures (Qs, Sections 4.6.2.4 and 4.6.3.3) can be obtained from irrational cuts. The atomic surfaces are continuous  $(n - d)$ -dimensional objects for IMs and CSs, and discrete  $(n - d)$ -dimensional objects for Qs. A class of aperiodic crystals with discrete fractal atomic surfaces also exists (Section 4.6.2.5). In this case the Hausdorff dimension (Hausdorff, 1919) of the atomic surface is not an integer number and smaller than  $n - d$ . The most outstanding characteristic feature of a fractal is its scale invariance: the object appears similar to itself 'from near as from far, that is, whatever the scale' (Gouyet, 1996).

To overcome the problems connected with experimental resolution, the translational symmetry of periodic crystals is used as a hard constraint in the course of the determination of their structures. Hence, space-group symmetry is taken for granted and only the local atomic configuration in a unit cell (actually, asymmetric unit) remains to be determined. In reciprocal space, this assumption corresponds to a condensation of Bragg reflections with finite full width at half maximum (FWHM) to  $\delta$  peaks accurately located at the reciprocal-lattice nodes. Diffuse diffraction phenomena are mostly neglected. This extrapolation to the existence of an ideal crystal is generally out of the question even if samples of very poor quality (high mosaicity, microdomain structure, defects, . . .) are investigated.

The same practice is convenient for the determination of real aperiodic structures once the type of idealized aperiodic ordering is 'known'. Again, the global ordering principle is taken as a hard

## 4.6. RECIPROCAL-SPACE IMAGES OF APERIODIC CRYSTALS

constraint. For instance, the question of whether a structure is commensurately or incommensurately modulated can only be answered within a given experimental resolution. Experimentally, the ratio of the wavelength of a modulation to the period of the underlying lattice can always be determined as a rational number only. Saying that a structure is incommensurately modulated, with the above ratio being an irrational number, simply means that the experimental results can be better understood, modelled and interpreted assuming an incommensurate modulation. For example, an incommensurate charge-density wave can be moved through an ideal crystal without changing the energy of the crystal. This is not so for a commensurate modulation. In some cases, the modulation period changes with temperature in discrete steps ('devil's staircase'), generating a series of commensurate superstructures ('lock-in structures'); in other cases, a continuous variation can be observed within the experimental resolution. The latter case will be described best by an incommensurately modulated structure.

However, if only the local structure of an aperiodic crystal is of interest, a structure analysis does not take much more experimental effort than for a regular crystal. In contrast, for the analysis of the global structure, *i.e.* the characterization of the type of its 'aperiodicity', diffraction experiments with the highest possible resolution are essential. Some problems connected with the structure analysis of aperiodic crystals are dealt with in Section 4.6.4.

To determine the long-range order – whether a real 'quasicrystal' is perfectly quasiperiodic, on average quasiperiodic, a crystalline approximant or a nanodomain structure – requires information from experiments that are sensitive to changes of the global structure. Hence, one needs diffraction experiments that allow the accurate determination of the spatial intensity distribution. Consequently, the limiting factors for such experiments are the maximum spatial and intensity resolution of the diffraction and detection equipment, as well as the size and quality of the sample. Nevertheless, the resolution available on state-of-the-art standard synchrotron-beamline equipment is sufficient to test whether the ordering of atoms in an aperiodic crystal reaches the same degree of perfection as found in high-quality silicon. Of course, the higher the sample quality the more necessary it is to account for dynamical diffraction effects such as reflection broadening and displacement. Otherwise, a misinterpretation may bias the global structure modelling.

The following sections present an aid to the characterization of aperiodic crystals based on information from diffraction experiments and give a survey of aperiodic crystals from the viewpoint of the experimentally accessible reciprocal space. Characteristic features of the diffraction patterns of the different types of aperiodic crystals are shown. A standard way of determining the metrics and finding the optimum  $nD$  embedding is described. Structure-factor formulae for general and special cases are given.

### 4.6.2. The $n$ -dimensional description of aperiodic crystals

#### 4.6.2.1. Basic concepts

An incommensurate modulation of a lattice-periodic structure destroys its translational symmetry in direct and reciprocal space. In the early seventies, a method was suggested by de Wolff (1974) for restoring the lost lattice symmetry by considering the diffraction pattern of an *incommensurately modulated structure* (IMS) as a projection of an  $nD$  reciprocal lattice upon the physical space.  $n$ , the dimension of the superspace, is always larger than or equal to  $d$ , the dimension of the physical space. This leads to a simple method for the description and characterization of IMSs as well as a variety of new possibilities in their structure analysis. The  $nD$  embedding method is well established today and can be applied to all aperiodic crystals with reciprocal-space structure equivalent to a  $\mathbb{Z}$  module

with finite rank  $n$  (Janssen, 1988). The dimension of the embedding space is determined by the rank of the  $\mathbb{Z}$  module, *i.e.* by the number of reciprocal-basis vectors necessary to allow for indexing all Bragg reflections with integer numbers. The point symmetry of the  $3D$  reciprocal space (Fourier spectrum) constrains the point symmetry of the  $nD$  reciprocal lattice and restricts the number of possible  $nD$  symmetry groups.

In the following sections, the  $nD$  descriptions of the four main classes of aperiodic crystals are demonstrated on simple  $1D$  examples of incommensurately modulated phases, composite crystals, quasicrystals and structures with fractally shaped atomic surfaces. The main emphasis is placed on quasicrystals that show scaling symmetry, a new and unusual property in structural crystallography. A detailed discussion of the different types of  $3D$  aperiodic crystals follows in Section 4.6.3.

#### 4.6.2.2. $1D$ incommensurately modulated structures

A periodic deviation of atomic parameters from a reference structure (*basic structure*, BS) is called a *modulated structure* (MS). In the case of mutual incommensurability of the basic structure and the modulation period, the structure is called incommensurately modulated. Otherwise, it is called commensurately modulated. The modulated atomic parameters may be one or several of the following:

- (a) coordinates,
- (b) occupancy factors,
- (c) thermal displacement parameters,
- (d) orientation of the magnetic moment.

An incommensurately modulated structure can be described in a dual way by its *basic structure*  $s(\mathbf{r})$  and a *modulation function*  $f(t)$ . This allows the structure-factor formula to be calculated and a full symmetry characterization employing representation theory to be performed (de Wolff, 1984). A more general method is the  $nD$  description: it relates the  $dD$  aperiodic incommensurately modulated structure to a periodic structure in  $nD$  space. This simplifies the symmetry analysis and structure-factor calculation, and allows more powerful structure-determination techniques.

The  $nD$  embedding method is demonstrated in the following  $1D$  example of a displacively modulated structure. A basic structure  $s(\mathbf{r}) = s(\mathbf{r} + n\mathbf{a})$ , with period  $a$  and  $n \in \mathbb{Z}$ , is modulated by a function  $f(t) = f(\mathbf{q} \cdot \mathbf{r}) = f(\alpha r) = f[\alpha r + (na/\alpha)]$ , with the satellite vector  $\mathbf{q} = \alpha \mathbf{a}^*$ , period  $\lambda = 1/q = a/\alpha$ , and  $\alpha$  a rational or irrational number yielding a commensurately or incommensurately modulated structure  $s_m(\mathbf{r})$  (Fig. 4.6.2.1).

If the  $1D$  IMS and its  $1D$  modulation function are properly combined in a  $2D$  parameter space  $\mathbf{V} = (\mathbf{V}^{\parallel}, \mathbf{V}^{\perp})$ , a  $2D$  lattice-periodic structure results (Fig. 4.6.2.2). The actual atoms are generated by the intersection of the  $1D$  physical (external, parallel) space  $\mathbf{V}^{\parallel}$  with the continuous *hyperatoms*. The hyperatoms have the shape of the modulation function along the perpendicular (internal, complementary) space  $\mathbf{V}^{\perp}$ . They result from a convolution of the physical-space atoms with their modulation functions.

A basis  $\mathbf{d}_1, \mathbf{d}_2$  ( $D$  basis) of the  $2D$  hyperlattice  $\Sigma = \{\mathbf{r} = \sum_{i=1}^2 n_i \mathbf{d}_i | n_i \in \mathbb{Z}\}$  is given by

$$\mathbf{d}_1 = \begin{pmatrix} a \\ -\alpha/c \end{pmatrix}_V, \mathbf{d}_2 = \begin{pmatrix} 0 \\ 1/c \end{pmatrix}_V,$$

where  $a$  is the translation period of the BS and  $c$  is an arbitrary constant. The components of the basis vectors are given on a  $2D$  orthogonal coordinate system ( $V$  basis). The components of the basis vector  $\mathbf{d}_1$  are simply the parallel-space period  $a$  of the BS and  $\alpha$  times the perpendicular-space component of the basis vector  $\mathbf{d}_2$ . The vector  $\mathbf{d}_2$  is always parallel to the perpendicular space and its length is one period of the modulation function in arbitrary units (this is expressed by the arbitrary factor  $1/c$ ). An atom at position  $\mathbf{r}$

4. DIFFUSE SCATTERING AND RELATED TOPICS

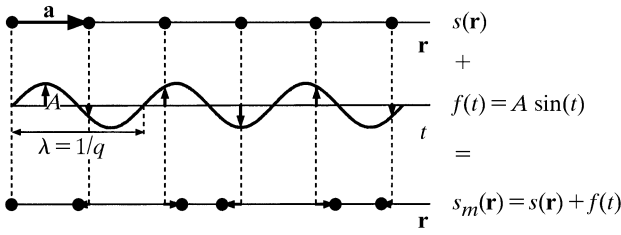


Fig. 4.6.2.1. The combination of a basic structure  $s(\mathbf{r})$ , with period  $a$ , and a sinusoidal modulation function  $f(t)$ , with amplitude  $A$ , period  $\lambda$  and  $t = \mathbf{q} \cdot \mathbf{r}$ , gives a modulated structure (MS)  $s_m(\mathbf{r})$ . The MS is aperiodic if  $a$  and  $\lambda$  are on incommensurate length scales. The filled circles represent atoms.

of the BS is displaced by an amount given by the modulation function  $f(t)$ , with  $f(t) = f(\mathbf{q} \cdot \mathbf{r})$ . Hence, the perpendicular-space variable  $t$  has to adopt the value  $\mathbf{q} \cdot \mathbf{r} = \alpha \mathbf{a}^* \cdot r \mathbf{a} = \alpha r$  for the physical-space variable  $\mathbf{r}$ . This can be achieved by assigning the slope  $\alpha$  to the basis vector  $\mathbf{d}_1$ . The choice of the parameter  $c$  has no influence on the actual MS, *i.e.* the way in which the 2D structure is cut by the parallel space (Fig. 4.6.2.2c).

The basis of the lattice  $\Sigma^* = \{\mathbf{H} = \sum_{i=1}^2 h_i \mathbf{d}_i^* | h_i \in \mathbb{Z}\}$ , reciprocal to  $\Sigma$ , can be obtained from the condition  $\mathbf{d}_i \cdot \mathbf{d}_j^* = \delta_{ij}$ :

$$\mathbf{d}_1^* = \begin{pmatrix} a^* \\ 0 \end{pmatrix}_V, \mathbf{d}_2^* = \begin{pmatrix} \alpha a^* \\ c \end{pmatrix}_V,$$

with  $a^* = 1/a$ . The metric tensors for the reciprocal and direct 2D lattices for  $c = 1$  are

$$G^* = \begin{pmatrix} a^{*2} & \alpha a^{*2} \\ \alpha a^{*2} & 1 + \alpha^2 a^{*2} \end{pmatrix} \quad \text{and} \quad G = \begin{pmatrix} a^2 + \alpha^2 & -\alpha \\ -\alpha & 1 \end{pmatrix}.$$

The choice of an arbitrary number for  $c$  has no influence on the metrics of the physical-space components of the IMS in direct or reciprocal space.

The Fourier transform of the *hypercrystal* depicted in Fig. 4.6.2.2 gives the weighted reciprocal lattice shown in Fig. 4.6.2.3. The 1D diffraction pattern  $M^* = \{\mathbf{H}^\parallel = \sum_{i=1}^2 h_i \mathbf{a}_i^* | h_i \in \mathbb{Z}\}$  in physical space is obtained by a projection of the weighted 2D reciprocal lattice  $\Sigma^*$  along  $\mathbf{V}^\perp$  as the Fourier transform of a section in direct space corresponds to a projection in reciprocal space and *vice versa*:

$$M^* = \{\mathbf{H}^\parallel\} \xleftarrow{\text{projection } \pi^\parallel \text{ onto } \mathbf{V}^\parallel} \Sigma^* = \{\mathbf{H} = (\mathbf{H}^\parallel, \mathbf{H}^\perp)\}.$$

Reciprocal-lattice points lying in physical space are referred to as *main reflections*, all others as *satellite reflections*. All Bragg reflections can be indexed with integer numbers  $h_1, h_2$  in the 2D description  $\mathbf{H} = h_1 \mathbf{d}_1^* + h_2 \mathbf{d}_2^*$ . In the physical-space description, the diffraction vector can be written as  $\mathbf{H}^\parallel = h \mathbf{a}^* + m \mathbf{q} = \mathbf{a}^* (h_1 + \alpha h_2)$ , with  $\mathbf{q} = \alpha \mathbf{a}^*$  for the satellite vector and  $m \in \mathbb{Z}$  the order of the satellite reflection. For a detailed discussion of the embedding and symmetry description of IMSs see, for example, Janssen *et al.* (1999).

A commensurately modulated structure with  $\alpha' = m/n$  and  $\lambda = (n/m)a$ ,  $m, n \in \mathbb{Z}$ , and with  $c = 1$ , can be generated by

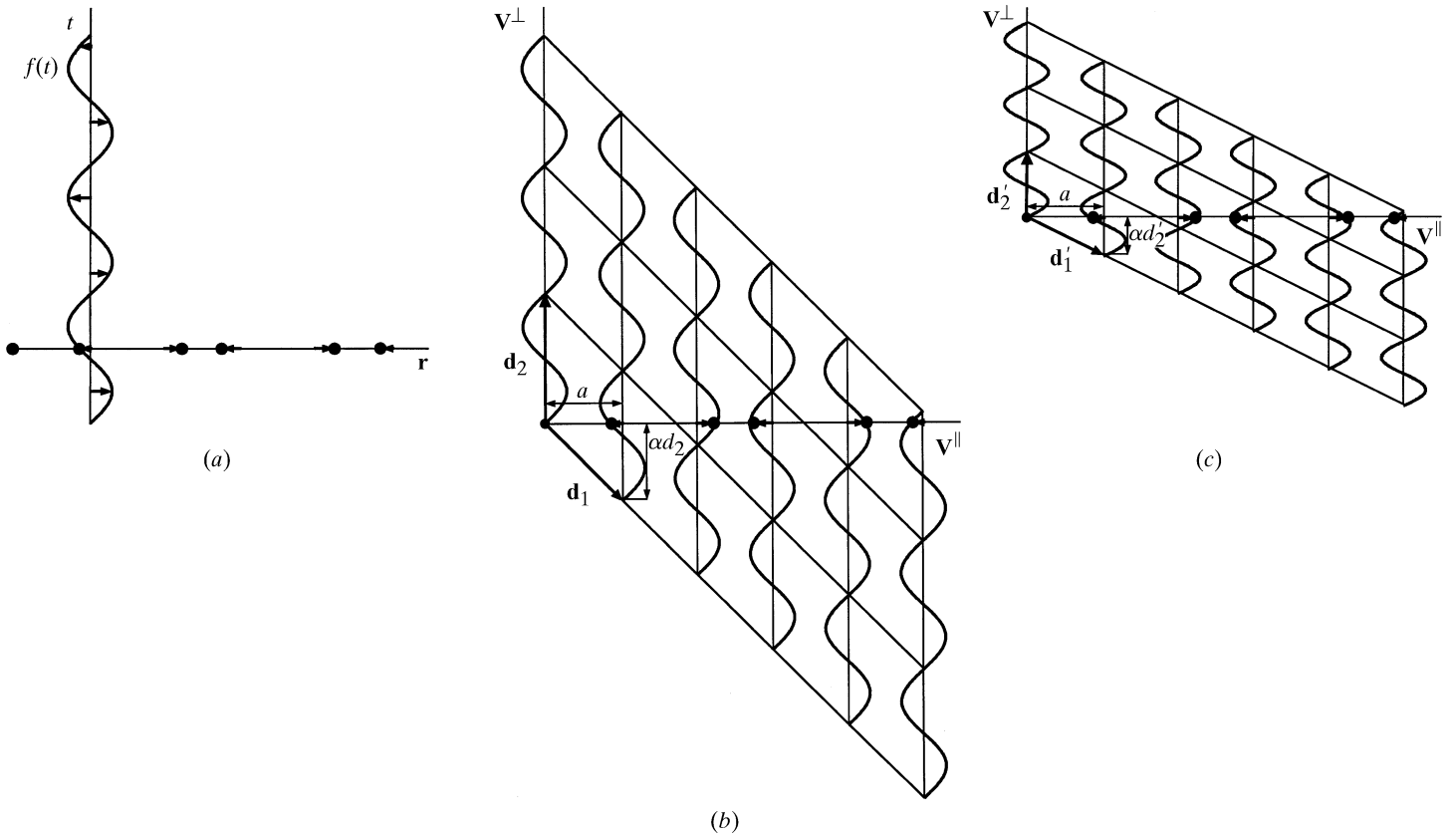


Fig. 4.6.2.2. 2D embedding of the sinusoidally modulated structure illustrated in Fig. 4.6.2.1. The correspondence between the actual displacement of an atom in the 1D structure and the modulation function defined in one additional dimension is illustrated in part (a). Adding to each atom its modulation function in this orthogonal dimension (perpendicular space  $\mathbf{V}^\perp$ ) yields a periodic arrangement in 2D space  $\mathbf{V}$ , part (b). The MS results as a special section of the 2D periodic structure along the parallel space  $\mathbf{V}^\parallel$ . It is obvious from a comparison of (b) and (c) that the actual MS is independent of the perpendicular-space scale.

#### 4.6. RECIPROCAL-SPACE IMAGES OF APERIODIC CRYSTALS

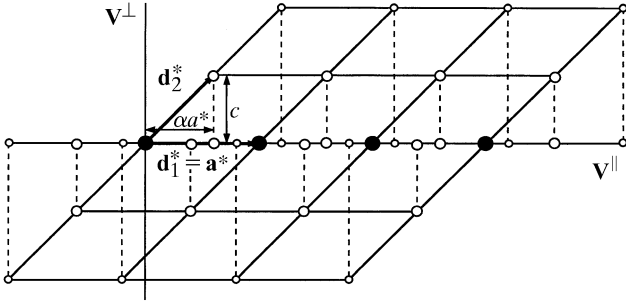


Fig. 4.6.2.3. Schematic representation of the 2D reciprocal-space embedding of the 1D sinusoidally modulated structure depicted in Figs. 4.6.2.1 and 4.6.2.2. Main reflections are marked by filled circles and satellite reflections by open circles. The sizes of the circles are roughly related to the reflection intensities. The actual 1D diffraction pattern of the 1D MS results from a projection of the 2D reciprocal space onto the parallel space. The correspondence between 2D reciprocal-lattice positions and their projected images is indicated by dashed lines.

shearing the 2D lattice  $\Sigma$  with a shear matrix  $S_m$ :

$$\mathbf{d}'_i = \sum_{j=1}^2 S_{mij} \mathbf{d}_j, \text{ with } S_m = \begin{pmatrix} 1 & -x \\ 0 & 1 \end{pmatrix}_D \text{ and } x = \alpha' - \alpha,$$

$$\mathbf{d}'_1 = \mathbf{d}_1 - x \mathbf{d}_2 = \begin{pmatrix} a \\ -\alpha \end{pmatrix}_V - (\alpha' - \alpha) \begin{pmatrix} 0 \\ 1 \end{pmatrix}_V = \begin{pmatrix} a \\ -\alpha' \end{pmatrix}_V,$$

$$\mathbf{d}'_2 = \mathbf{d}_2 = \begin{pmatrix} 0 \\ 1 \end{pmatrix}_V.$$

The subscript  $D$  ( $V$ ) following the shear matrix indicates that it is acting on the  $D$  ( $V$ ) basis. The shear matrix does not change the distances between the atoms in the basic structure. In reciprocal space, using the inverted and transposed shear matrix, one obtains

$$\mathbf{d}'_i{}^* = \sum_{j=1}^2 (S_m^{-1})_{ij}^T \mathbf{d}_j^*, \text{ with } (S_m^{-1})^T = \begin{pmatrix} 1 & 0 \\ x & 1 \end{pmatrix}_D \text{ and } x = \alpha' - \alpha,$$

$$\mathbf{d}'_1{}^* = \mathbf{d}_1^* = \begin{pmatrix} a^* \\ 0 \end{pmatrix}_V,$$

$$\mathbf{d}'_2{}^* = x \mathbf{d}_1^* + \mathbf{d}_2^* = (\alpha' - \alpha) \begin{pmatrix} a^* \\ 0 \end{pmatrix}_V + \begin{pmatrix} 0 \\ 1 \end{pmatrix}_V = \begin{pmatrix} \alpha' a^* \\ 1 \end{pmatrix}_V.$$

##### 4.6.2.3. 1D composite structures

In the simplest case, a *composite structure* (CS) consists of two intergrown periodic structures with mutually incommensurate lattices. Owing to mutual interactions, each subsystem may be modulated with the period of the other. Consequently, CSs can be considered as coherent intergrowths of two or more incommensurately modulated substructures. The substructures have at least the origin of their reciprocal lattices in common. However, in all known cases, at least one common reciprocal-lattice plane exists. This means that at least one particular projection of the composite structure exhibits full lattice periodicity.

The unmodulated (basic) 1D subsystems of a 1D incommensurate intergrowth structure can be related to each other in a 2D parameter space  $\mathbf{V} = (\mathbf{V}^{\parallel}, \mathbf{V}^{\perp})$  (Fig. 4.6.2.4). The actual atoms result from the intersection of the physical space  $\mathbf{V}^{\parallel}$  with the hypercrystal. The hyperatoms correspond to a convolution of the real atoms with infinite lines parallel to the basis vectors  $\mathbf{d}_1$  and  $\mathbf{d}_2$  of the 2D hyperlattice  $\Sigma = \{\mathbf{r} = \sum_{i=1}^2 n_i \mathbf{d}_i | n_i \in \mathbb{Z}\}$ .

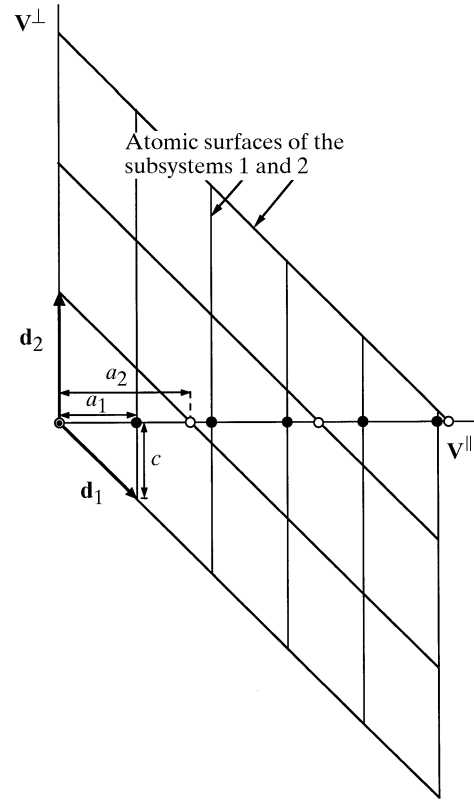


Fig. 4.6.2.4. 2D embedding of a 1D composite structure without mutual interaction of the subsystems. Filled and empty circles represent the atoms of the unmodulated substructures with periods  $a_1$  and  $a_2$ , respectively. The atoms result from the parallel-space cut of the linear atomic surfaces parallel to  $\mathbf{d}_1$  and  $\mathbf{d}_2$ .

An appropriate basis is given by

$$\mathbf{d}_1 = \begin{pmatrix} a_1 \\ -c \end{pmatrix}_V, \mathbf{d}_2 = \begin{pmatrix} 0 \\ c(a_2/a_1) \end{pmatrix}_V,$$

where  $a_1$  and  $a_2$  are the lattice parameters of the two substructures and  $c$  is an arbitrary constant. Taking into account the interactions between the subsystems, each one becomes modulated with the period of the other. Consequently, in the 2D description, the shape of the hyperatoms is determined by their modulation functions (Fig. 4.6.2.5).

A basis of the reciprocal lattice  $\Sigma^* = \{\mathbf{H} = \sum_{i=1}^2 h_i \mathbf{d}_i^* | h_i \in \mathbb{Z}\}$  can be obtained from the condition  $\mathbf{d}_i \cdot \mathbf{d}_j^* = \delta_{ij}$ :

$$\mathbf{d}_1^* = \begin{pmatrix} a_1^* \\ 0 \end{pmatrix}_V, \mathbf{d}_2^* = \begin{pmatrix} a_2^* \\ (a_2^*/ca_1^*) \end{pmatrix}_V.$$

The metric tensors for the reciprocal and the direct 2D lattices for  $c = 1$  are

$$G^* = \begin{pmatrix} a_1^{*2} & a_1^* a_2^* \\ a_1^* a_2^* & (1 + a_1^{*2})(a_2^*/a_1^*)^2 \end{pmatrix} \text{ and } G = \begin{pmatrix} 1 + a_1^2 & -a_2/a_1 \\ -a_2/a_1 & (a_2/a_1)^2 \end{pmatrix}.$$

The Fourier transforms of the hypercrystals depicted in Figs. 4.6.2.4 and 4.6.2.5 correspond to the weighted reciprocal lattices illustrated in Figs. 4.6.2.6 and 4.6.2.7. The 1D diffraction patterns  $M^* = \{\mathbf{H}^{\parallel} = \sum_{i=1}^2 h_i \mathbf{a}_i^* | h_i \in \mathbb{Z}\}$  in physical space are obtained by a projection of the weighted 2D reciprocal lattices  $\Sigma^*$  upon  $\mathbf{V}^{\parallel}$ . All Bragg reflections can be indexed with integer numbers  $h_1, h_2$  in both the 2D description  $\mathbf{H} = h_1 \mathbf{d}_1^* + h_2 \mathbf{d}_2^*$  and in the 1D physical-space description with two parallel basis vectors  $\mathbf{H}^{\parallel} = h_1 \mathbf{a}_1^* + h_2 \mathbf{a}_2^*$ .

#### 4. DIFFUSE SCATTERING AND RELATED TOPICS

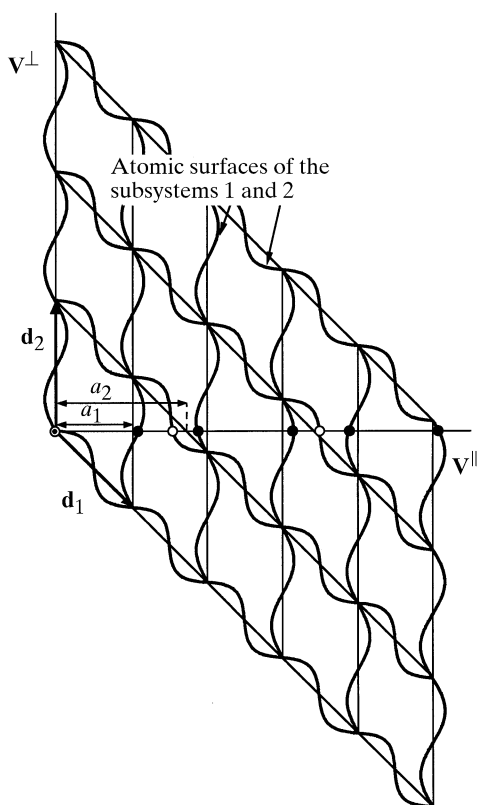


Fig. 4.6.2.5. 2D embedding of a 1D composite structure with mutual interaction of the subsystems causing modulations. Filled and empty circles represent the modulated subsystems with periods  $a_1$  and  $a_2$  of the basic subsystems, respectively. The atoms result from the parallel-space cut of the sinusoidal atomic surfaces running parallel to  $\mathbf{d}_1$  and  $\mathbf{d}_2$ .

The reciprocal-lattice points  $\mathbf{H} = h_1 \mathbf{d}_1^*$  and  $\mathbf{H} = h_2 \mathbf{d}_2^*$ ,  $h_1, h_2 \in \mathbb{Z}$ , on the main axes  $\mathbf{d}_1^*$  and  $\mathbf{d}_2^*$  are the main reflections of the two subsystems. All other reflections are referred to as satellite reflections. Their intensities differ from zero only in the case of modulated subsystems. Each reflection of one subsystem coincides with exactly one reflection of the other subsystem.

##### 4.6.2.4. 1D quasiperiodic structures

The Fibonacci sequence, the best investigated example of a 1D quasiperiodic structure, can be obtained from the substitution rule  $\sigma: S \rightarrow L, L \rightarrow LS$ , replacing the letter S by L and the letter L by the

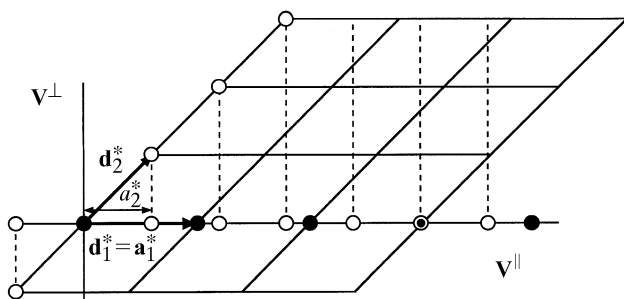


Fig. 4.6.2.6. Schematic representation of the reciprocal space of the embedded 1D composite structure depicted in Fig. 4.6.2.4. Filled and empty circles represent the reflections generated by the subsystems with periods  $a_1$  and  $a_2$ , respectively. The actual 1D diffraction pattern of the 1D CS results from a projection of the 2D reciprocal space onto the parallel space. The correspondence between 2D reciprocal-lattice positions and their projected images is indicated by dashed lines.

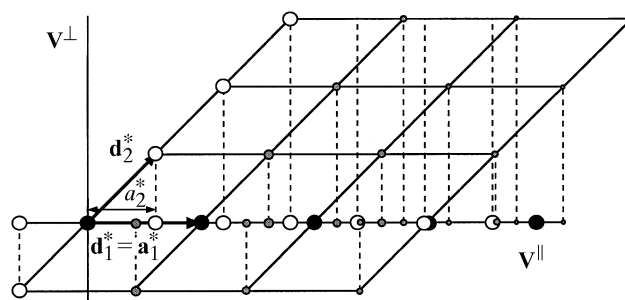


Fig. 4.6.2.7. Schematic representation of the reciprocal space of the embedded 1D composite structure depicted in Fig. 4.6.2.5. Filled and empty circles represent the main reflections of the two subsystems. The satellite reflections generated by the modulated subsystems are shown as grey circles. The diameters of the circles are roughly proportional to the intensities of the reflections. The actual 1D diffraction pattern of the 1D CS results from a projection of the 2D reciprocal space onto the parallel space. The correspondence between 2D reciprocal-lattice positions and their projected images is indicated by dashed lines.

word LS (see *e.g.* Luck *et al.*, 1993). Applying the substitution matrix

$$S = \begin{pmatrix} 0 & 1 \\ 1 & 1 \end{pmatrix}$$

associated with  $\sigma$ , this rule can be written in the form

$$\begin{pmatrix} S \\ L \end{pmatrix} \rightarrow \begin{pmatrix} 0 & 1 \\ 1 & 1 \end{pmatrix} \begin{pmatrix} S \\ L \end{pmatrix} = \begin{pmatrix} L \\ L + S \end{pmatrix}.$$

$S$  gives the sum of letters,  $L + S = S + L$ , and not their order. Consequently, the same substitution matrix can also be applied, for instance, to the substitution  $\sigma': S \rightarrow L, L \rightarrow SL$ . The repeated action of  $S$  on the alphabet  $A = \{S, L\}$  yields the words  $A_n = \sigma^n(S)$  and  $B_n = \sigma^n(L) = A_{n+1}$  as illustrated in Table 4.6.2.1. The frequencies of letters contained in the words  $A_n$  and  $B_n$  can be calculated by applying the  $n$ th power of the transposed substitution matrix on the unit vector. From

$$\begin{pmatrix} \nu_{n+1}^A \\ \nu_{n+1}^B \end{pmatrix} = S^T \begin{pmatrix} \nu_n^A \\ \nu_n^B \end{pmatrix}$$

it follows that

$$\begin{pmatrix} \nu_n^A \\ \nu_n^B \end{pmatrix} = (S^T)^n \begin{pmatrix} 1 \\ 1 \end{pmatrix}.$$

In the case of the Fibonacci sequence,  $\nu_n^B$  gives the total number of letters S and L, and  $\nu_n^A$  the number of letters L.

An infinite Fibonacci sequence, *i.e.* a word  $B_n$  with  $n \rightarrow \infty$ , remains invariant under inflation (deflation). Inflation (deflation) means that the number of letters L, S increases (decreases) under the action of the (inverted) substitution matrix  $S$ . Inflation and deflation represent self-similarity (scaling) symmetry operations on the infinite Fibonacci sequence. A more detailed discussion of the scaling properties of the Fibonacci chain in direct and reciprocal space will be given later.

The Fibonacci numbers  $F_n = F_{n-1} + F_{n-2}$  form a series with  $\lim_{n \rightarrow \infty} (F_{n+1}/F_n) = \tau$  {the golden mean  $\tau = [1 + (5)^{1/2}]/2 = 2 \cos(\pi/5) = 1.618 \dots$ }. The ratio of the frequencies of L and S in the Fibonacci sequence converges to  $\tau$  if the sequence goes to infinity. The continued fraction expansion of the golden mean  $\tau$ ,

#### 4.6. RECIPROCAL-SPACE IMAGES OF APERIODIC CRYSTALS

Table 4.6.2.1. *Expansion of the Fibonacci sequence*  $B_n = \sigma^n(L)$  by repeated action of the substitution rule  $\sigma$ :  
 $S \rightarrow L, L \rightarrow LS$

$\nu_L, \nu_S$  are the frequencies of the letters L and S in word  $B_n$ .

| $B_n$         | $\nu_L$   | $\nu_S$  | $n$      |
|---------------|-----------|----------|----------|
| L             | 1         | 0        | 0        |
| LS            | 1         | 1        | 1        |
| LSL           | 2         | 1        | 2        |
| LSLLS         | 3         | 2        | 3        |
| LSLLSLSL      | 5         | 3        | 4        |
| LSLLSLSLLS    | 8         | 5        | 5        |
| LSLLSLSLLSLSL | 13        | 8        | 6        |
| $\vdots$      | $\vdots$  | $\vdots$ | $\vdots$ |
|               | $F_{n+1}$ | $F_n$    | $n$      |

$$\tau = 1 + \frac{1}{1 + \frac{1}{1 + \frac{1}{1 + \dots}}}$$

contains only the number 1. This means that  $\tau$  is the ‘most irrational’ number, *i.e.* the irrational number with the worst truncated continued fraction approximation to it. This might be one of the reasons for the stability of quasiperiodic systems, where  $\tau$  plays a role. The strong irrationality may impede the lock-in into commensurate systems (*rational approximants*).

By associating intervals (*e.g.* atomic distances) with length ratio  $\tau$  to 1 to the letters L and S, a quasiperiodic structure  $s(\mathbf{r})$  (*Fibonacci chain*) can be obtained. The invariance of the ratio of lengths  $L/S = (L + S)/L = \tau$  is responsible for the invariance of the Fibonacci chain under scaling by a factor  $\tau^n, n \in \mathbb{Z}$ . Owing to a minimum atomic distance S in real crystal structures, the full set of inverse symmetry operators  $\tau^{-n}$  does not exist. Consequently, the set of scaling operators  $s = \{\tau^0 = 1, \tau^1, \dots\}$  forms only a semi-group, *i.e.* an associative groupoid. Groupoids are the most general algebraic sets satisfying only one of the group axioms: the associative law. The scaling properties of the Fibonacci sequence can be derived from the eigenvalues of the scaling matrix  $S$ . For this purpose the equation

$$\det |S - \lambda I| = 0$$

with eigenvalue  $\lambda$  and unit matrix  $I$  has to be solved. The evaluation of the determinant yields the characteristic polynomial

$$\lambda^2 - \lambda - 1 = 0,$$

yielding in turn the eigenvalues  $\lambda_1 = [1 + (5)^{1/2}]/2 = \tau$ ,  $\lambda_2 = [1 - (5)^{1/2}]/2 = -1/\tau$  and the eigenvectors  $\mathbf{w}_1 = \begin{pmatrix} 1 \\ \tau \end{pmatrix}$ ,  $\mathbf{w}_2 = \begin{pmatrix} 1 \\ -1/\tau \end{pmatrix}$ . Rewriting the eigenvalue equation gives for the first (*i.e.* the largest) eigenvalue

$$\begin{pmatrix} 0 & 1 \\ 1 & 1 \end{pmatrix} \begin{pmatrix} 1 \\ \tau \end{pmatrix} = \begin{pmatrix} \tau \\ 1 + \tau \end{pmatrix} = \begin{pmatrix} \tau \\ \tau^2 \end{pmatrix} = \tau \begin{pmatrix} 1 \\ \tau \end{pmatrix}.$$

Identifying the eigenvector  $\begin{pmatrix} 1 \\ \tau \end{pmatrix}$  with  $\begin{pmatrix} S \\ L \end{pmatrix}$  shows that an infinite

Fibonacci sequence  $s(\mathbf{r})$  remains invariant under scaling by a factor  $\tau$ . This scaling operation maps each new lattice vector  $\tau\mathbf{r}$  upon a vector  $\mathbf{r}$  of the original lattice:

$$s(\tau\mathbf{r}) = s(\mathbf{r}).$$

Considering periodic lattices, these eigenvalues are integer numbers. For quasiperiodic ‘lattices’ (*quasilattices*) they always correspond to *algebraic numbers* (*Pisot numbers*). A Pisot number is the solution of a polynomial equation with integer coefficients. It is larger than one, whereas the modulus of its conjugate is smaller than unity:  $\lambda_1 > 1$  and  $|\lambda_2| < 1$  (Luck *et al.*, 1993). The total lengths  $l_n^A$  and  $l_n^B$  of the words  $A_n, B_n$  can be determined from the equations  $l_n^A = \lambda_1^n l^A$  and  $l_n^B = \lambda_1^n l^B$  with the eigenvalue  $\lambda_1$ . The left Perron–Frobenius eigenvector  $\mathbf{w}_1$  of  $S$ , *i.e.* the left eigenvector associated with  $\lambda_1$ , determines the ratio S:L to 1: $\tau$ . The right Perron–Frobenius eigenvector  $\mathbf{w}_1$  of  $S$  associated with  $\lambda_1$  gives the relative frequencies, 1 and  $\tau$ , for the letters S and L (for a definition of the Perron–Frobenius theorem see Luck *et al.*, 1993, and references therein).

The general case of an alphabet  $A = \{L_1 \dots L_k\}$  with  $k$  letters (intervals)  $L_i$ , of which at least two are on incommensurate length scales and which transform with the substitution matrix  $S$ ,

$$L'_i \rightarrow \sum_{j=1}^k S_{ij} L_j,$$

can be treated analogously.  $S$  is a  $k \times k$  matrix with non-negative integer coefficients. Its eigenvalues are solutions of a polynomial equation of rank  $k$  with integer coefficients (algebraic or Pisot numbers). The dimension  $n$  of the embedding space is generically equal to the number of letters (intervals)  $k$  involved by the substitution rule. From substitution rules, infinitely many different 1D quasiperiodic sequences can be generated. However, their atomic surfaces in the  $nD$  description are generically of fractal shape (see Section 4.6.2.5).

The quasiperiodic 1D density distribution  $\rho(\mathbf{r})$  of the Fibonacci chain can be represented by the Fourier series

$$\rho(\mathbf{r}) = (1/V) \sum_{\mathbf{H}^{\parallel}} F(\mathbf{H}^{\parallel}) \exp(-2\pi i \mathbf{H}^{\parallel} \cdot \mathbf{r}),$$

with  $\mathbf{H}^{\parallel} \in \mathbb{R}$  (the set of real numbers). The Fourier coefficients  $F(\mathbf{H}^{\parallel})$  form a Fourier module  $M^* = \{\mathbf{H}^{\parallel} = \sum_{i=1}^2 h_i \mathbf{a}_i^* | h_i \in \mathbb{Z}\}$  equivalent to a  $\mathbb{Z}$  module of rank 2. Thus a periodic function in 2D space can be defined by

$$\rho(\mathbf{r}^{\parallel}, \mathbf{r}^{\perp}) = (1/V) \sum_{\mathbf{H}} F(\mathbf{H}) \exp[-2\pi i (\mathbf{H}^{\parallel} \cdot \mathbf{r}^{\parallel} + \mathbf{H}^{\perp} \cdot \mathbf{r}^{\perp})],$$

where  $\mathbf{r} = (\mathbf{r}^{\parallel}, \mathbf{r}^{\perp}) \in \Sigma$  and  $\mathbf{H} = (\mathbf{H}^{\parallel}, \mathbf{H}^{\perp}) \in \Sigma^*$  are, by construction, direct and reciprocal lattice vectors (Figs. 4.6.2.8 and 4.6.2.9):

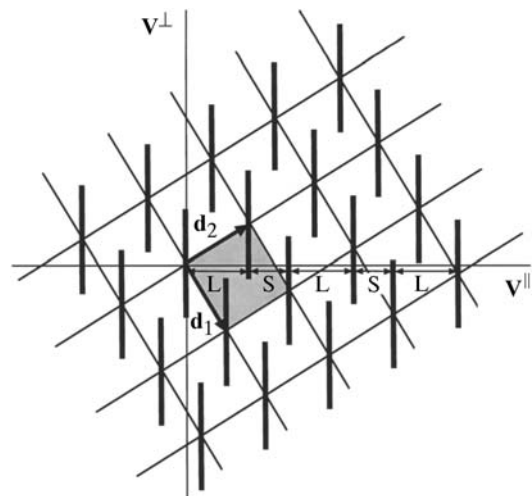


Fig. 4.6.2.8. 2D embedding of the Fibonacci chain. The short and long distances S and L, generated by the intersection of the atomic surfaces with the physical space  $\mathbf{V}^{\parallel}$ , are indicated. The atomic surfaces are represented by bars parallel to  $\mathbf{V}^{\perp}$ . Their lengths correspond to the projection of one unit cell (shaded) upon  $\mathbf{V}^{\perp}$ .

#### 4. DIFFUSE SCATTERING AND RELATED TOPICS

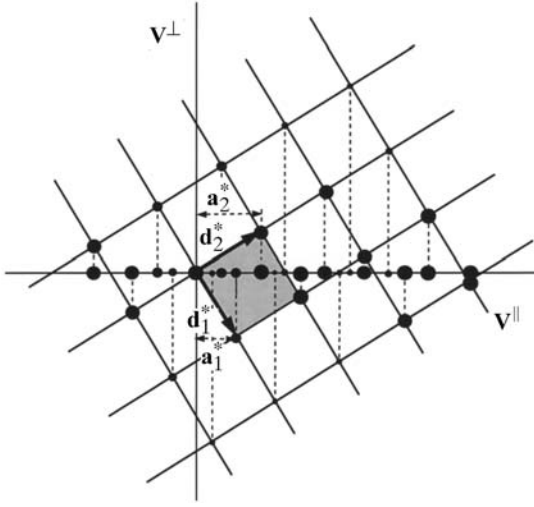


Fig. 4.6.2.9. Schematic representation of the reciprocal space of the embedded Fibonacci chain depicted in Fig. 4.6.2.8. The physical-space reciprocal basis  $\mathbf{a}_1^*$  and  $\mathbf{a}_2^*$  is marked. The diameters of the filled circles are roughly proportional to the reflection intensities. One 2D reciprocal-lattice unit cell is shadowed. The actual 1D diffraction pattern of the 1D Fibonacci chain results from a projection of the 2D reciprocal space onto the parallel space. The correspondence between 2D reciprocal-lattice positions and their projected images is indicated by dashed lines.

$$\mathbf{r} = n_1 \mathbf{d}_1 + n_2 \mathbf{d}_2, \text{ with } \mathbf{d}_1 = \frac{1}{a^*(2+\tau)} \begin{pmatrix} 1 \\ -\tau \end{pmatrix}_V,$$

$$\mathbf{d}_2 = \frac{1}{a^*(2+\tau)} \begin{pmatrix} \tau \\ 1 \end{pmatrix}_V;$$

$$\mathbf{H} = h_1 \mathbf{d}_1^* + h_2 \mathbf{d}_2^*, \text{ with } \mathbf{d}_1^* = a^* \begin{pmatrix} 1 \\ -\tau \end{pmatrix}_V, \mathbf{d}_2^* = a^* \begin{pmatrix} \tau \\ 1 \end{pmatrix}_V.$$

The 1D Fibonacci chain results from the cut of the parallel (physical) space with the 2D lattice  $\Sigma$  decorated with line elements for the *atomic surfaces* (acceptance domains). In this description, the atomic surfaces correspond simply to the projection of one 2D unit cell upon the perpendicular-space coordinate. This satisfies the condition that each unit cell contributes exactly to one point of the Fibonacci chain (*primitive unit cell*). The physical space  $\mathbf{V}^{\parallel}$  is related to the eigenspace of the substitution matrix  $S$  associated with its eigenvalue  $\lambda_1 = \tau$ . The perpendicular space  $\mathbf{V}^{\perp}$  corresponds to the eigenspace of the substitution matrix  $S$  associated with its eigenvalue  $\lambda_2 = -1/\tau$ . Thus, the physical space scales to powers of  $\tau$  and the perpendicular space to powers of  $-1/\tau$ .

By block-diagonalization, the reducible substitution (scaling) matrix  $S$  can be decomposed into two non-equivalent irreducible representations. These can be assigned to the two 1D orthogonal subspaces  $\mathbf{V}^{\parallel}$  and  $\mathbf{V}^{\perp}$  forming the 2D embedding space  $\mathbf{V} = \mathbf{V}^{\parallel} \oplus \mathbf{V}^{\perp}$ . Thus, using  $WSW^{-1} = S_V = S_V^{\parallel} \oplus S_V^{\perp}$ , where

$$W = \begin{pmatrix} 1 & \tau \\ -\tau & 1 \end{pmatrix} = (\mathbf{d}_1^* \quad \mathbf{d}_2^*),$$

one obtains

$$\begin{pmatrix} 1 & \tau \\ -\tau & 1 \end{pmatrix} \begin{pmatrix} 0 & 1 \\ 1 & 1 \end{pmatrix}_D \begin{pmatrix} 1 & \tau \\ -\tau & 1 \end{pmatrix}^{-1} = \begin{pmatrix} \tau & 0 \\ 0 & -1/\tau \end{pmatrix}_V \\ = \begin{pmatrix} S^{\parallel} & 0 \\ 0 & S^{\perp} \end{pmatrix}_V,$$

the scaling operations  $S^{\parallel}$  and  $S^{\perp}$  in parallel and in perpendicular space as indicated by the partition lines.

The metric tensors for the reciprocal and the direct 2D square lattices read

$$G^* = |a^*|^2(2+\tau) \begin{pmatrix} 1 & 0 \\ 0 & 1 \end{pmatrix} \text{ and } G = \frac{1}{|a^*|^2(2+\tau)} \begin{pmatrix} 1 & 0 \\ 0 & 1 \end{pmatrix}.$$

The short distance  $S$  of the Fibonacci sequence is related to  $a^*$  by

$$S = 1/[a^*(2+\tau)] \\ = \min \left\{ |\pi^{\parallel}(\mathbf{d}_i - \mathbf{d}_j)| \mid |\pi^{\perp}(\mathbf{d}_i - \mathbf{d}_j)| < \Omega_{AS} \wedge i, j \in \mathbb{Z} \right\},$$

with the projectors  $\pi^{\parallel}$  and  $\pi^{\perp}$  onto  $\mathbf{V}^{\parallel}$  and  $\mathbf{V}^{\perp}$ . The *point density*  $\rho_p$  of the Fibonacci chain, i.e. the number of vertices per unit length, can be calculated using the formula

$$\rho_p = \frac{\Omega_{AS}}{\Omega_{UC}} = \frac{(1+\tau)/[a^*(2+\tau)]}{1/[|a^*|^2(2+\tau)]} = a^* \tau^2,$$

where  $\Omega_{AS}$  and  $\Omega_{UC}$  are the areas of the atomic surface and of the 2D unit cell, respectively.

For an infinite Fibonacci sequence generated from the intervals  $S$  and  $L$  an average distance  $d$  can be calculated:

$$d = \lim_{n \rightarrow \infty} \frac{F_n S + F_{n+1} L}{F_n + F_{n+1}} = \lim_{n \rightarrow \infty} \frac{F_n(S + \tau L)}{F_n(1 + \tau)} = \frac{S(1 + \tau^2)}{(1 + \tau)} = (3 - \tau)S.$$

Therefrom, the point density can also be calculated:

$$\rho_p = 1/d = 1/[(3 - \tau)S] = [a^*(2 + \tau)]/(3 - \tau) = a^* \tau^2.$$

An approximant structure of the Fibonacci sequence with a unit cell containing  $m$  intervals  $L$  and  $n$  intervals  $S$  can be generated by shearing the 2D lattice  $\Sigma$  by the shear matrix  $S_m$ ,

$$S_m = \frac{1}{2 + \tau} \begin{pmatrix} \tau^2 + x\tau + 1 & -x \\ x\tau^2 & \tau^2 - x\tau + 1 \end{pmatrix}_D,$$

where  $x = (n\tau - m)/(m\tau + n)$ :

$$\mathbf{d}'_i = \sum_{j=1}^2 S_{mij} \mathbf{d}_j;$$

$$\mathbf{d}'_1 = \frac{1}{2 + \tau} [(\tau^2 + x\tau + 1)\mathbf{d}_1 - x\mathbf{d}_2]$$

$$= \frac{1}{(2 + \tau)a^*} \begin{pmatrix} 1 \\ -\tau - x \end{pmatrix}_V$$

$$= \frac{1}{(2 + \tau)a^*} \begin{pmatrix} 1 \\ -\frac{2n\tau + m\tau}{m\tau + n} \end{pmatrix}_V,$$

$$\mathbf{d}'_2 = \frac{1}{2 + \tau} [x\tau^2 \mathbf{d}_1 + (\tau^2 - x\tau + 1)\mathbf{d}_2]$$

$$= \frac{1}{(2 + \tau)a^*} \begin{pmatrix} \tau \\ -x\tau + 1 \end{pmatrix}_V$$

$$= \frac{1}{(2 + \tau)a^*} \begin{pmatrix} \tau \\ \frac{2m\tau - n\tau}{m\tau + n} \end{pmatrix}_V.$$

This shear matrix does not change the magnitudes of the intervals  $L$  and  $S$ . In reciprocal space the inverted and transposed shear matrix is applied on the reciprocal basis,

#### 4.6. RECIPROCAL-SPACE IMAGES OF APERIODIC CRYSTALS

$$(S_m^{-1})^T = \frac{1}{2+\tau} \begin{pmatrix} \tau^2 - x\tau + 1 & -x\tau^2 \\ x & \tau^2 + x\tau + 1 \end{pmatrix}_D,$$

where  $x = (n\tau - m)/(m\tau + n)$ :

$$\mathbf{d}_i^* = \sum_{j=1}^2 (S_m^{-1})_{ij}^T \mathbf{d}_j^*;$$

$$\begin{aligned} \mathbf{d}_1^* &= \frac{1}{2+\tau} \left[ (\tau^2 - x\tau + 1)\mathbf{d}_1^* - x\tau^2 \mathbf{d}_2^* \right] \\ &= a^* \begin{pmatrix} 1 - x\tau \\ -\tau \end{pmatrix}_V \\ &= a^* \begin{pmatrix} 2m\tau - n\tau \\ m\tau + n \\ -\tau \end{pmatrix}_V, \end{aligned}$$

$$\begin{aligned} \mathbf{d}_2^* &= \frac{1}{2+\tau} \left[ x\mathbf{d}_1^* + (\tau^2 + x\tau + 1)\mathbf{d}_2^* \right] \\ &= a^* \begin{pmatrix} \tau + x \\ 1 \end{pmatrix}_V \\ &= a^* \begin{pmatrix} 2n\tau + m\tau \\ m\tau + n \\ 1 \end{pmatrix}_V. \end{aligned}$$

The point  $x_n(t)$  of the  $n$ th interval L or S of an infinite Fibonacci sequence is given by

$$x_n(t) = \{x_0 + n(3 - \tau) - (\tau - 1)[\text{frac}(n\tau + t) - (1/2)]\}S,$$

where  $t$  is the phase of the modulation function  $y(t) = (\tau - 1)[\text{frac}(n\tau + t) - (1/2)]$  (Janssen, 1986). Thus, the Fibonacci sequence can also be dealt with as an incommensurately modulated structure. This is a consequence of the fact that for 1D structures only the crystallographic point symmetries 1 and  $\bar{1}$  allow the existence of a periodic average structure.

The embedding of the Fibonacci chain as an incommensurately modulated structure can be performed as follows:

(1) select a subset  $\Lambda^* \subset M^*$  of strong reflections for main reflections  $\mathbf{H} = h\mathbf{a}^*$ ,  $h \in \mathbb{Z}$ ;

(2) define a satellite vector  $\mathbf{q} = \alpha\mathbf{a}^*$  pointing from each main reflection to the next satellite reflection.

One possible way of indexing based on the same  $\mathbf{a}^*$  as defined above is illustrated in Fig. 4.6.2.10. The scattering vector is given by  $\mathbf{H}^{\parallel} = h(\tau + 1)\mathbf{a}^* + m\mathbf{q}$ , where  $\mathbf{q} = \tau\mathbf{a}^*$ , or, in the 2D representation,  $\mathbf{H} = h_1\mathbf{d}_1^* + h_2\mathbf{d}_2^*$ , where  $\mathbf{d}_1^* = a^* \begin{pmatrix} 1 + \tau \\ 0 \end{pmatrix}_V$  and  $\mathbf{d}_2^* = a^* \begin{pmatrix} \tau \\ 1 \end{pmatrix}_V$ , with the direct basis

$$\mathbf{d}_1 = \frac{1}{a^*(1 + \tau)} \begin{pmatrix} 1 \\ -\tau \end{pmatrix}_V, \quad \mathbf{d}_2 = \frac{1}{a^*} \begin{pmatrix} 0 \\ 1 \end{pmatrix}_V.$$

The modulation function is saw-tooth-like (Fig. 4.6.2.11).

##### 4.6.2.5. 1D structures with fractal atomic surfaces

A 1D structure with a *fractal atomic surface* (Hausdorff dimension 0.9157... ) can be derived from the Fibonacci sequence by squaring its substitution matrix  $S$ :

$$\begin{pmatrix} S \\ L \end{pmatrix} \rightarrow \begin{pmatrix} 1 & 1 \\ 1 & 2 \end{pmatrix} \begin{pmatrix} S \\ L \end{pmatrix} = \begin{pmatrix} S + L \\ S + 2L \end{pmatrix}$$

with  $S^2 = \begin{pmatrix} 1 & 1 \\ 1 & 2 \end{pmatrix}$ ,

corresponding to the substitution rule  $S \rightarrow SL, L \rightarrow LLS$  as well

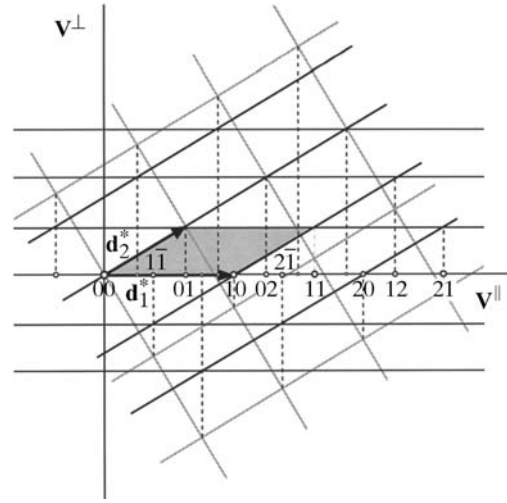


Fig. 4.6.2.10. Reciprocal space of the embedded Fibonacci chain as a modulated structure. Several main and satellite reflections are indexed. The square reciprocal lattice of the quasicrystal description illustrated in Fig. 4.6.2.9 is indicated by grey lines. The reflections located on  $\mathbf{V}^{\parallel}$  can be considered to be projected either from the 2D square lattice of the embedding as for a QS or from the 2D oblique lattice of the embedding as for an IMS.

as two other non-equivalent ones (see Janssen, 1995). The eigenvalues  $\lambda_i$  are obtained by calculating

$$\det |S - \lambda I| = 0.$$

The evaluation of the determinant gives the characteristic polynomial

$$\lambda^2 - 3\lambda + 1 = 0,$$

with the solutions  $\lambda_{1,2} = [3 \pm (5)^{1/2}]/2$ , with  $\lambda_1 = \tau^2$  and  $\lambda_2 = 1/\tau^2 = 2 - \tau$ , and the same eigenvectors  $\mathbf{w}_1 = \begin{pmatrix} 1 \\ \tau \end{pmatrix}$ ,  $\mathbf{w}_2 = \begin{pmatrix} 1 \\ -1/\tau \end{pmatrix}$  as for the Fibonacci sequence. Rewriting the eigenvalue equation gives

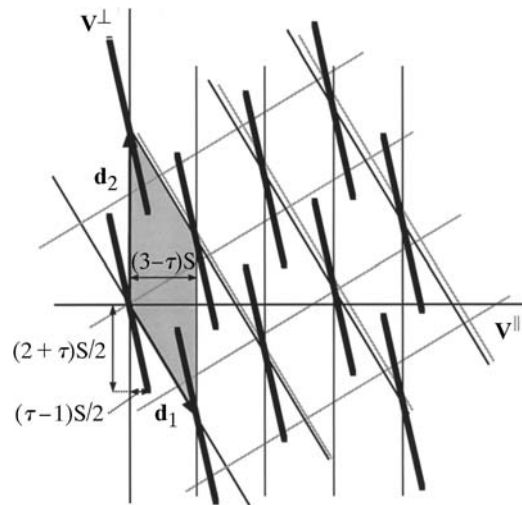


Fig. 4.6.2.11. 2D direct-space embedding of the Fibonacci chain as a modulated structure. The average period is  $(3 - \tau)S$ . The square lattice in the quasicrystal description shown in Fig. 4.6.2.8 is indicated by grey lines. The rod-like atomic surfaces are now inclined relative to  $\mathbf{V}^{\parallel}$  and arranged so as to give a saw-tooth modulation wave.

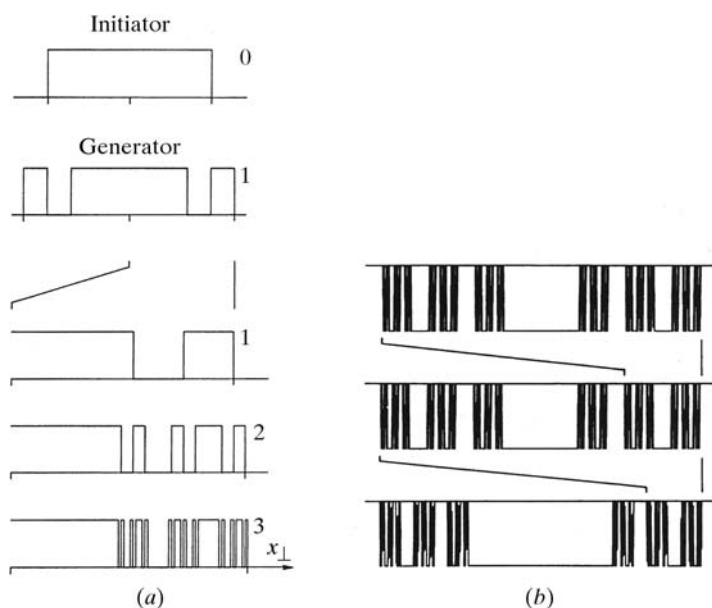


Fig. 4.6.2.12. (a) Three steps in the development of the fractal atomic surface of the squared Fibonacci sequence starting from an initiator and a generator. The action of the generator is to cut a piece from each side of the initiator and to add it where the initiator originally ended. This is repeated, cutting thinner and thinner pieces each time from the generated structures. (b) Magnification sequence of the fractal atomic surface illustrating its self-similarity. Each successive figure represents a magnification of a selected portion of the previous figure (from Zobetz, 1993).

$$\begin{pmatrix} 1 & 1 \\ 1 & 2 \end{pmatrix} \begin{pmatrix} 1 \\ \tau \end{pmatrix} = \begin{pmatrix} \tau + 1 \\ 2\tau + 1 \end{pmatrix} = \begin{pmatrix} \tau^2 \\ \tau^3 \end{pmatrix} = \tau^2 \begin{pmatrix} 1 \\ \tau \end{pmatrix}.$$

Identifying the eigenvector  $\begin{pmatrix} 1 \\ \tau \end{pmatrix}$  with  $\begin{pmatrix} S \\ L \end{pmatrix}$  shows that the infinite 1D sequence  $s(\mathbf{r})$  multiplied by powers of its eigenvalue  $\tau^2$  (scaling operation) remains invariant (each new lattice point coincides with one of the original lattice):

$$s(\tau^2 \mathbf{r}) = s(\mathbf{r}).$$

The fractal sequence can be described on the same reciprocal and direct bases as the Fibonacci sequence. The only difference in the 2D direct-space description is the fractal character of the perpendicular-space component of the hyperatoms (Fig. 4.6.2.12) (see Zobetz, 1993).

### 4.6.3. Reciprocal-space images

#### 4.6.3.1. Incommensurately modulated structures (IMs)

One-dimensionally modulated structures are the simplest representatives of IMs. The vast majority of the one hundred or so IMs known so far belong to this class (Cummins, 1990). However, there is also an increasing number of IMs with 2D or 3D modulation. The dimension  $d$  of the modulation is defined by the number of rationally independent modulation wave vectors (satellite vectors)  $\mathbf{q}_i$  (Fig. 4.6.3.1). The electron-density function of a  $dD$  modulated 3D crystal can be represented by the Fourier series

$$\rho(\mathbf{r}) = (1/V) \sum_{\mathbf{H}} F(\mathbf{H}) \exp(-2\pi i \mathbf{H} \cdot \mathbf{r}).$$

The Fourier coefficients (*structure factors*)  $F(\mathbf{H})$  differ from zero only for reciprocal-space vectors  $\mathbf{H} = \sum_{i=1}^3 h_i \mathbf{a}_i^* + \sum_{j=1}^d m_j \mathbf{q}_j =$

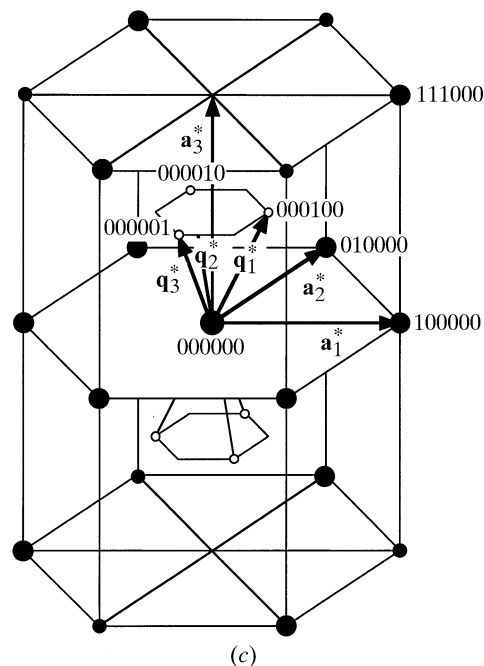
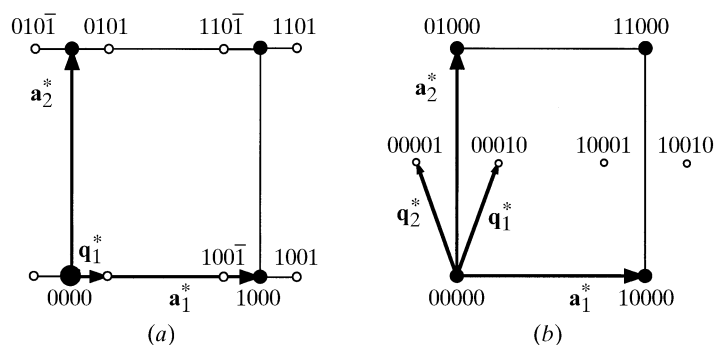


Fig. 4.6.3.1. Schematic diffraction patterns for IMs with (a) 1D, (b) 2D and (c) 3D modulation. The satellite vectors correspond to  $\mathbf{q} = \alpha_1 \mathbf{a}_1^*$  in (a),  $\mathbf{q}_1 = \alpha_{11} \mathbf{a}_1^* + (1/2) \mathbf{a}_2^*$  and  $\mathbf{q}_2 = -\alpha_{12} \mathbf{a}_1^* + (1/2) \mathbf{a}_2^*$ , where  $\alpha_{11} = \alpha_{12}$ , in (b), and  $\mathbf{q}_1 = \alpha_{11} \mathbf{a}_1^* + \alpha_{31} \mathbf{a}_3^*$ ,  $\mathbf{q}_2 = \alpha_{12} (-\mathbf{a}_1^* + \mathbf{a}_2^*) + \alpha_{32} \mathbf{a}_3^*$ ,  $\mathbf{q}_3 = -\alpha_{13} \mathbf{a}_2^* + \alpha_{33} \mathbf{a}_3^*$ , where  $\alpha_{11} = \alpha_{12} = \alpha_{13}$  and  $\alpha_{31} = \alpha_{32} = \alpha_{33}$ , in (c). The areas of the circles are proportional to the reflection intensities. Main (filled circles) and satellite (open circles) reflections are indexed (after Janner *et al.*, 1983b).

$\sum_{i=1}^{3+d} h_i \mathbf{a}_i^*$  with  $h_i, m_j \in \mathbb{Z}$ . The  $d$  satellite vectors are given by  $\mathbf{q}_j = \mathbf{a}_{3+j}^* = \sum_{i=1}^3 \alpha_{ij} \mathbf{a}_i^*$ , with  $\alpha_{ij}$  a  $3 \times d$  matrix  $\sigma$ . In the case of an IM, at least one entry to  $\sigma$  has to be irrational. The wavelength of the modulation function is  $\lambda_j = 1/q_j$ . The set of vectors  $\mathbf{H}$  forms a Fourier module  $M^* = \{\mathbf{H} = \sum_{i=1}^{3+d} h_i \mathbf{a}_i^* | h_i \in \mathbb{Z}\}$  of rank  $n = 3 + d$ , which can be decomposed into a rank 3 and a rank  $d$  submodule  $M^* = M_1^* \oplus M_2^*$ .  $M_1^* = \{h_1 \mathbf{a}_1^* + h_2 \mathbf{a}_2^* + h_3 \mathbf{a}_3^*\}$  corresponds to a  $\mathbb{Z}$  module of rank 3 in a 3D subspace (the physical space),  $M_2^* = \{h_4 \mathbf{a}_4^* + \dots + h_{3+d} \mathbf{a}_{3+d}^*\}$  corresponds to a  $\mathbb{Z}$  module of rank  $d$  in a  $dD$  subspace (perpendicular space). The submodule  $M_1$  is identical to the 3D reciprocal lattice  $\Lambda^*$  of the average structure.  $M_2$  results from the projection of the perpendicular-space component of the  $(3 + d)D$  reciprocal lattice  $\Sigma^*$  upon the physical space. Owing to the coincidence of one subspace with the physical space, the dimension of the embedding space is given as  $(3 + d)D$  and not as  $nD$ . This terminology points out the special role of the physical space.

Hence the reciprocal-basis vectors  $\mathbf{a}_i^*, i = 1, \dots, 3 + d$ , can be considered to be physical-space projections of reciprocal-basis

## 4.6. RECIPROCAL-SPACE IMAGES OF APERIODIC CRYSTALS

vectors  $\mathbf{d}_i^*$ ,  $i = 1, \dots, 3 + d$ , spanning a  $(3 + d)$ D reciprocal lattice  $\Sigma^*$ :

$$\Sigma^* = \left\{ \mathbf{H} = \sum_{i=1}^{3+d} h_i \mathbf{d}_i^* \mid h_i \in \mathbb{Z} \right\},$$

$$\mathbf{d}_i^* = (\mathbf{a}_i^*, \mathbf{0}), \quad i = 1, \dots, 3 \quad \text{and} \quad \mathbf{d}_{3+j}^* = (\mathbf{a}_{3+j}^*, c\mathbf{e}_j^*), \quad j = 1, \dots, d.$$

The first vector component of  $\mathbf{d}_i^*$  refers to the physical space, the second to the perpendicular space spanned by the mutually orthogonal unit vectors  $\mathbf{e}_j$ .  $c$  is an arbitrary constant which can be set to 1 without loss of generality.

A direct lattice  $\Sigma$  with basis  $\mathbf{d}_i$ ,  $i = 1, \dots, 3 + d$  and  $\mathbf{d}_i \cdot \mathbf{d}_j^* = \delta_{ij}$ , can be constructed according to

$$\Sigma = \left\{ \mathbf{r} = \sum_{i=1}^{3+d} m_i \mathbf{d}_i \mid m_i \in \mathbb{Z} \right\},$$

$$\mathbf{d}_i = \left( \mathbf{a}_i, -\sum_{j=1}^d \alpha_{ij} (1/c) \mathbf{e}_j \right), \quad i = 1, \dots, 3$$

$$\text{and } \mathbf{d}_{3+j} = \left( \mathbf{0}, (1/c) \mathbf{e}_j^* \right), \quad j = 1, \dots, d.$$

Consequently, the aperiodic structure in physical space  $\mathbf{V}^{\parallel}$  is equivalent to a 3D section of the  $(3 + d)$ D hypercrystal.

### 4.6.3.1.1. Indexing

The 3D reciprocal space  $M^*$  of a  $(3 + d)$ D IMS consists of two separable contributions,

$$M^* = \left\{ \mathbf{H} = \sum_{i=1}^3 h_i \mathbf{a}_i^* + \sum_{j=1}^d m_j \mathbf{q}_j \right\},$$

the set of main reflections ( $m_j = 0$ ) and the set of satellite reflections ( $m_j \neq 0$ ) (Fig. 4.6.3.1). In most cases, the modulation is only a weak perturbation of the crystal structure. The main reflections are related to the average structure, the satellites to the difference between average and actual structure. Consequently, the satellite reflections are generally much weaker than the main reflections and can be easily identified. Once the set of main reflections has been separated, a conventional basis  $\mathbf{a}_i^*$ ,  $i = 1, \dots, 3$ , for  $\Lambda^*$  is chosen.

The only ambiguity is in the assignment of rationally independent satellite vectors  $\mathbf{q}_j$ . They should be chosen inside the reciprocal-space unit cell (Brillouin zone) of  $\Lambda^*$  in such a way as to give a minimal number  $d$  of additional dimensions. If satellite vectors reach the Brillouin-zone boundary, centred  $(3 + d)$ D Bravais lattices are obtained. The star of satellite vectors has to be invariant under the point-symmetry group of the diffraction pattern. There should be no contradiction to a reasonable physical modulation model concerning period or propagation direction of the modulation wave. More detailed information on how to find the optimum basis and the correct setting is given by Janssen *et al.* (1999) and Janner *et al.* (1983a,b).

### 4.6.3.1.2. Diffraction symmetry

The Laue symmetry group  $K^L = \{R\}$  of the Fourier module  $M^*$ ,

$$M^* = \left\{ \mathbf{H} = \sum_{i=1}^3 h_i \mathbf{a}_i^* + \sum_{j=1}^d m_j \mathbf{q}_j = \sum_{i=1}^{3+d} h_i \mathbf{a}_i^* \right\}, \quad \Lambda^* = \left\{ \mathbf{H} = \sum_{i=1}^3 h_i \mathbf{a}_i^* \right\},$$

is isomorphous to or a subgroup of one of the 11 3D crystallographic Laue groups leaving  $\Lambda^*$  invariant. The action of the point-group symmetry operators  $R$  on the reciprocal basis  $\mathbf{a}_i^*$ ,  $i = 1, \dots, 3 + d$ , can be written as

$$R\mathbf{a}_i^* = \sum_{j=1}^{3+d} \Gamma_{ij}^T(R) \mathbf{a}_j^*, \quad i = 1, \dots, 3 + d.$$

The  $(3 + d) \times (3 + d)$  matrices  $\Gamma^T(R)$  form a finite group of integral matrices which are reducible, since  $R$  is already an orthogonal transformation in 3D physical space. Consequently,  $R$  can be expressed as pair of orthogonal transformations ( $R^{\parallel}, R^{\perp}$ ) in 3D physical and  $d$ D perpendicular space, respectively. Owing to their mutual orthogonality, no symmetry relationship exists between the set of main reflections and the set of satellite reflections.  $\Gamma^T(R)$  is the transpose of  $\Gamma(R)$  which acts on vector components in direct space.

For the  $(3 + d)$ D direct-space (*superspace*) symmetry operator  $(R_s, \mathbf{t}_s)$  and its matrix representation  $\Gamma(R_s, \mathbf{t}_s)$  on  $\Sigma$ , the following decomposition can be performed:

$$\Gamma(R_s) = \begin{pmatrix} \Gamma^{\parallel}(R) & 0 \\ \Gamma^M(R) & \Gamma^{\perp}(R) \end{pmatrix} \quad \text{and} \quad \mathbf{t}_s = (\mathbf{t}_3, \mathbf{t}_d).$$

$\Gamma^{\parallel}(R)$  is a  $3 \times 3$  matrix,  $\Gamma^{\perp}(R)$  is a  $d \times d$  matrix and  $\Gamma^M(R)$  is a  $d \times 3$  matrix. The translation operator  $\mathbf{t}_s$  consists of a 3D vector  $\mathbf{t}_3$  and a  $d$ D vector  $\mathbf{t}_d$ . According to Janner & Janssen (1979),  $\Gamma^M(R)$  can be derived from  $\Gamma^M(R) = \sigma \Gamma^{\parallel}(R) - \Gamma^{\perp}(R) \sigma$ .  $\Gamma^M(R)$  has integer elements only as it contains components of primitive-lattice vectors of  $\Lambda^*$ , whereas  $\sigma$  in general consists of a rational and an irrational part:  $\sigma = \sigma^i + \sigma^r$ . Thus, only the rational part gives rise to nonzero entries in  $\Gamma^M(R)$ . With the order of the Laue group denoted by  $N$ , one obtains  $\sigma^i \equiv (1/N) \sum_R \Gamma^{\perp}(R) \sigma \Gamma^{\parallel}(R)^{-1}$ , where  $\Gamma^{\perp}(R) \sigma^i \Gamma^{\parallel}(R)^{-1} = \sigma^i$ , implying that  $\Gamma^M(R) = \sigma^r \Gamma^{\parallel}(R) - \Gamma^{\perp}(R) \sigma^r$  and  $0 = \sigma^i \Gamma^{\parallel}(R) - \Gamma^{\perp}(R) \sigma^i$ .

*Example:* In the case of a 3D IMS with 1D modulation ( $d = 1$ ) the  $3 \times d$  matrix

$$\sigma = \begin{pmatrix} \alpha_1 \\ \alpha_2 \\ \alpha_3 \end{pmatrix}$$

has the components of the wavevector  $\mathbf{q} = \sum_{i=1}^3 \alpha_i \mathbf{a}_i^* = \mathbf{q}^i + \mathbf{q}^r$ .  $\Gamma^{\perp}(R) = \varepsilon = \pm 1$  because for  $d = 1$ ,  $\mathbf{q}$  can only be transformed into  $\pm \mathbf{q}$ . Corresponding to  $\mathbf{q}^i \equiv (1/N) \sum_R \varepsilon R \mathbf{q}$ , one obtains  $R^T \mathbf{q}^i \equiv \varepsilon \mathbf{q}^i$  (modulo  $\Lambda^*$ ). The  $3 \times 1$  row matrix  $\Gamma^M(R)$  is equivalent to the difference vector between  $R^T \mathbf{q}$  and  $\varepsilon \mathbf{q}$  (Janssen *et al.*, 1999).

For a monoclinic modulated structure with point group  $2/m$  for  $M^*$  (unique axis  $\mathbf{a}_3$ ) and satellite vector  $\mathbf{q} = (1/2)\mathbf{a}_1^* + \alpha_3 \mathbf{a}_3^*$ , with  $\alpha_3$  an irrational number, one obtains

$$\begin{aligned} \mathbf{q}^i &\equiv (1/N) \sum_R \varepsilon R \mathbf{q} \\ &= \frac{1}{4} \left( +1 \cdot \begin{pmatrix} 1 & 0 & 0 \\ 0 & 1 & 0 \\ 0 & 0 & 1 \end{pmatrix} \begin{pmatrix} 1/2 \\ 0 \\ \alpha_3 \end{pmatrix} \right. \\ &\quad + 1 \cdot \begin{pmatrix} \bar{1} & 0 & 0 \\ 0 & \bar{1} & 0 \\ 0 & 0 & 1 \end{pmatrix} \begin{pmatrix} 1/2 \\ 0 \\ \alpha_3 \end{pmatrix} - 1 \cdot \begin{pmatrix} \bar{1} & 0 & 0 \\ 0 & \bar{1} & 0 \\ 0 & 0 & \bar{1} \end{pmatrix} \begin{pmatrix} 1/2 \\ 0 \\ \alpha_3 \end{pmatrix} \\ &\quad \left. - 1 \cdot \begin{pmatrix} 1 & 0 & 0 \\ 0 & 1 & 0 \\ 0 & 0 & \bar{1} \end{pmatrix} \begin{pmatrix} 1/2 \\ 0 \\ \alpha_3 \end{pmatrix} \right) \\ &= \begin{pmatrix} 0 \\ 0 \\ \alpha_3 \end{pmatrix}. \end{aligned}$$

From the relations  $R^T \mathbf{q}^i \equiv \varepsilon \mathbf{q}^i$  (modulo  $\Lambda^*$ ), it can be shown that

#### 4. DIFFUSE SCATTERING AND RELATED TOPICS

the symmetry operations 1 and 2 are associated with the perpendicular-space transformations  $\varepsilon = 1$ , and  $m$  and  $\bar{1}$  with  $\varepsilon = -1$ . The matrix  $\Gamma^M(R)$  is given by

$$\begin{aligned}\Gamma^M(2) &= \sigma^r \Gamma^\parallel(2) - \Gamma^\perp(2) \sigma^r \\ &= \begin{pmatrix} 1/2 \\ 0 \\ 0 \end{pmatrix} \begin{pmatrix} \bar{1} & 0 & 0 \\ 0 & \bar{1} & 0 \\ 0 & 0 & 1 \end{pmatrix} - (+1) \begin{pmatrix} 1/2 \\ 0 \\ 0 \end{pmatrix} = \begin{pmatrix} \bar{1} \\ 0 \\ 0 \end{pmatrix}\end{aligned}$$

for the operation 2, for instance.

The matrix representations  $\Gamma^T(R_s)$  of the symmetry operators  $R$  in reciprocal  $(3+d)$ D superspace decompose according to

$$\Gamma^T(R_s) = \begin{pmatrix} \Gamma^\parallel T(R) & \Gamma^{MT}(R) \\ 0 & \Gamma^\perp T(R) \end{pmatrix}.$$

Phase relationships between modulation functions of symmetry-equivalent atoms can give rise to systematic extinctions of different classes of satellite reflections. The extinction rules may include indices of both main and satellite reflections. A full list of systematic absences is given in the table of  $(3+1)$ D superspace groups (Janssen *et al.*, 1999). Thus, once point symmetry and systematic absences are found, the superspace group can be obtained from the tables in a way analogous to that used for regular 3D crystals. A different approach for the symmetry description of IMSs from the 3D Fourier-space perspective has been given by Dräger & Mermin (1996).

##### 4.6.3.1.3. Structure factor

The structure factor of a periodic structure is defined as the Fourier transform of the density distribution  $\rho(\mathbf{r})$  of its unit cell (UC):

$$F(\mathbf{H}) = \int_{\text{UC}} \rho(\mathbf{r}) \exp(2\pi i \mathbf{H} \cdot \mathbf{r}) \, d\mathbf{r}.$$

The same is valid in the case of the  $(3+d)$ D description of IMSs. The parallel- and perpendicular-space components are orthogonal to each other and can be separated. The Fourier transform of the parallel-space component of the electron-density distribution of a single atom gives the usual atomic scattering factors  $f_k(\mathbf{H}^\parallel)$ . For the structure-factor calculation, one does not need to use  $\rho(\mathbf{r})$  explicitly. The hyperatoms correspond to the convolution of the electron-density distribution in 3D physical space with the modulation function in  $d$ D perpendicular space. Therefore, the Fourier transform of the  $(3+d)$ D hyperatoms is simply the product of the Fourier transform  $f_k(\mathbf{H}^\parallel)$  of the physical-space component with the Fourier transform of the perpendicular-space component, the modulation function.

For a general *displacive modulation* one obtains for the  $i$ th coordinate  $x_{ik}$  of the  $k$ th atom in 3D physical space

$$x_{ik} = \bar{x}_{ik} + u_{ik}(\bar{x}_4, \dots, \bar{x}_{3+d}), \quad i = 1, \dots, 3,$$

where  $\bar{x}_{ik}$  are the basic-structure coordinates and  $u_{ik}(\bar{x}_4, \dots, \bar{x}_{3+d})$  are the modulation functions with unit periods in their arguments (Fig. 4.6.3.2). The arguments are  $\bar{x}_{3+j} = \alpha_{ij} \bar{x}_{ik}^0 + t_j$ ,  $j = 1, \dots, d$ , where  $\bar{x}_{ik}^0$  are the coordinates of the  $k$ th atom referred to the origin of its unit cell and  $t_j$  are the phases of the modulation functions. The modulation functions  $u_{ik}(\bar{x}_4, \dots, \bar{x}_{3+d})$  themselves can be expressed in terms of a Fourier series as

$$\begin{aligned}u_{ik}(\bar{x}_4, \dots, \bar{x}_{3+d}) &= \sum_{n_1=1}^{\infty} \dots \sum_{n_d=1}^{\infty} \left\{ {}^u C_{ik}^{n_1 \dots n_d} \cos[2\pi(n_1 \bar{x}_4 + \dots + n_d \bar{x}_{3+d})] \right. \\ &\quad \left. + {}^u S_{ik}^{n_1 \dots n_d} \sin[2\pi(n_1 \bar{x}_4 + \dots + n_d \bar{x}_{3+d})] \right\},\end{aligned}$$

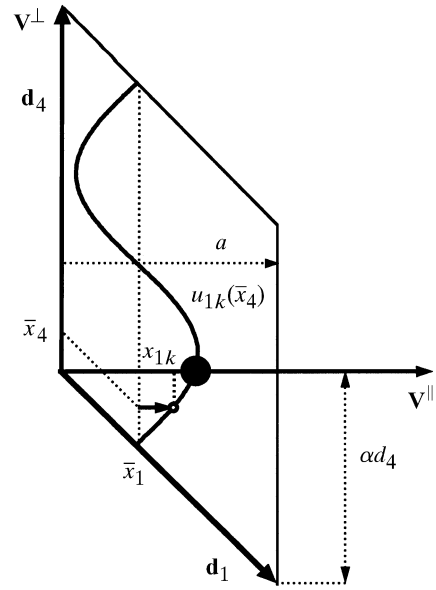


Fig. 4.6.3.2. The relationships between the coordinates  $x_{1k}, x_{4k}, \bar{x}_1, \bar{x}_4$  and the modulation function  $u_{1k}$  in a special section of the  $(3+d)$ D space.

where  $n_j$  are the orders of harmonics for the  $j$ th modulation wave of the  $i$ th component of the  $k$ th atom and their amplitudes are  ${}^u C_{ik}^{n_1 \dots n_d}$  and  ${}^u S_{ik}^{n_1 \dots n_d}$ .

Analogous expressions can be derived for a *density modulation*, i.e., the modulation of the occupation probability  $p_k(\bar{x}_4, \dots, \bar{x}_{3+d})$ :

$$\begin{aligned}p_k(\bar{x}_4, \dots, \bar{x}_{3+d}) &= \sum_{n_1=1}^{\infty} \dots \sum_{n_d=1}^{\infty} \left\{ {}^p C_k^{n_1 \dots n_d} \cos[2\pi(n_1 \bar{x}_4 + \dots + n_d \bar{x}_{3+d})] \right. \\ &\quad \left. + {}^p S_k^{n_1 \dots n_d} \sin[2\pi(n_1 \bar{x}_4 + \dots + n_d \bar{x}_{3+d})] \right\},\end{aligned}$$

and for the modulation of the tensor of thermal parameters  $B_{ijk}(\bar{x}_4, \dots, \bar{x}_{3+d})$ :

$$\begin{aligned}B_{ijk}(\bar{x}_4, \dots, \bar{x}_{3+d}) &= \sum_{n_1=1}^{\infty} \dots \sum_{n_d=1}^{\infty} \left\{ {}^B C_{ijk}^{n_1 \dots n_d} \cos[2\pi(n_1 \bar{x}_4 + \dots + n_d \bar{x}_{3+d})] \right. \\ &\quad \left. + {}^B S_{ijk}^{n_1 \dots n_d} \sin[2\pi(n_1 \bar{x}_4 + \dots + n_d \bar{x}_{3+d})] \right\}.\end{aligned}$$

The resulting structure-factor formula is

$$\begin{aligned}F(\mathbf{H}) &= \sum_{k=1}^{N'} \sum_{(R, \mathbf{t})} \int_0^1 d\bar{x}_4 \dots \int_0^1 d\bar{x}_{3+d} f_k(\mathbf{H}^\parallel) p_k \\ &\quad \times \exp \left( - \sum_{i,j=1}^{3+d} h_i [R B_{ijk} R^T] h_j + 2\pi i \sum_{j=1}^{3+d} h_j R x_{jk} + h_j t_j \right)\end{aligned}$$

for summing over the set  $(R, \mathbf{t})$  of superspace symmetry operations and the set of  $N'$  atoms in the asymmetric unit of the  $(3+d)$ D unit cell (Yamamoto, 1982). Different approaches without numerical integration based on analytical expressions including Bessel functions have also been developed. For more information see Paciorek & Chapuis (1994), Petricek, Maly & Cisarova (1991), and references therein.

For illustration, some fundamental IMSs will be discussed briefly (see Korekawa, 1967; Böhm, 1977).

*Harmonic density modulation.* A harmonic density modulation can result on average from an ordered distribution of vacancies on atomic positions. For an IMS with  $N$  atoms per unit cell one obtains

#### 4.6. RECIPROCAL-SPACE IMAGES OF APERIODIC CRYSTALS

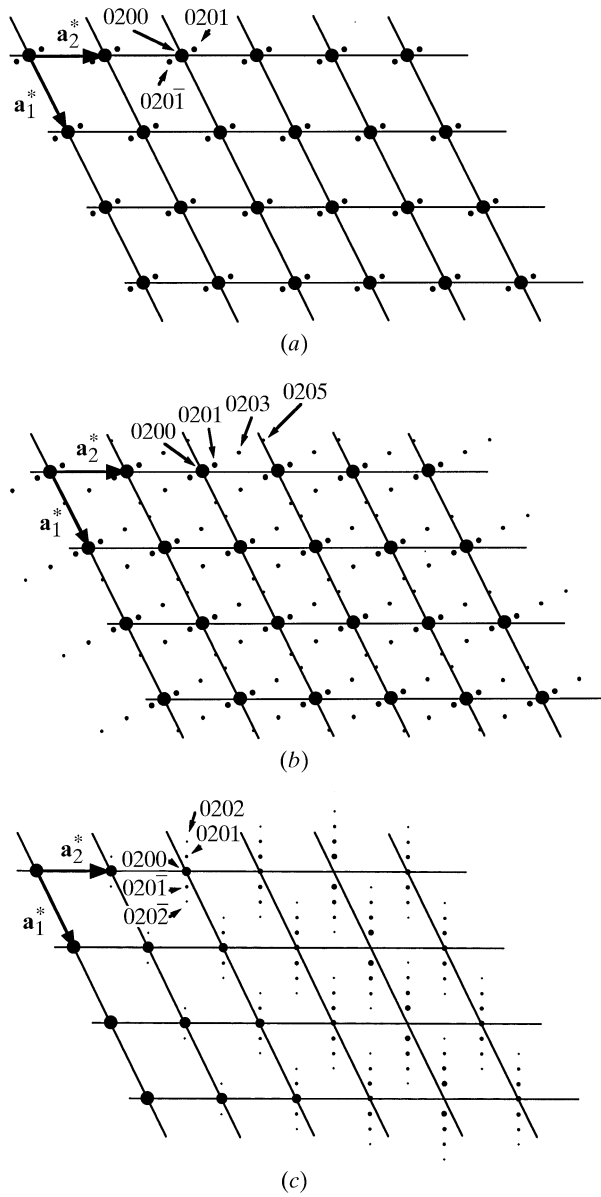


Fig. 4.6.3.3. Schematic diffraction patterns for 3D IMSs with (a) 1D harmonic and (b) rectangular density modulation. The modulation direction is parallel to  $\mathbf{a}_2$ . In (a) only first-order satellites exist; in (b), all odd-order satellites can be present. In (c), the diffraction pattern of a harmonic displacive modulation along  $\mathbf{a}_1$  with amplitudes parallel to  $\mathbf{a}_2^*$  is depicted. Several reflections are indexed. The areas of the circles are proportional to the reflection intensities.

for a harmonic modulation of the occupancy factor

$$p_k = (p_k^0/2) \{1 + \cos[2\pi(\bar{x}_{4,k} + \varphi_k)]\}, \quad 0 \leq p_k^0 \leq 1,$$

the structure-factor formula for the  $m$ th order satellite ( $0 \leq m \leq 1$ )

$$F_0(\mathbf{H}) = (1/2) \sum_{k=1}^N f_k(\mathbf{H}^{\parallel}) T_k(\mathbf{H}^{\parallel}) \exp(2\pi i \mathbf{H} \cdot \mathbf{r}_k),$$

$$F_m(\mathbf{H}) = (1/2) \sum_{k=1}^N f_k(\mathbf{H}^{\parallel}) T_k(\mathbf{H}^{\parallel}) (p_k^0/2)^{|m|} \exp \left[ 2\pi i \left( \sum_{i=1}^3 h_i x_{ik} + m \varphi_k \right) \right].$$

Thus, a linear correspondence exists between the structure-factor magnitudes of the satellite reflections and the amplitude of the density modulation. Furthermore, only first-order satellites exist, since the modulation wave consists only of one term. An important criterion for the existence of a density modulation is that a pair of

satellites around the origin of the reciprocal lattice exists (Fig. 4.6.3.3).

*Symmetric rectangular density modulation.* The box-function-like modulated occupancy factor can be expanded into a Fourier series,

$$p_k = p_k^0 (4/\pi) \left\{ \sum_{n=1}^{\infty} [(-1)^{n+1} / (2n-1)] \cos[2\pi(2n-1)(\bar{x}_{4,k} + \varphi_k)] \right\}, \quad 0 \leq p_k^0 \leq 1,$$

and the resulting structure factor of the  $m$ th order satellite is

$$F_0(\mathbf{H}) = (1/2) \sum_{k=1}^N f_k(\mathbf{H}^{\parallel}) T_k(\mathbf{H}^{\parallel}) \exp \left( 2\pi i \sum_{i=1}^3 h_i x_{ik} \right),$$

$$F_m(\mathbf{H}) = (1/\pi m) \sin(m\pi/2) \sum_{k=1}^N f_k(\mathbf{H}^{\parallel}) T_k(\mathbf{H}^{\parallel}) p_k^0 \times \exp \left[ 2\pi i \left( \sum_{i=1}^3 h_i x_{ik} + m \varphi_k \right) \right].$$

According to this formula, only odd-order satellites occur in the diffraction pattern. Their structure-factor magnitudes decrease linearly with the order  $|m|$  (Fig. 4.6.3.3b)

*Harmonic displacive modulation.* The displacement of the atomic coordinates is given by the function

$$x_{ik} = x_{ik}^0 + A_{ik} \cos[2\pi(\bar{x}_{4,k} + \varphi_k)], \quad i = 1, \dots, 3,$$

and the structure factor by

$$F_0(\mathbf{H}) = \sum_{k=1}^N f_k(\mathbf{H}^{\parallel}) T_k(\mathbf{H}^{\parallel}) J_0(2\pi \mathbf{H}^{\parallel} \cdot \mathbf{A}_k) \exp \left( 2\pi i \sum_{i=1}^3 h_i x_{ik} \right),$$

$$F_m(\mathbf{H}) = \sum_{k=1}^N f_k(\mathbf{H}^{\parallel}) T_k(\mathbf{H}^{\parallel}) J_m(2\pi \mathbf{H}^{\parallel} \cdot \mathbf{A}_k) \times \exp \left[ 2\pi i \left( \sum_{i=1}^3 h_i x_{ik} + m \varphi_k \right) \right].$$

The structure-factor magnitudes of the  $m$ th-order satellite reflections are a function of the  $m$ th-order Bessel functions. The arguments of the Bessel functions are proportional to the scalar products of the amplitude and the diffraction vector. Consequently, the intensity of the satellites will vary characteristically as a function of the length of the diffraction vector. Each main reflection is accompanied by an infinite number of satellite reflections (Figs. 4.6.3.3c and 4.6.3.4).

#### 4.6.3.2. Composite structures (CSs)

Composite structures consist of  $N$  mutually incommensurate substructures with  $N$  basic sublattices  $\Lambda_{\nu} = \{\mathbf{a}_{1\nu}, \mathbf{a}_{2\nu}, \mathbf{a}_{3\nu}\}$ , with  $\nu = 1, \dots, N$ . The reciprocal sublattices  $\Lambda_{\nu}^* = \{\mathbf{a}_{1\nu}^*, \mathbf{a}_{2\nu}^*, \mathbf{a}_{3\nu}^*\}$ , with  $\nu = 1, \dots, N$ , have either only the origin of the reciprocal lattice or one or two reciprocal-lattice directions in common. Thus, one needs  $(3+d) < 3N$  reciprocal-basis vectors for integer indexing of diffraction patterns that show Bragg reflections at positions given by the Fourier module  $M^*$ . The CSs discovered to date have at least one lattice direction in common and consist of a maximum number of  $N = 3$  substructures. They can be divided in three main classes: channel structures, columnar packings and layer packings (see van Smaalen, 1992, 1995).

In the following, the approach of Janner & Janssen (1980b) and van Smaalen (1992, 1995, and references therein) for the description of CSs is used. The set of diffraction vectors of a CS, *i.e.* its Fourier module  $M^* = \{\sum_{i=1}^{3+d} h_i \mathbf{a}_i^*\}$ , can be split into the contributions of the  $\nu$  subsystems by employing  $3 \times (3+d)$  matrices  $Z_{ik\nu}$  with integer coefficients  $\mathbf{a}_{i\nu}^* = \sum_{k=1}^{3+d} Z_{ik\nu} \mathbf{a}_k^*$ ,

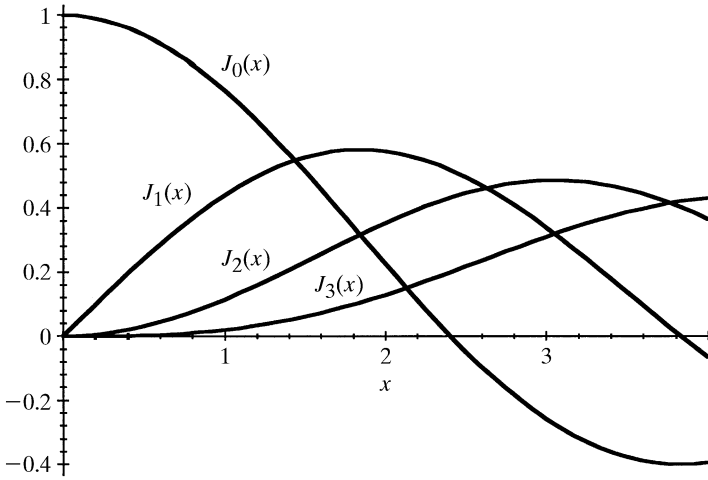


Fig. 4.6.3.4. The relative structure-factor magnitudes of  $m$ th-order satellite reflections for a harmonic displacive modulation are proportional to the values of the  $m$ th-order Bessel function  $J_m(x)$ .

$i = 1, \dots, 3$ . In the general case, each subsystem will be modulated with the periods of the others due to their mutual interactions. Thus, in general, CSs consist of several intergrown incommensurately modulated substructures. The satellite vectors  $\mathbf{q}_{j\nu}$ ,  $j = 1, \dots, d$ , referred to the  $\nu$ th subsystem can be obtained from  $M^*$  by applying the  $d \times (3+d)$  integer matrices  $V_{jk\nu}$ :  $\mathbf{q}_{j\nu} = \sum_{k=1}^{3+d} V_{jk\nu} \mathbf{a}_k^*$ ,  $j = 1, \dots, d$ . The matrices consisting of the components  $\sigma_\nu$  of the satellite vectors  $\mathbf{q}_{j\nu}$  with regard to the reciprocal sublattices  $\Lambda_\nu^*$  can be calculated by  $\sigma_\nu = (V_{3\nu} + V_{d\nu}\sigma)(Z_{3\nu} + Z_{d\nu}\sigma)^{-1}$ , where the subscript 3 refers to the  $3 \times 3$  submatrix of physical space and the subscript  $d$  to the  $d \times d$  matrix of the internal space. The juxtaposition of the  $3 \times (3+d)$  matrix  $Z_\nu$  and the  $d \times (3+d)$  matrix  $V_\nu$  defines the non-singular  $(3+d) \times (3+d)$  matrix  $W_\nu$ ,

$$W_\nu = \begin{pmatrix} Z_\nu \\ V_\nu \end{pmatrix}.$$

This matrix allows the reinterpretation of the Fourier module  $M^*$  as the Fourier module  $M_\nu^* = M^*W_\nu$  of a  $d$ -dimensionally modulated subsystem  $\nu$ . It also describes the coordinate transformation between the superspace basis  $\Sigma$  and  $\Sigma_\nu$ .

The superspace description is obtained analogously to that for IMSs (see Section 4.6.3.1) by considering the 3D Fourier module  $M^*$  of rank  $3+d$  as the projection of a  $(3+d)$ D reciprocal lattice  $\Sigma^*$  upon the physical space. Thus, one obtains for the definition of the direct and reciprocal  $(3+d)$  lattices (Janner & Janssen, 1980b)

$$\Sigma^* : \begin{cases} \mathbf{a}_i^* &= (\mathbf{a}_i^*, \mathbf{0}) & i = 1, \dots, 3 \\ \mathbf{a}_{3+j}^* &= (\mathbf{a}_{3+j}^*, \mathbf{e}_j^*) & j = 1, \dots, d \end{cases}$$

$$\Sigma : \begin{cases} \mathbf{a}_i &= (\mathbf{a}_i, -\sum_{j=1}^d \sigma_{ji} \mathbf{e}_j) & i = 1, \dots, 3 \\ \mathbf{a}_{3+j} &= (\mathbf{0}, \mathbf{e}_j) & j = 1, \dots, d. \end{cases}$$

#### 4.6.3.2.1. Indexing

The indexing of diffraction patterns of composite structures can be performed in the following way:

- (1) find the minimum number of reciprocal lattices  $\Lambda_\nu^*$  necessary to index the diffraction pattern;
- (2) find a basis for  $M^*$ , the union of sublattices  $\Lambda_\nu^*$ ;
- (3) find the appropriate superspace embedding.

The  $(3+d)$  vectors  $\mathbf{a}_i^*$  forming a basis for the 3D Fourier module  $M^* = \{\sum_{i=1}^{3+d} h_i \mathbf{a}_i^*\}$  can be chosen such that  $\mathbf{a}_1^*$ ,  $\mathbf{a}_2^*$  and  $\mathbf{a}_3^*$  are

linearly independent. Then the remaining  $d$  vectors can be described as a linear combination of the first three, defining the  $d \times 3$  matrix  $\sigma$ :  $\mathbf{a}_{3+j}^* = \sum_{i=1}^{3+d} \sigma_{ji} \mathbf{a}_i^*$ ,  $j = 1, \dots, d$ . This is formally equivalent to the reciprocal basis obtained for an IMS (see Section 4.6.3.1) and one can proceed in an analogous way to that for IMSs.

#### 4.6.3.2.2. Diffraction symmetry

The symmetry of CSs can be described with basically the same formalism as used for IMSs. This is a consequence of the formally equivalent applicability of the higher-dimensional approach, in particular of the superspace-group theory developed for IMSs [see Janner & Janssen (1980a,b); van Smaalen (1991, 1992); Yamamoto (1992a)].

#### 4.6.3.2.3. Structure factor

The structure factor  $F(\mathbf{H})$  of a composite structure consists of the weighted contributions of the subsystem structure factors  $F_\nu(\mathbf{H}_\nu)$ :

$$F(\mathbf{H}) = \sum_\nu |J_\nu| F_\nu(\mathbf{H}_\nu);$$

$$F_\nu(\mathbf{H}) = \sum_{(R^\nu, \mathbf{t}^\nu)} \sum_{k=1}^{N'} \int_0^1 d\mathbf{x}_{4,k}^\nu \dots \int_0^1 d\mathbf{x}_{3+d,k}^\nu f_k^\nu(\mathbf{H}^\parallel) P_k^\nu \times \exp \left( - \sum_{i,j=1}^{3+d} h_i^\nu [R^\nu B_{ijk}^\nu R^{\nu T}] h_j^\nu + 2\pi i \sum_{j=1}^{3+d} h_j^\nu R^\nu x_{jk}^\nu + h_j^\nu t_j^\nu \right),$$

with coefficients similar to those for IMSs.

The weights are the Jacobians of the transformations from  $\mathbf{t}_\nu$  to  $\mathbf{t}$ , and  $\mathbf{H}_\nu$  are the reflection indices with respect to the subsystem Fourier modules  $M_\nu^*$  (van Smaalen, 1995, and references therein).

The relative values of  $|J_\nu|$ , where  $J_\nu = \det [(V_{d\nu} - \sigma_\nu \cdot Z_{d\nu})^{-1}]$ , are related to the volume ratios of the contributing subsystems. The subsystem structure factors correspond to those for IMSs (see Section 4.6.3.1). Besides this formula, based on the publications of Yamamoto (1982) and van Smaalen (1995), different structure-factor equations have been discussed (Kato, 1990; Petricek, Maly, Coppens *et al.*, 1991).

#### 4.6.3.3. Quasiperiodic structures (QSs)

##### 4.6.3.3.1. 3D structures with 1D quasiperiodic order

Structures with quasiperiodic order in one dimension and lattice symmetry in the other two dimensions are the simplest representatives of quasicrystals. A few phases of this structure type have been identified experimentally (see Steurer, 1990). Since the Fibonacci chain represents the most important model of a 1D quasiperiodic structure, it will be used in this section to represent the quasiperiodic direction of 3D structures with 1D quasiperiodic order. As discussed in Section 4.6.2.4, 1D quasiperiodic structures are on the borderline between quasiperiodic and incommensurately modulated structures. They can be described using either of the two approaches. In the following, the quasiperiodic description will be preferred to take account of the scaling symmetry.

The electron-density-distribution function  $\rho(\mathbf{r})$  of a 1D quasiperiodically ordered 3D crystal can be represented by a Fourier series:

$$\rho(\mathbf{r}) = (1/V) \sum_{\mathbf{H}} F(\mathbf{H}) \exp(-2\pi i \mathbf{H} \cdot \mathbf{r}).$$

The Fourier coefficients (structure factors)  $F(\mathbf{H})$  differ from zero only for reciprocal-space vectors  $\mathbf{H} = \sum_{i=1}^3 h_i^\parallel \mathbf{a}_i^*$  with  $h_1^\parallel \in \mathbb{R}$ ,  $h_2^\parallel, h_3^\parallel \in \mathbb{Z}$  or with integer indexing  $\mathbf{H} = \sum_{i=1}^4 h_i \mathbf{a}_i^*$  with  $h_i \in \mathbb{Z}$ . The set of all vectors  $\mathbf{H}$  forms a Fourier module  $M^* = \{\mathbf{H}^\parallel = \sum_{i=1}^4 h_i \mathbf{a}_i^* | h_i \in \mathbb{Z}\}$  of rank 4 which can be decomposed into two rank 2 submodules  $M^* = M_1^* \oplus M_2^*$ .  $M_1^* = \{h_1 \mathbf{a}_1^* + h_2 \mathbf{a}_2^*\}$  corresponds

#### 4.6. RECIPROCAL-SPACE IMAGES OF APERIODIC CRYSTALS

to a  $\mathbb{Z}$  module of rank 2 in a 1D subspace,  $M_2^* = \{h_3\mathbf{a}_3^* + h_4\mathbf{a}_4^*\}$  corresponds to a  $\mathbb{Z}$  module of rank 2 in a 2D subspace. Consequently, the first submodule can be considered as a projection from a 2D reciprocal lattice,  $M_1^* = \pi^\parallel(\Sigma^*)$ , while the second submodule is of the form of a reciprocal lattice,  $M_2^* = \Lambda^*$ .

Hence, the reciprocal-basis vectors  $\mathbf{a}_i^*$ ,  $i = 1, \dots, 4$ , can be considered to be projections of reciprocal-basis vectors  $\mathbf{d}_i^*$ ,  $i = 1, \dots, 4$ , spanning a 4D reciprocal lattice, onto the physical space  $\Sigma^* = \{\mathbf{H} = \sum_{i=1}^4 h_i \mathbf{d}_i^* | h_i \in \mathbb{Z}\}$ , with

$$\mathbf{d}_1^* = a_1^* \begin{pmatrix} 1 \\ -\tau \\ 0 \\ 0 \end{pmatrix}, \quad \mathbf{d}_2^* = a_1^* \begin{pmatrix} \tau \\ 1 \\ 0 \\ 0 \end{pmatrix}, \quad \mathbf{d}_3^* = a_3^* \begin{pmatrix} 0 \\ 0 \\ 1 \\ 0 \end{pmatrix}, \quad \mathbf{d}_4^* = a_4^* \begin{pmatrix} 0 \\ 0 \\ 0 \\ 1 \end{pmatrix}.$$

A direct lattice  $\Sigma$  with basis  $\mathbf{d}_i$ ,  $i = 1, \dots, 4$  and  $\mathbf{d}_i \cdot \mathbf{d}_j^* = \delta_{ij}$ , can be constructed according to (compare Fig. 4.6.2.8)  $\Sigma = \{\mathbf{r} = \sum_{i=1}^4 m_i \mathbf{d}_i | m_i \in \mathbb{Z}\}$ , with

$$\mathbf{d}_1 = \frac{1}{a_1^*(2+\tau)} \begin{pmatrix} 1 \\ -\tau \\ 0 \\ 0 \end{pmatrix}, \quad \mathbf{d}_2 = \frac{1}{a_1^*(2+\tau)} \begin{pmatrix} \tau \\ 1 \\ 0 \\ 0 \end{pmatrix},$$

$$\mathbf{d}_3 = \frac{1}{a_3^*} \begin{pmatrix} 0 \\ 0 \\ 1 \\ 0 \end{pmatrix}, \quad \mathbf{d}_4 = \frac{1}{a_4^*} \begin{pmatrix} 0 \\ 0 \\ 0 \\ 1 \end{pmatrix}.$$

Consequently, the structure in physical space  $\mathbf{V}^\parallel$  is equivalent to a 3D section of the 4D hypercrystal.

##### 4.6.3.3.1.1. Indexing

The reciprocal space of the Fibonacci chain is densely filled with Bragg reflections (Figs. 4.6.2.9 and 4.6.3.5). According to the  $nD$  embedding method, the shorter the parallel-space distance  $\Delta \mathbf{H}^\parallel = \mathbf{H}_2^\parallel - \mathbf{H}_1^\parallel$  between two Bragg reflections, the larger the corresponding perpendicular-space distance  $\Delta \mathbf{H}^\perp = \mathbf{H}_2^\perp - \mathbf{H}_1^\perp$  becomes. Since the structure factor  $F(\mathbf{H})$  decreases rapidly as a function of  $\mathbf{H}^\perp$  (Fig. 4.6.3.6), 'neighbouring' reflections of strong Bragg peaks are extremely weak and, consequently, the reciprocal space appears to be filled with *discrete* Bragg peaks even for low-resolution experiments.

This property allows an unambiguous identification of a correct set of reciprocal-basis vectors. However, infinitely many sets allowing a correct indexing of the diffraction pattern with integer indices exist. Nevertheless, an optimum basis (low indices are assigned to strong reflections) can be derived: the intensity distribution, not the metrics, characterizes the best choice of indexing. Once the minimum distance  $S$  in the structure is identified from chemical considerations, the reciprocal basis should be chosen as described in Section 4.6.2.4. It has to be kept in mind, however, that the identification of the metrics is not sufficient to distinguish in the 1D aperiodic case between an incommensurately modulated structure, a quasiperiodic structure or special kinds of structures with fractally shaped atomic surfaces.

A correct set of reciprocal-basis vectors can be identified in the following way:

- (1) Find pairs of strong reflections whose physical-space diffraction vectors are related to each other by the factor  $\tau$ .
- (2) Index these reflections by assigning an appropriate value to  $a^*$ . This value should be derived from the shortest interatomic distance  $S$  expected in the structure.
- (3) The reciprocal basis is correct if all observable Bragg reflections can be indexed with integer numbers.

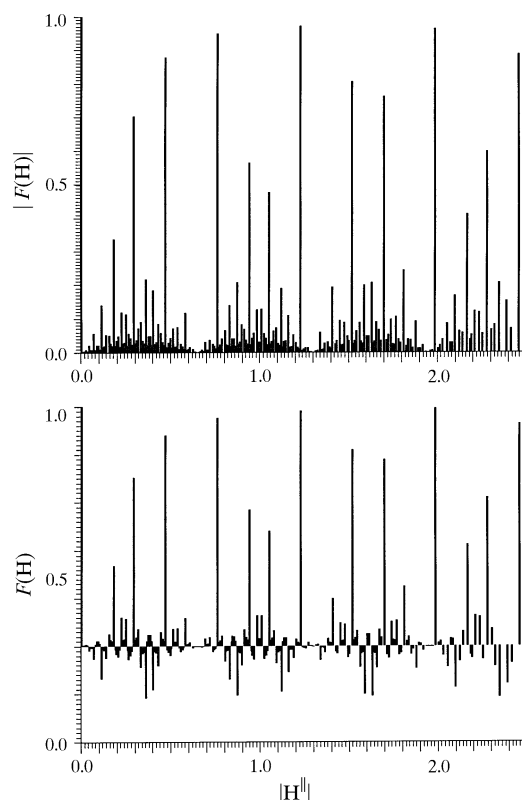


Fig. 4.6.3.5. The structure factors  $F(\mathbf{H})$  (below) and their magnitudes  $|F(\mathbf{H})|$  (above) of a Fibonacci chain decorated with equal point atoms are shown as a function of the parallel-space component  $|\mathbf{H}^\parallel|$  of the diffraction vector. The short distance in the Fibonacci chain is  $S = 2.5 \text{ \AA}$ , all structure factors within  $0 \leq |\mathbf{H}^\parallel| \leq 2.5 \text{ \AA}^{-1}$  have been calculated and normalized to  $F(00) = 1$ .

##### 4.6.3.3.1.2. Diffraction symmetry

The possible Laue symmetry group  $K^{3D}$  of the Fourier module  $M^* = \{\mathbf{H}^\parallel = \sum_{i=1}^4 h_i \mathbf{a}_i^* | h_i \in \mathbb{Z}\}$  is any one of the direct product  $K^{3D} = K^{2D} \otimes K^{1D} \otimes \bar{1}$ .  $K^{2D}$  corresponds to one of the ten crystallographic 2D point groups,  $K^{1D} = \{1\}$  in the general case of a quasiperiodic stacking of periodic layers. Consequently, the nine Laue groups  $\bar{1}, 2/m, mmm, 4/m, 4/mmm, \bar{3}, \bar{3}m, 6/m$  and  $6/mmm$  are possible. These are all 3D crystallographic Laue groups except for the two cubic ones.

The (unweighted) Fourier module shows only 2D lattice symmetry. In the third dimension, the submodule  $M_1^*$  remains invariant under the scaling symmetry operation  $S^n M_1^* = \tau^n M_1^*$  with  $n \in \mathbb{Z}$ . The scaling symmetry operators  $S^n$  form an infinite group  $s = \{\dots, S^{-1}, S^0, S^1, \dots\}$  of reciprocal-basis transformations  $S^n$  in superspace,

$$S^n = \begin{pmatrix} 0 & 1 & 0 & 0 \\ 1 & 1 & 0 & 0 \\ 0 & 0 & 1 & 0 \\ 0 & 0 & 0 & 1 \end{pmatrix}_D^n, \quad S^{-1} = \begin{pmatrix} \bar{1} & 1 & 0 & 0 \\ 1 & 0 & 0 & 0 \\ 0 & 0 & 1 & 0 \\ 0 & 0 & 0 & 1 \end{pmatrix}_D,$$

$$S^0 = \begin{pmatrix} 1 & 0 & 0 & 0 \\ 0 & 1 & 0 & 0 \\ 0 & 0 & 1 & 0 \\ 0 & 0 & 0 & 1 \end{pmatrix}_D,$$

and act on the reciprocal basis  $\mathbf{d}_i^*$  in superspace.

#### 4. DIFFUSE SCATTERING AND RELATED TOPICS

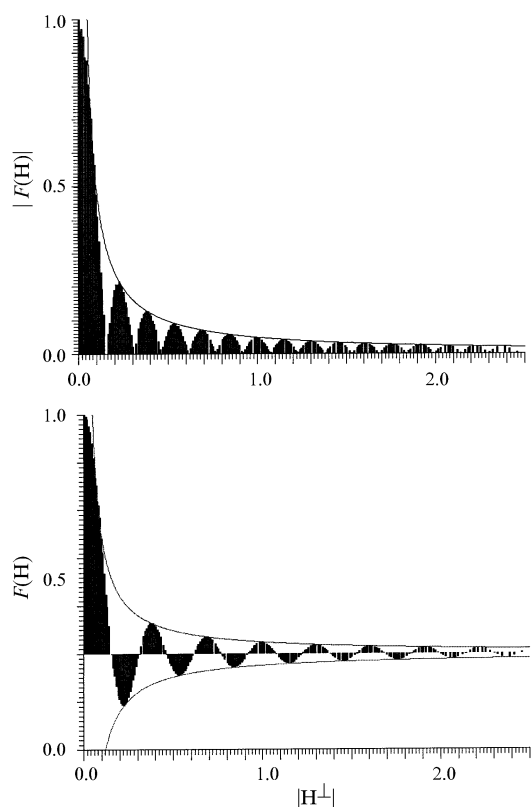


Fig. 4.6.3.6. The structure factors  $F(\mathbf{H})$  (below) and their magnitudes  $|F(\mathbf{H})|$  (above) of a Fibonacci chain decorated with equal point atoms are shown as a function of the perpendicular-space component  $|\mathbf{H}^\perp|$  of the diffraction vector. The short distance in the Fibonacci chain is  $S = 2.5 \text{ \AA}$ , all structure factors within  $0 \leq |\mathbf{H}| \leq 2.5 \text{ \AA}^{-1}$  have been calculated and normalized to  $F(00) = 1$ .

##### 4.6.3.3.1.3. Structure factor

The structure factor of a periodic structure is defined as the Fourier transform of the density distribution  $\rho(\mathbf{r})$  of its unit cell (UC):

$$F(\mathbf{H}) = \int_{\text{UC}} \rho(\mathbf{r}) \exp(2\pi i \mathbf{H} \cdot \mathbf{r}) \, d\mathbf{r}.$$

The same is valid in the case of the  $nD$  description of a quasiperiodic structure. The parallel- and perpendicular-space components are orthogonal to each other and can be separated. In the case of the 1D Fibonacci sequence, the Fourier transform of the parallel-space component of the electron-density distribution of a single atom gives the usual atomic scattering factor  $f(\mathbf{H}^\parallel)$ . Parallel to  $x^\perp$ ,  $\rho(\mathbf{r})$  adopts values  $\neq 0$  only within the interval  $-(1+\tau)/[2a^*(2+\tau)] \leq x^\perp \leq (1+\tau)/[2a^*(2+\tau)]$  and one obtains

$$F(\mathbf{H}) = f(\mathbf{H}^\parallel) [a^*(2+\tau)] / (1+\tau) \times \int_{-(1+\tau)/[2a^*(2+\tau)]}^{+(1+\tau)/[2a^*(2+\tau)]} \exp(2\pi i \mathbf{H}^\perp \cdot x^\perp) \, dx^\perp.$$

The factor  $[a^*(2+\tau)] / (1+\tau)$  results from the normalization of the structure factors to  $F(\mathbf{0}) = f(0)$ . With

$$\begin{aligned} \mathbf{H} &= h_1 \mathbf{d}_1^* + h_2 \mathbf{d}_2^* + h_3 \mathbf{d}_3^* + h_4 \mathbf{d}_4^* \\ &= h_1 a_1^* \begin{pmatrix} 1 \\ -\tau \\ 0 \\ 0 \end{pmatrix} + h_2 a_1^* \begin{pmatrix} \tau \\ 1 \\ 0 \\ 0 \end{pmatrix} + h_3 a_3^* \begin{pmatrix} 0 \\ 0 \\ 1 \\ 0 \end{pmatrix} + h_4 a_4^* \begin{pmatrix} 0 \\ 0 \\ 0 \\ 1 \end{pmatrix} \end{aligned}$$

and  $\mathbf{H}^\perp = a_1^*(-\tau h_1 + h_2)$  the integrand can be rewritten as

$$F(\mathbf{H}) = f(\mathbf{H}^\parallel) [a^*(2+\tau)] / (1+\tau) \times \int_{-(1+\tau)/[2a^*(2+\tau)]}^{+(1+\tau)/[2a^*(2+\tau)]} \exp[2\pi i(-\tau h_1 + h_2)x^\perp] \, dx^\perp,$$

yielding

$$F(\mathbf{H}) = f(\mathbf{H}^\parallel) (2+\tau) / [2\pi i(-\tau h_1 + h_2)(1+\tau)] \times \exp[2\pi i(-\tau h_1 + h_2)x^\perp] \Big|_{-(1+\tau)/[2a^*(2+\tau)]}^{+(1+\tau)/[2a^*(2+\tau)]}.$$

Using  $\sin x = (e^{ix} - e^{-ix})/2i$  gives

$$F(\mathbf{H}) = f(\mathbf{H}^\parallel) (2+\tau) / [\pi(-\tau h_1 + h_2)(1+\tau)] \times \sin[\pi(1+\tau)(-\tau h_1 + h_2)] / (2+\tau).$$

Thus, the structure factor has the form of the function  $\sin(x)/x$  with  $x$  a perpendicular reciprocal-space coordinate. The upper and lower limiting curves of this function are given by the hyperbolae  $\pm 1/x$  (Fig. 4.6.3.6). The continuous shape of  $F(\mathbf{H})$  as a function of  $\mathbf{H}^\perp$  allows the estimation of an overall temperature factor and atomic scattering factor for reflection-data normalization (compare Figs. 4.6.3.6 and 4.6.3.7).

In the case of a 3D crystal structure which is quasiperiodic in one direction, the structure factor can be written in the form

$$F(\mathbf{H}) = \sum_{k=1}^n [T_k(\mathbf{H}) f_k(\mathbf{H}^\parallel) g_k(\mathbf{H}^\perp) \exp(2\pi i \mathbf{H} \cdot \mathbf{r}_k)].$$

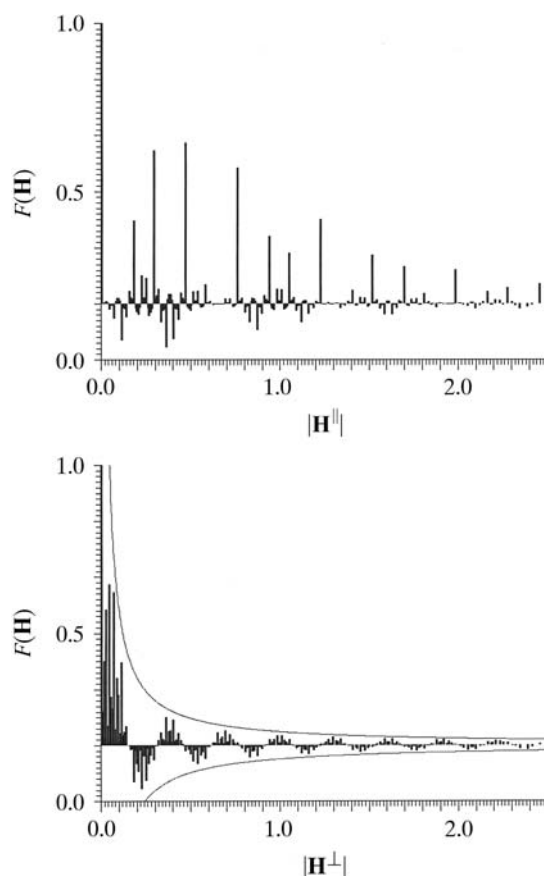


Fig. 4.6.3.7. The structure factors  $F(\mathbf{H})$  of the Fibonacci chain decorated with aluminium atoms ( $U_{\text{overall}} = 0.005 \text{ \AA}^2$ ) as a function of the parallel (above) and the perpendicular (below) component of the diffraction vector. The short distance is  $S = 2.5 \text{ \AA}$ , all structure factors within  $0 \leq |\mathbf{H}| \leq 2.5 \text{ \AA}^{-1}$  have been calculated and normalized to  $F(00) = 1$ .

#### 4.6. RECIPROCAL-SPACE IMAGES OF APERIODIC CRYSTALS

The sum runs over all  $n$  averaged hyperatoms in the 4D unit cell of the structure. The *geometric form factor*  $g_k(\mathbf{H}^\perp)$  corresponds to the Fourier transform of the  $k$ th atomic surface,

$$g_k(\mathbf{H}^\perp) = (1/A_{\text{UC}}^\perp) \int_{A_k} \exp(2\pi i \mathbf{H}^\perp \cdot \mathbf{r}^\perp) d\mathbf{r}^\perp,$$

normalized to  $A_{\text{UC}}^\perp$ , the area of the 2D unit cell projected upon  $\mathbf{V}^\perp$ , and  $A_k$ , the area of the  $k$ th atomic surface.

The atomic temperature factor  $T_k(\mathbf{H})$  can also have perpendicular-space components. Assuming only harmonic (static or dynamic) displacements in parallel and perpendicular space one obtains, in analogy to the usual expression (Willis & Pryor, 1975),

$$\begin{aligned} T_k(\mathbf{H}) &= T_k(\mathbf{H}^\parallel, \mathbf{H}^\perp) \\ &= \exp(-2\pi^2 \mathbf{H}^\parallel T \langle \mathbf{u}_i^\parallel \mathbf{u}_j^{\parallel T} \rangle \mathbf{H}^\parallel) \exp(-2\pi^2 \mathbf{H}^\perp T \langle \mathbf{u}_i^\perp \mathbf{u}_j^{\perp T} \rangle \mathbf{H}^\perp), \end{aligned}$$

with

$$\langle \mathbf{u}_i^\parallel \mathbf{u}_j^{\parallel T} \rangle = \begin{pmatrix} \langle \mathbf{u}_1^{\parallel 2} \rangle & \langle \mathbf{u}_1^\parallel \cdot \mathbf{u}_2^{\parallel T} \rangle & \langle \mathbf{u}_1^\parallel \cdot \mathbf{u}_3^{\parallel T} \rangle \\ \langle \mathbf{u}_2^\parallel \cdot \mathbf{u}_1^{\parallel T} \rangle & \langle \mathbf{u}_2^{\parallel 2} \rangle & \langle \mathbf{u}_2^\parallel \cdot \mathbf{u}_3^{\parallel T} \rangle \\ \langle \mathbf{u}_3^\parallel \cdot \mathbf{u}_1^{\parallel T} \rangle & \langle \mathbf{u}_3^\parallel \cdot \mathbf{u}_2^{\parallel T} \rangle & \langle \mathbf{u}_3^{\parallel 2} \rangle \end{pmatrix}$$

and  $\langle \mathbf{u}_i^\perp \mathbf{u}_j^{\perp T} \rangle = \langle \mathbf{u}_i^{\perp 2} \rangle$ .

The elements of the type  $\langle \mathbf{u}_i \cdot \mathbf{u}_j^T \rangle$  represent the average values of the atomic displacements along the  $i$ th axis times the displacement along the  $j$ th axis on the  $V$  basis.

##### 4.6.3.3.1.4. Intensity statistics

In the following, only the properties of the quasiperiodic component of the 3D structure, namely the Fourier module  $M_1^*$ , are discussed. The intensities  $I(\mathbf{H})$  of the Fibonacci chain decorated with point atoms are only a function of the perpendicular-space component of the diffraction vector.  $|F(\mathbf{H})|$  and  $F(\mathbf{H})$  are illustrated in Figs. 4.6.3.5 and 4.6.3.6 as a function of  $\mathbf{H}^\parallel$  and of  $\mathbf{H}^\perp$ . The distribution of  $|F(\mathbf{H})|$  as a function of their frequencies clearly resembles a centric distribution, as can be expected from the centrosymmetric 2D sub-unit cell. The shape of the distribution function depends on the radius  $H_{\text{max}}$  of the limiting sphere in reciprocal space. The number of weak reflections increases with the square of  $H_{\text{max}}$ , that of strong reflections only linearly (strong reflections always have small  $\mathbf{H}^\perp$  components).

The weighted reciprocal space of the Fibonacci sequence contains an infinite number of Bragg reflections within a limited region of the physical space. Contrary to the diffraction pattern of a periodic structure consisting of point atoms on the lattice nodes, the Bragg reflections show intensities depending on the perpendicular-space components of their diffraction vectors.

The reciprocal space of a sequence generated from hyperatoms with fractally shaped atomic surfaces (squared Fibonacci sequence) is very similar to that of the Fibonacci sequence (Figs. 4.6.3.8 and 4.6.3.9). However, there are significantly more weak reflections in the diffraction pattern of the 'fractal' sequence, caused by the geometric form factor.

##### 4.6.3.3.1.5. Relationships between structure factors at symmetry-related points of the Fourier image

The two possible point-symmetry groups in the 1D quasiperiodic case,  $K^{1D} = 1$  and  $K^{1D} = \bar{1}$ , relate the structure factors to

$$\begin{aligned} 1 : & \quad F(\mathbf{H}) = -F(\bar{\mathbf{H}}), \\ \bar{1} : & \quad F(\mathbf{H}) = F(\bar{\mathbf{H}}). \end{aligned}$$

A 3D structure with 1D quasiperiodicity results from the stacking of atomic layers with distances following a quasiperiodic sequence.

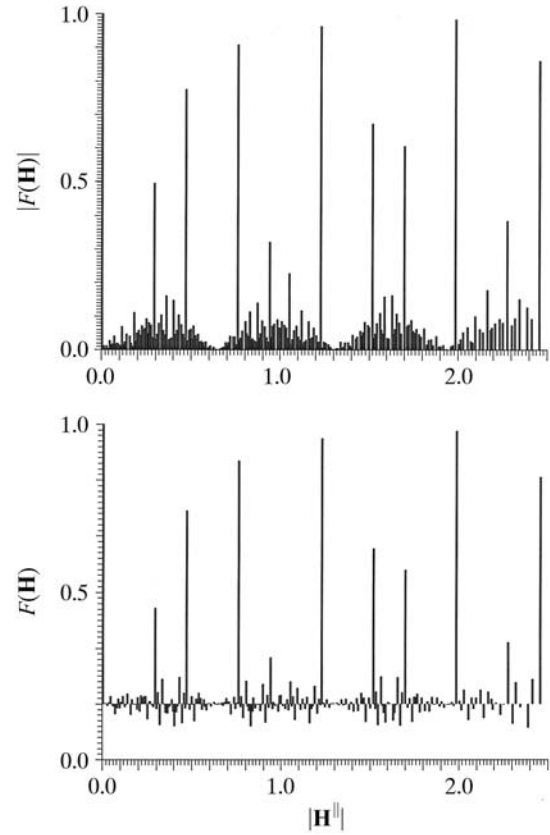


Fig. 4.6.3.8. The structure factors  $F(\mathbf{H})$  (below) and their magnitudes  $|F(\mathbf{H})|$  (above) of the squared Fibonacci chain decorated with equal point atoms are shown as a function of the parallel-space component  $|\mathbf{H}^\parallel|$  of the diffraction vector. The short<sub>1</sub> distance is  $S = 2.5 \text{ \AA}$ , all structure factors within  $0 \leq |\mathbf{H}| \leq 2.5 \text{ \AA}^{-1}$  have been calculated and normalized to  $F(00) = 1$ .

The point groups  $K^{3D}$  describing the symmetry of such structures result from the direct product  $K^{3D} = K^{2D} \otimes K^{1D}$ .  $K^{2D}$  corresponds to one of the ten crystallographic 2D point groups,  $K^{1D}$  can be  $\{1\}$  or  $\{1, m\}$ . Consequently, 18 3D point groups are possible.

Since 1D quasiperiodic sequences can be described generically as incommensurately modulated structures, their possible point and space groups are equivalent to a subset of the  $(3+1)$ D superspace groups for IMSs with satellite vectors of the type  $(00\gamma)$ , *i.e.*  $\mathbf{q} = \gamma \mathbf{c}^*$ , for the quasiperiodic direction  $[001]$  (Janssen *et al.*, 1999).

From the scaling properties of the Fibonacci sequence, some relationships between structure factors can be derived. Scaling the physical-space structure by a factor  $\tau^n$ ,  $n \in \mathbb{Z}$ , corresponds to a scaling of the perpendicular space by the inverse factor  $(-\tau)^{-n}$ . For the scaling of the corresponding reciprocal subspaces, the inverse factors compared to the direct spaces have to be applied.

The set of vectors  $\mathbf{r}$ , defining the vertices of a Fibonacci sequence  $s(\mathbf{r})$ , multiplied by a factor  $\tau$  coincides with a subset of the vectors defining the vertices of the original sequence (Fig. 4.6.3.10). The residual vertices correspond to a particular decoration of the scaled sequence, *i.e.* the sequence  $\tau^2 s(\mathbf{r})$ . The Fourier transform of the sequence  $s(\mathbf{r})$  then can be written as the sum of the Fourier transforms of the sequences  $\tau s(\mathbf{r})$  and  $\tau^2 s(\mathbf{r})$ ;

$$\sum_k \exp(2\pi i \mathbf{H} \cdot \mathbf{r}_k) = \sum_k \exp(2\pi i \mathbf{H} \tau \mathbf{r}_k) + \sum_k \exp[2\pi i \mathbf{H} (\tau^2 \mathbf{r}_k + \tau)].$$

In terms of structure factors, this can be reformulated as

$$F(\mathbf{H}) = F(\tau \mathbf{H}) + \exp(2\pi i \tau \mathbf{H}) F(\tau^2 \mathbf{H}).$$

Hence, phases of structure factors that are related by scaling symmetry can be determined from each other.

4. DIFFUSE SCATTERING AND RELATED TOPICS

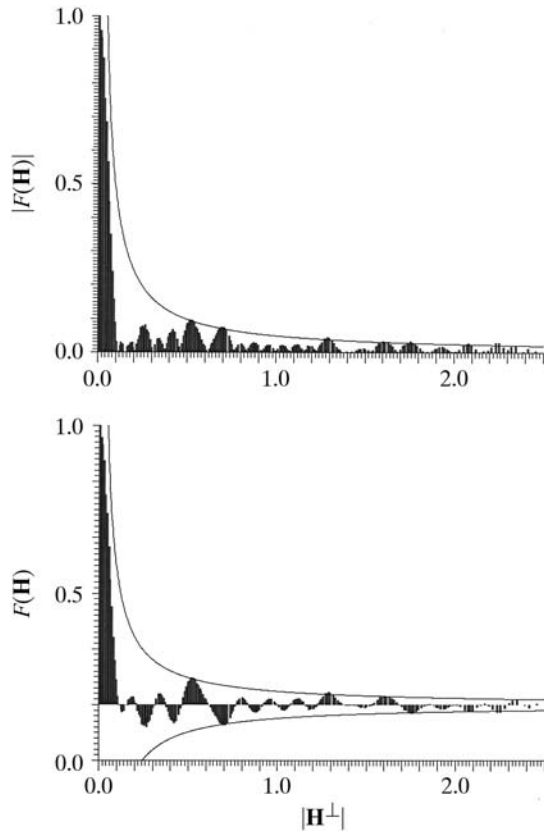


Fig. 4.6.3.9. The structure factors  $F(\mathbf{H})$  (below) and their magnitudes  $|F(\mathbf{H})|$  (above) of the squared Fibonacci chain decorated with equal point atoms are shown as a function of the perpendicular-space component  $|\mathbf{H}^\perp|$  of the diffraction vector. The short  $a_1$  distance is  $S = 2.5 \text{ \AA}$ , all structure factors within  $0 \leq |\mathbf{H}| \leq 2.5 \text{ \AA}^{-1}$  have been calculated and normalized to  $F(00) = 1$ .

Further scaling relationships in reciprocal space exist: scaling a diffraction vector  $\mathbf{H} = h_1 \mathbf{d}_1^* + h_2 \mathbf{d}_2^* = h_1 a^* \begin{pmatrix} 1 \\ -\tau \end{pmatrix}_V + h_2 a^* \begin{pmatrix} \tau \\ 1 \end{pmatrix}_V$  with the matrix  $S = \begin{pmatrix} 0 & 1 \\ 1 & 1 \end{pmatrix}_D$ ,

$$\begin{pmatrix} 0 & 1 \\ 1 & 1 \end{pmatrix}_D \begin{pmatrix} h_1 \\ h_2 \end{pmatrix}_D = \begin{pmatrix} F_n & F_{n+1} \\ F_{n+1} & F_{n+2} \end{pmatrix}_D \begin{pmatrix} h_1 \\ h_2 \end{pmatrix}_D = \begin{pmatrix} F_n h_1 + F_{n+1} h_2 \\ F_{n+1} h_1 + F_{n+2} h_2 \end{pmatrix}_D,$$

increases the magnitudes of structure factors assigned to this particular diffraction vector  $\mathbf{H}$ ,

$$|F(S^n \mathbf{H})| > |F(S^{n-1} \mathbf{H})| > \dots > |F(S \mathbf{H})| > |F(\mathbf{H})|.$$

This is due to the shrinking of the perpendicular-space component of the diffraction vector by powers of  $(-\tau)^{-n}$  while expanding the parallel-space component by  $\tau^n$  according to the eigenvalues  $\tau$  and  $-\tau^{-1}$  of  $S$  acting in the two eigenspaces  $\mathbf{V}^\parallel$  and  $\mathbf{V}^\perp$ :

$$\begin{aligned} \pi^\parallel(S \mathbf{H}) &= (h_2 + \tau(h_1 + h_2))a^* = (\tau h_1 + h_2(\tau + 1))a^* \\ &= \tau(h_1 + \tau h_2)a^*, \end{aligned}$$

$$\begin{aligned} \pi^\perp(S \mathbf{H}) &= (-\tau h_2 + h_1 + h_2)a^* = (h_1 - h_2(\tau - 1))a^* \\ &= -(1/\tau)(-\tau h_1 + h_2)a^*, \end{aligned}$$

$$|F(\tau^n \mathbf{H}^\parallel)| > |F(\tau^{n-1} \mathbf{H}^\parallel)| > \dots > |F(\tau \mathbf{H}^\parallel)| > |F(\mathbf{H}^\parallel)|.$$

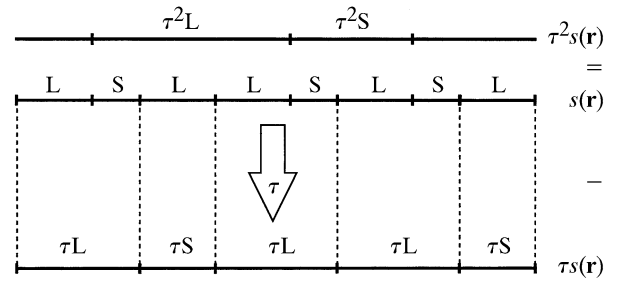


Fig. 4.6.3.10. Part . . . L S L L S L S L . . . of a Fibonacci sequence  $s(\mathbf{r})$  before and after scaling by the factor  $\tau$ . L is mapped onto  $\tau L$ , S onto  $\tau S = L$ . The vertices of the new sequence are a subset of those of the original sequence (the correspondence is indicated by dashed lines). The residual vertices  $\tau^2 s(\mathbf{r})$ , which give when decorating  $\tau s(\mathbf{r})$  the Fibonacci sequence  $s(\mathbf{r})$ , form a Fibonacci sequence scaled by a factor  $\tau^2$ .

Thus, for scaling  $n$  times we obtain

$$\begin{aligned} \pi^\perp(S^n \mathbf{H}) &= (-\tau(F_n h_1 + F_{n+1} h_2) + (F_{n+1} h_1 + F_{n+2} h_2))a^* \\ &= (h_1(-\tau F_n + F_{n+1}) + h_2(-\tau F_{n+1} + F_{n+2}))a^* \end{aligned}$$

with

$$\lim_{n \rightarrow \infty} (-\tau F_n + F_{n+1}) = 0 \text{ and } \lim_{n \rightarrow \infty} (-\tau F_{n+1} + F_{n+2}) = 0,$$

yielding eventually

$$\lim_{n \rightarrow \infty} (\pi^\perp(S^n \mathbf{H})) = 0 \text{ and } \lim_{n \rightarrow \infty} (F(S^n \mathbf{H})) = F(\mathbf{0}).$$

The scaling of the diffraction vectors  $\mathbf{H}$  by  $S^n$  corresponds to a hyperbolic rotation (Janner, 1992) with angle  $n\varphi$ , where  $\sinh \varphi = 1/2$  (Fig. 4.6.3.11):

$$\begin{aligned} \begin{pmatrix} 0 & 1 \\ 1 & 1 \end{pmatrix}^{2n} &= \begin{pmatrix} \cosh 2n\varphi & \sinh 2n\varphi \\ \sinh 2n\varphi & \cosh 2n\varphi \end{pmatrix}, \\ \begin{pmatrix} 0 & 1 \\ 1 & 1 \end{pmatrix}^{2n+1} &= \begin{pmatrix} \sinh[(2n+1)\varphi] & \cosh[(2n+1)\varphi] \\ \cosh[(2n+1)\varphi] & \sinh[(2n+1)\varphi] \end{pmatrix}. \end{aligned}$$

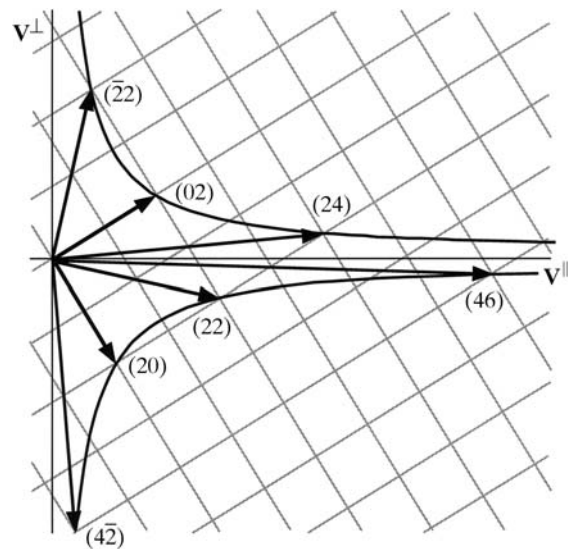


Fig. 4.6.3.11. Scaling operations of the Fibonacci sequence. The scaling operation  $S$  acts six times on the diffraction vector  $\mathbf{H} = (4\bar{2})$  yielding the sequence  $(4\bar{2}) \rightarrow (22) \rightarrow (20) \rightarrow (02) \rightarrow (22) \rightarrow (24) \rightarrow (46)$ .

#### 4.6. RECIPROCAL-SPACE IMAGES OF APERIODIC CRYSTALS

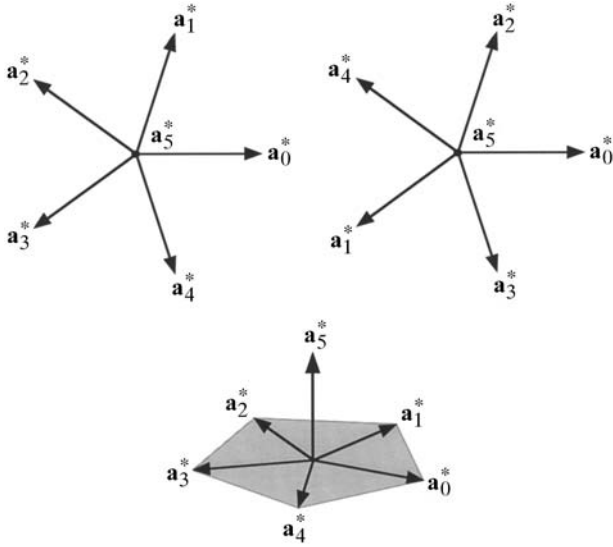


Fig. 4.6.3.12. Reciprocal basis of the decagonal phase in the 5D description projected upon  $\mathbf{V}^{\parallel}$  (above left) and  $\mathbf{V}^{\perp}$  (above right). Below, a perspective physical-space view is shown.

##### 4.6.3.3.2. Decagonal phases

A structure quasiperiodic in two dimensions, periodic in the third dimension and with decagonal diffraction symmetry is called a decagonal phase. Its holohedral Laue symmetry group is  $K = 10/mmm$ . All reciprocal-space vectors  $\mathbf{H} \in M^*$  can be represented on a basis ( $V$  basis)  $\mathbf{a}_i^* = a_i^* (\cos 2\pi i/5, \sin 2\pi i/5, 0)$ ,  $i = 1, \dots, 4$  and  $\mathbf{a}_5^* = a_5^* (0, 0, 1)$  (Fig. 4.6.3.12) as  $\mathbf{H} = \sum_{i=1}^5 h_i \mathbf{a}_i^*$ . The vector components refer to a Cartesian coordinate system in physical (parallel) space. Thus, from the number of independent reciprocal-basis vectors necessary to index the Bragg reflections with integer numbers, the dimension of the embedding space has to be at least five. This can also be shown in a different way (Hermann, 1949).

The set  $M^*$  of all vectors  $\mathbf{H}$  remains invariant under the action of the symmetry operators of the point group  $10/mmm$ . The symmetry-adapted matrix representations for the point-group generators, the tenfold rotation  $\alpha = 10$ , the reflection plane  $\beta = m_2$  (normal of the reflection plane along the vectors  $\mathbf{a}_i^* \mathbf{a}_{i+3}^*$  with  $i = 1, \dots, 4$  modulo 5) and the inversion operation  $\Gamma(\gamma) = \bar{1}$  may be written in the form

$$\Gamma(\alpha) = \begin{pmatrix} 0 & 1 & \bar{1} & 0 & 0 \\ 0 & 1 & 0 & \bar{1} & 0 \\ 0 & 1 & 0 & 0 & 0 \\ \bar{1} & 1 & 0 & 0 & 0 \\ 0 & 0 & 0 & 0 & 1 \end{pmatrix}_D, \quad \Gamma(\beta) = \begin{pmatrix} 0 & 0 & 0 & 1 & 0 \\ 0 & 0 & 1 & 0 & 0 \\ 0 & 1 & 0 & 0 & 0 \\ 1 & 0 & 0 & 0 & 0 \\ 0 & 0 & 0 & 0 & 1 \end{pmatrix}_D$$

$$\Gamma(\gamma) = \begin{pmatrix} \bar{1} & 0 & 0 & 0 & 0 \\ 0 & \bar{1} & 0 & 0 & 0 \\ 0 & 0 & \bar{1} & 0 & 0 \\ 0 & 0 & 0 & \bar{1} & 0 \\ 0 & 0 & 0 & 0 & \bar{1} \end{pmatrix}_D.$$

By block-diagonalization, these reducible symmetry matrices can be decomposed into non-equivalent irreducible representations. These can be assigned to the two orthogonal subspaces forming the 5D embedding space  $\mathbf{V} = \mathbf{V}^{\parallel} \oplus \mathbf{V}^{\perp}$ , the 3D parallel (physical) subspace  $\mathbf{V}^{\parallel}$  and the perpendicular 2D subspace  $\mathbf{V}^{\perp}$ . Thus, using  $W\Gamma W^{-1} = \Gamma_V = \Gamma_V^{\parallel} \oplus \Gamma_V^{\perp}$ , we obtain

$$\Gamma_V(\alpha) = \left( \begin{array}{ccc|cc} \cos(\pi/5) & -\sin(\pi/5) & 0 & 0 & 0 \\ \sin(\pi/5) & \cos(\pi/5) & 0 & 0 & 0 \\ 0 & 0 & 1 & 0 & 0 \\ \hline 0 & 0 & 0 & \cos(3\pi/5) & -\sin(3\pi/5) \\ 0 & 0 & 0 & \sin(3\pi/5) & \cos(3\pi/5) \end{array} \right)_V$$

$$= \left( \begin{array}{c|c} \Gamma^{\parallel}(\alpha) & 0 \\ \hline 0 & \Gamma^{\perp}(\alpha) \end{array} \right)_V,$$

$$\Gamma_V(\beta) = \left( \begin{array}{ccc|cc} 1 & 0 & 0 & 0 & 0 \\ 0 & \bar{1} & 0 & 0 & 0 \\ 0 & 0 & 1 & 0 & 0 \\ \hline 0 & 0 & 0 & \bar{1} & 0 \\ 0 & 0 & 0 & 0 & 1 \end{array} \right)_V, \quad \Gamma_V(\gamma) = \left( \begin{array}{ccc|cc} \bar{1} & 0 & 0 & 0 & 0 \\ 0 & \bar{1} & 0 & 0 & 0 \\ \hline 0 & 0 & \bar{1} & 0 & 0 \\ 0 & 0 & 0 & \bar{1} & 0 \\ 0 & 0 & 0 & 0 & \bar{1} \end{array} \right)_V,$$

where

$$W = \left( \begin{array}{ccccc|c} a_1^* \cos(2\pi/5) & a_2^* \cos(4\pi/5) & a_3^* \cos(6\pi/5) & a_4^* \cos(8\pi/5) & 0 & 0 \\ a_1^* \sin(2\pi/5) & a_2^* \sin(4\pi/5) & a_3^* \sin(6\pi/5) & a_4^* \sin(8\pi/5) & 0 & 0 \\ 0 & 0 & 0 & 0 & 0 & a_5^* \\ \hline a_1^* \cos(6\pi/5) & a_2^* \cos(2\pi/5) & a_3^* \cos(8\pi/5) & a_4^* \cos(4\pi/5) & 0 & 0 \\ a_1^* \sin(6\pi/5) & a_2^* \sin(2\pi/5) & a_3^* \sin(8\pi/5) & a_4^* \sin(4\pi/5) & 0 & 0 \end{array} \right)_V.$$

The column vectors of the matrix  $W$  give the parallel- (above the partition line) and perpendicular-space components (below the partition line) of a reciprocal basis in  $V$  space. Thus,  $W$  can be rewritten using the physical-space reciprocal basis defined above as

$$W = (\mathbf{d}_1^*, \mathbf{d}_2^*, \mathbf{d}_3^*, \mathbf{d}_4^*, \mathbf{d}_5^*),$$

yielding the reciprocal basis  $\mathbf{d}_i^*$ ,  $i = 1, \dots, 5$ , in the 5D embedding space ( $D$  space):

$$\mathbf{d}_i^* = a_i^* \begin{pmatrix} \cos(2\pi i/5) \\ \sin(2\pi i/5) \\ 0 \\ \cos(6\pi i/5) \\ \sin(6\pi i/5) \end{pmatrix}_V, \quad i = 1, \dots, 4 \quad \text{and} \quad \mathbf{d}_5^* = a_5^* \begin{pmatrix} 0 \\ 0 \\ 1 \\ 0 \\ 0 \end{pmatrix}_V.$$

The  $5 \times 5$  symmetry matrices can each be decomposed into a  $3 \times 3$  matrix and a  $2 \times 2$  matrix. The first one,  $\Gamma^{\parallel}$ , acts on the parallel-space component, the second one,  $\Gamma^{\perp}$ , on the perpendicular-space component. In the case of  $\Gamma(\alpha)$ , the coupling factor between a rotation in parallel and perpendicular space is 3. Thus, a  $\pi/5$  rotation in physical space is related to a  $3\pi/5$  rotation in perpendicular space (Fig. 4.6.3.12).

With the condition  $\mathbf{d}_i^* \cdot \mathbf{d}_j^* = \delta_{ij}$ , a basis in direct 5D space is obtained:

$$\mathbf{d}_i = \frac{2}{5a_i^*} \begin{pmatrix} \cos(2\pi i/5) - 1 \\ \sin(2\pi i/5) \\ 0 \\ \cos(6\pi i/5) - 1 \\ \sin(6\pi i/5) \end{pmatrix}, \quad i = 1, \dots, 4, \quad \text{and} \quad \mathbf{d}_5 = \frac{1}{a_5^*} \begin{pmatrix} 0 \\ 0 \\ 1 \\ 0 \\ 0 \end{pmatrix}.$$

The metric tensors  $G, G^*$  are of the type

$$\begin{pmatrix} A & C & C & C & 0 \\ C & A & C & C & 0 \\ C & C & A & C & 0 \\ C & C & C & A & 0 \\ 0 & 0 & 0 & 0 & B \end{pmatrix}$$

with  $A = 2a_1^{*2}, B = a_5^{*2}, C = -(1/2)a_1^{*2}$  for the reciprocal space and  $A = 4/5a_1^{*2}, B = 1/a_5^{*2}, C = 2/5a_1^{*2}$  for the direct space. Thus, for the lattice parameters in reciprocal space we obtain

#### 4. DIFFUSE SCATTERING AND RELATED TOPICS

$d_i^* = a_i^*(2)^{1/2}$ ,  $i = 1, \dots, 4$ ;  $d_5^* = a_5^*$ ;  $\alpha_{ij}^* = 104.5^\circ$ ,  $i, j = 1, \dots, 4$ ;  $\alpha_{i5}^* = 90^\circ$ ,  $i = 1, \dots, 4$ , and for those in direct space  $d_i = 2/[a_i^*(5)^{1/2}]$ ,  $i = 1, \dots, 4$ ;  $d_5 = 1/a_5^*$ ;  $\alpha_{ij} = 60^\circ$ ,  $i, j = 1, \dots, 4$ ;  $\alpha_{i5} = 90^\circ$ ,  $i = 1, \dots, 4$ . The volume of the 5D unit cell can be calculated from the metric tensor  $G$ :

$$V = [\det(G)]^{1/2} = \frac{4}{5(5)^{1/2}(a_1^*)^4 a_5^*} = \frac{(5)^{1/2}}{4} (d_1)^4 d_5.$$

Since decagonal phases are only quasiperiodic in two dimensions, it is sufficient to demonstrate their characteristics on a 2D example, the canonical *Penrose tiling* (Penrose, 1974). It can be constructed from two unit tiles: a skinny (acute angle  $\alpha_s = \pi/5$ ) and a fat (acute angle  $\alpha_f = 2\pi/5$ ) rhomb with equal edge lengths  $a_r$  and areas  $A_s = a_r^2 \sin(\pi/5)$ ,  $A_f = a_r^2 \sin(2\pi/5)$  (Fig. 4.6.3.13). The areas and frequencies of these two unit tiles in the Penrose tiling are both in a ratio 1 to  $\tau$ . By replacing each skinny and fat rhomb according to the inflation rule, a  $\tau$ -inflated tiling is obtained. Inflation (deflation) means that the number of tiles is inflated (deflated), their edge lengths are decreased (increased) by a factor  $\tau$ . By infinite repetition of this inflation operation, an infinite Penrose

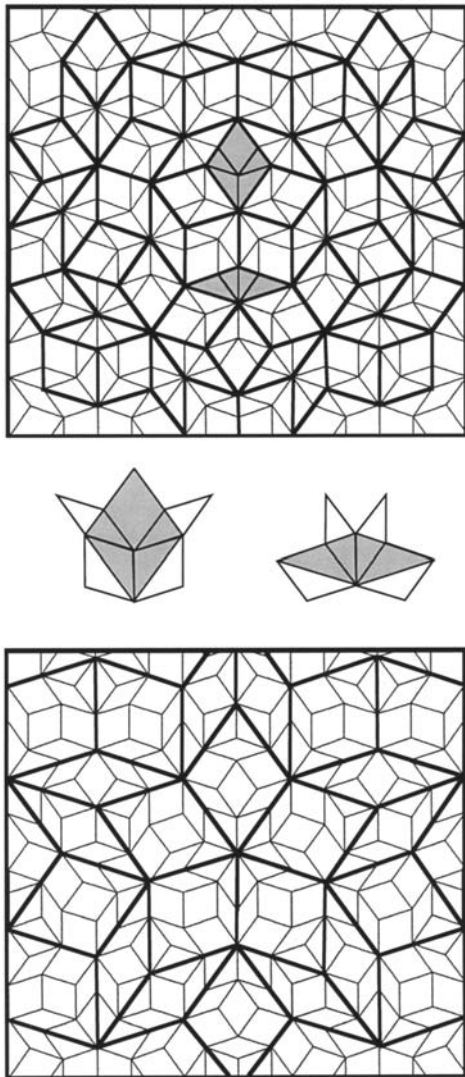


Fig. 4.6.3.13. A section of a Penrose tiling (thin lines) superposed by its  $\tau$ -deflated tiling (above, thick lines) and by its  $\tau^2$ -deflated tiling (below, thick lines). In the middle, the inflation rule of the Penrose tiling is illustrated.

tiling is generated. Consequently, this substitution operation leaves the tiling invariant.

From Fig. 4.6.3.13 it can be seen that the sets of vertices of the deflated tilings are subsets of the set of vertices of the original tiling. The  $\tau$ -deflated tiling is dual to the original tiling; a further deflation by a factor  $\tau$  gives the original tiling again. However, the edge lengths of the tiles are increased by a factor  $\tau^2$ , and the tiling is rotated around  $36^\circ$ . Only the fourth deflation of the original tiling yields the original tiling in its original orientation but with all lengths multiplied by a factor  $\tau^4$ .

Contrary to the reciprocal-space scaling behaviour of  $M^* = \{\mathbf{H}^{\parallel} = \sum_{i=1}^4 h_i \mathbf{a}_i^* | h_i \in \mathbb{Z}\}$ , the set of vertices  $M = \{\mathbf{r} = \sum_{i=1}^4 n_i \mathbf{a}_i | n_i \in \mathbb{Z}\}$  of the Penrose tiling is not invariant by scaling the length scale simply by a factor  $\tau$  using the scaling matrix  $S$ :

$$S = \begin{pmatrix} 0 & 1 & 0 & \bar{1} \\ 0 & 1 & 1 & \bar{1} \\ \bar{1} & 1 & 1 & 0 \\ \bar{1} & 0 & 1 & 0 \end{pmatrix}_D \quad \text{acting on vectors } \mathbf{r} = \begin{pmatrix} n_1 \\ n_2 \\ n_3 \\ n_4 \end{pmatrix}_D.$$

The square of  $S$ , however, maps all vertices of the Penrose tiling upon other ones:

$$S^2 = \begin{pmatrix} 1 & 1 & 0 & \bar{1} \\ 0 & 2 & 1 & \bar{1} \\ \bar{1} & 1 & 2 & 0 \\ \bar{1} & 0 & 1 & 1 \end{pmatrix}_D, \quad \Gamma(\alpha)S^2 = \begin{pmatrix} 1 & 1 & \bar{1} & \bar{1} \\ 1 & 2 & 0 & \bar{2} \\ 0 & 2 & 1 & \bar{1} \\ \bar{1} & 1 & 1 & 0 \end{pmatrix}_D.$$

$S^2$  corresponds to a hyperbolic rotation with  $\chi = \cosh^{-1}(3/2)$  in superspace (Janner, 1992). However, only operations of the type  $S^{4n}$ ,  $n = 0, 1, 2, \dots$ , scale the Penrose tiling in a way which is equivalent to the ( $4n$ th) substitutional operations discussed above. The rotoscaling operation  $\Gamma(\alpha)S^2$ , also a symmetry operation of the Penrose tiling, leaves a pentagram invariant as demonstrated in Fig. 4.6.3.14 (Janner, 1992). Block-diagonalization of the scaling matrix  $S$  decomposes it into two non-equivalent irreducible representations which give the scaling properties in the two orthogonal subspaces of the 4D embedding space,  $\mathbf{V} = \mathbf{V}^{\parallel} \oplus \mathbf{V}^{\perp}$ , the 2D parallel (physical) subspace  $\mathbf{V}^{\parallel}$  and the perpendicular 2D subspace  $\mathbf{V}^{\perp}$ . Thus, using  $WSW^{-1} = S_V \oplus S_V^{\perp}$ , we obtain

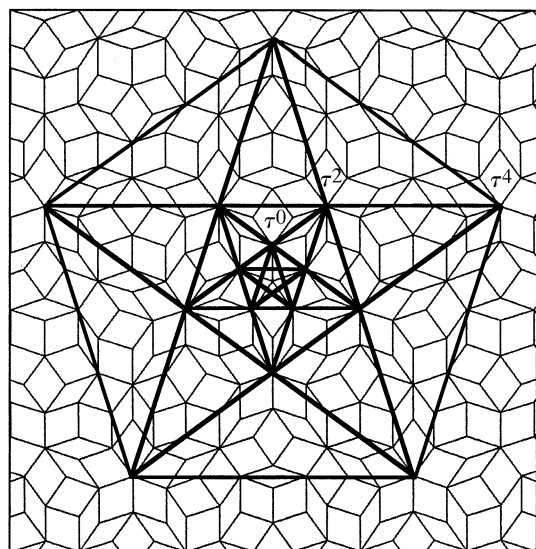


Fig. 4.6.3.14. Scaling symmetry of a pentagram superposed on the Penrose tiling. A vector pointing to a corner of a pentagon (star) is mapped by the rotoscaling operation (rotation around  $\pi/5$  and dilatation by a factor  $\tau^2$ ) onto the next largest pentagon (star).

#### 4.6. RECIPROCAL-SPACE IMAGES OF APERIODIC CRYSTALS

$$S_V = \left( \begin{array}{cc|cc} \tau & 0 & 0 & 0 \\ 0 & \tau & 0 & 0 \\ \hline 0 & 0 & -1/\tau & 0 \\ 0 & 0 & 0 & -1/\tau \end{array} \right)_V = \left( \begin{array}{c|c} S_V^{\parallel} & 0 \\ \hline 0 & S_V^{\perp} \end{array} \right)_V,$$

where

$$W = \begin{pmatrix} a_1^* \cos(2\pi/5) & a_2^* \cos(4\pi/5) & a_3^* \cos(6\pi/5) & a_4^* \cos(8\pi/5) \\ a_1^* \sin(2\pi/5) & a_2^* \sin(4\pi/5) & a_3^* \sin(6\pi/5) & a_4^* \sin(8\pi/5) \\ \hline a_1^* \cos(4\pi/5) & a_2^* \cos(8\pi/5) & a_3^* \cos(2\pi/5) & a_4^* \cos(6\pi/5) \\ a_1^* \sin(4\pi/5) & a_2^* \sin(8\pi/5) & a_3^* \sin(2\pi/5) & a_4^* \sin(6\pi/5) \end{pmatrix}.$$

The 2D Penrose tiling can also be embedded canonically in the 5D space. Canonically means that the 5D lattice is hypercubic and that the projection of one unit cell upon the 3D perpendicular space  $V^{\perp}$ , giving a rhomb-icosahedron, defines the atomic surface. However, the parallel-space image  $\mathbf{a}_i^*$ ,  $i = 1, \dots, 4$ , with  $\mathbf{a}_0^* = -(\mathbf{a}_1^* + \mathbf{a}_2^* + \mathbf{a}_3^* + \mathbf{a}_4^*)$ , of the 5D basis  $\mathbf{d}_i^*$ ,  $i = 1, \dots, 4$  is not linearly independent. Consequently, the atomic surface consists of only a subset of the points contained in the rhomb-icosahedron: five equidistant pentagons (one with diameter zero) resulting as sections of the rhomb-icosahedron with five equidistant parallel planes (Fig. 4.6.3.15). The linear dependence of the 5D basis allows the embedding in the 4D space. The resulting hyper-rhombohedral hyperlattice is spanned by the basis  $\mathbf{d}_i$ ,  $i = 1, \dots, 4$ , discussed above. The atomic surfaces occupy the positions  $p/5(1111)$ ,  $p = 1, \dots, 4$ , on the body diagonal of the 4D unit cell. Neighbouring pentagons are in an *anti* position to each other (Fig. 4.6.3.16). Thus the 4D unit cell is decorated centrosymmetrically. The edge length  $a_r$  of a Penrose rhomb is related to the length of physical-space basis vectors  $a_i^*$  by  $a_r = \tau S$ , with the smallest distance  $S = (2\tau/5a_i^*)$ ,  $i = 1, \dots, 4$ . The *point density* (number of vertices per unit area) of a Penrose tiling with Penrose rhombs of edge length  $a_r$  can be calculated from the ratio of the relative number of unit tiles in the tiling to their area:

$$\rho = \frac{1 + \tau}{a_r^2 [\sin(\pi/5) + \tau \sin(2\pi/5)]} = (5/2)a_i^{*2} (2 - \tau)^2 \tan(2\pi/5).$$

This is equivalent to the calculation from the 4D description,

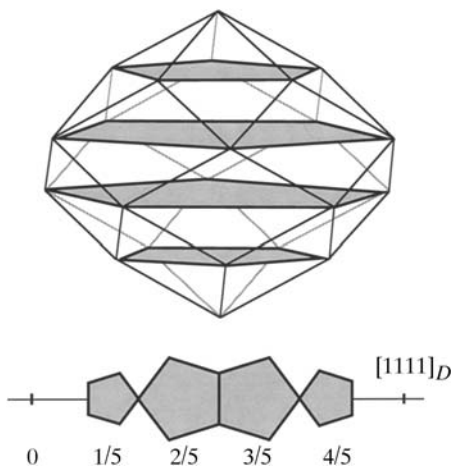


Fig. 4.6.3.15. Atomic surface of the Penrose tiling in the 5D hypercubic description. The projection of the 5D hypercubic unit cell upon  $V^{\perp}$  gives a rhomb-icosahedron (above). The Penrose tiling is generated by four equidistant pentagons (shaded) inscribed in the rhomb-icosahedron. Below is a perpendicular-space projection of the same pentagons, which are located on the  $[1111]_D$  diagonal of the 4D hyper-rhombohedral unit cell in the 4D description.

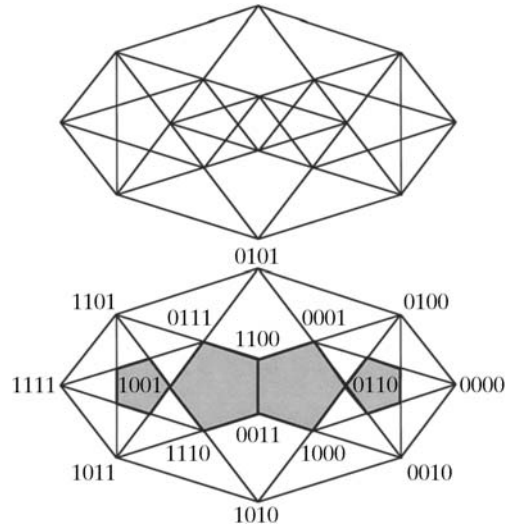


Fig. 4.6.3.16. Projection of the 4D hyper-rhombohedral unit cell of the Penrose tiling in the 4D description upon the perpendicular space. In the upper drawing all edges between the 16 corners are shown. In the lower drawing the corners are indexed and the four pentagonal atomic surfaces of the Penrose tiling are shaded.

$$\rho = \frac{\sum_{i=1}^4 \Omega_{AS}^i}{\Omega_{UC}} = \frac{\sum_{i=1}^4 (5/2)\lambda^2 \sin(2\pi/5)}{4/[5(5)^{1/2}|a_i^*|^4]} = (5/2)a_i^{*2} (2 - \tau)^2 \tan(2\pi/5),$$

where  $\Omega_{AS}$  and  $\Omega_{UC}$  are the area of the atomic surface and the volume of the 4D unit cell, respectively. The pentagon radii are  $\lambda_{1,4} = 2(2 - \tau)/5a^*$  and  $\lambda_{2,3} = 2(\tau - 1)/5a^*$  for the atomic surfaces in  $(p/5)(1111)$  with  $p = 1, 4$  and  $p = 2, 3$ . A detailed discussion of the properties of Penrose tiling is given in the papers of Penrose (1974, 1979), Jaric (1986) and Pavlovitch & Kleman (1987).

##### 4.6.3.3.2.1. Indexing

The indexing of the submodule  $M_1^*$  of the diffraction pattern of a decagonal phase is not unique. Since  $M_1^*$  corresponds to a  $\mathbb{Z}$  module of rank 4 with decagonal point symmetry, it is invariant under scaling by  $\tau^n$ ,  $n \in \mathbb{Z}$ :  $S^n M^* = \tau^n M^*$ . Nevertheless, an optimum basis (low indices are assigned to strong reflections) can be derived: not the metrics, as for regular periodic crystals, but the intensity distribution characterizes the best choice of indexing.

A correct set of reciprocal-basis vectors can be identified experimentally in the following way:

(1) Find directions of systematic absences or pseudo-absences determining the possible orientations of the reciprocal-basis vectors (see Rabson *et al.*, 1991).

(2) Find pairs of strong reflections whose physical-space diffraction vectors are related to each other by the factor  $\tau$ .

(3) Index these reflections by assigning an appropriate value to  $a^*$ . This value should be derived from the shortest interatomic distance  $S$  and the edge length of the unit tiles expected in the structure.

(4) The reciprocal basis is correct if all observable Bragg reflections can be indexed with integer numbers.

##### 4.6.3.3.2.2. Diffraction symmetry

The diffraction symmetry of decagonal phases can be described by the Laue groups  $10/mmm$  or  $10/m$ . The set of all vectors  $\mathbf{H}$  forms a Fourier module  $M^* = \{\mathbf{H}^{\parallel} = \sum_{i=1}^5 h_i \mathbf{a}_i^* | h_i \in \mathbb{Z}\}$  of rank 5 in physical space which can be decomposed into two submodules



## 4.6. RECIPROCAL-SPACE IMAGES OF APERIODIC CRYSTALS

Table 4.6.3.1. 3D point groups of order  $k$  describing the diffraction symmetry and corresponding 5D decagonal space groups with reflection conditions (see Rabson et al., 1991)

| 3D point group                         | $k$ | 5D space group                           | Reflection condition   |
|--|-----|--|--|
| $\frac{10}{m} \frac{2}{m} \frac{2}{m}$ | 40  | $P \frac{10}{m} \frac{2}{m} \frac{2}{m}$ | No condition   |
|  |     | $P \frac{10}{m} \frac{2}{c} \frac{2}{c}$ | $h_1 h_2 h_2 h_1 h_5 : h_5 = 2n$<br>$h_1 h_2 h_2 h_1 h_5 : h_5 = 2n$ |
|  |     | $P \frac{10}{m} \frac{2}{m} \frac{2}{c}$ | $h_1 h_2 h_2 h_1 h_5 : h_5 = 2n$                                     |
|  |     | $P \frac{10}{m} \frac{2}{c} \frac{2}{m}$ | $h_1 h_2 h_2 h_1 h_5 : h_5 = 2n$                                     |
| $\frac{10}{m}$                         | 20  | $P \frac{10}{m}$                         | No condition   |
|  |     | $P \frac{10}{m}$                         | $0000h_5 : h_5 = 2n$   |
| 1022                                   | 20  | $P1022$                                  | No condition   |
|  |     | $P10_22$                                 | $0000h_5 : jh_5 = 10n$   |
| 10 $mm$                                | 20  | $P10mm$                                  | No condition   |
|  |     | $P10cc$                                  | $h_1 h_2 h_2 h_1 h_5 : h_5 = 2n$<br>$h_1 h_2 h_2 h_1 h_5 : h_5 = 2n$ |
|  |     | $P10_5mc$                                | $h_1 h_2 h_2 h_1 h_5 : h_5 = 2n$                                     |
|  |     | $P10_5cm$                                | $h_1 h_2 h_2 h_1 h_5 : h_5 = 2n$                                     |
| $\overline{10}m2$                      | 20  | $P\overline{10}m2$                       | No condition   |
|  |     | $P\overline{10}c2$                       | $h_1 h_2 h_2 h_1 h_5 : h_5 = 2n$                                     |
|  |     | $P\overline{10}2m$                       | No condition   |
|  |     | $P\overline{10}2c$                       | $h_1 h_2 h_2 h_1 h_5 : h_5 = 2n$                                     |
| 10                                     | 10  | $P10$                                    | No condition   |
|  |     | $P10_j$                                  | $0000h_5 : jh_5 = 10n$   |

$$F(\mathbf{H}) = \sum_{k=1}^N f_k(\mathbf{H}^{\parallel}) T_k(\mathbf{H}^{\parallel}, \mathbf{H}^{\perp}) g_k(\mathbf{H}^{\perp}) \exp(2\pi i \mathbf{H} \cdot \mathbf{r}_k),$$

with 5D diffraction vectors  $\mathbf{H} = \sum_{i=1}^5 h_i \mathbf{d}_i^*$ ,  $N$  hyperatoms, parallel-space atomic scattering factor  $f_k(\mathbf{H}^{\parallel})$ , temperature factor  $T_k(\mathbf{H}^{\parallel}, \mathbf{H}^{\perp})$  and perpendicular-space geometric form factor  $g_k(\mathbf{H}^{\perp})$ .  $T_k(\mathbf{H}^{\parallel}, \mathbf{0})$  is equivalent to the conventional Debye–Waller factor and  $T_k(\mathbf{0}, \mathbf{H}^{\perp})$  describes random fluctuations along the perpendicular-space coordinate. These fluctuations cause characteristic jumps of vertices in physical space (*phason flips*). Even random phason flips map the vertices onto positions which can still be described by physical-space vectors of the type  $\mathbf{r} = \sum_{i=1}^5 n_i \mathbf{a}_i$ . Consequently, the set  $M = \{\mathbf{r} = \sum_{i=1}^5 n_i \mathbf{a}_i | n_i \in \mathbb{Z}\}$  of all possible vectors forms a  $\mathbb{Z}$  module. The shape of the atomic surfaces corresponds to a selection rule for the positions actually occupied. The geometric form factor  $g_k(\mathbf{H}^{\perp})$  is equivalent to the Fourier transform of the *atomic surface*, i.e. the 2D perpendicular-space component of the 5D *hyperatoms*.

For example, the canonical Penrose tiling  $g_k(\mathbf{H}^{\perp})$  corresponds to the Fourier transform of pentagonal atomic surfaces:

$$g_k(\mathbf{H}^{\perp}) = (1/A_{\text{UC}}^{\perp}) \int_{A_k} \exp(2\pi i \mathbf{H}^{\perp} \cdot \mathbf{r}) \, d\mathbf{r},$$

where  $A_{\text{UC}}^{\perp}$  is the area of the 5D unit cell projected upon  $\mathbf{V}^{\perp}$  and  $A_k$  is the area of the  $k$ th atomic surface. The area  $A_{\text{UC}}^{\perp}$  can be calculated using the formula

$$A_{\text{UC}}^{\perp} = (4/25a_i^{*2})[(7 + \tau) \sin(2\pi/5) + (2 + \tau) \sin(4\pi/5)].$$

Evaluating the integral by decomposing the pentagons into triangles, one obtains

$$g_k(\mathbf{H}^{\perp}) = \frac{1}{A_{\text{UC}}^{\perp}} \sin\left(\frac{2\pi}{5}\right) \times \sum_{j=0}^4 \frac{A_j [\exp(iA_{j+1}\lambda_k) - 1] - A_{j+1} [\exp(iA_j\lambda_k) - 1]}{A_j A_{j+1} (A_j - A_{j+1})}$$

with  $j = 0, \dots, 4$  running over the five triangles, where the radii of the pentagons are  $\lambda_j$ ,  $A_j = 2\pi \mathbf{H}^{\perp} \cdot \mathbf{e}_j$ ,

$$\mathbf{H}^{\perp} = \pi^{\perp}(\mathbf{H}) = \sum_{j=0}^4 h_j a_j^* \begin{pmatrix} 0 \\ 0 \\ 0 \\ \cos(6\pi j/5) \\ \sin(6\pi j/5) \end{pmatrix}$$

and the vectors

$$\mathbf{e}_j = \frac{1}{a_j^*} \begin{pmatrix} 0 \\ 0 \\ 0 \\ \cos(2\pi j/5) \\ \sin(2\pi j/5) \end{pmatrix} \text{ with } j = 0, \dots, 4.$$

As shown by Ishihara & Yamamoto (1988), the Penrose tiling can be considered to be a superstructure of a pentagonal tiling with only one type of pentagonal atomic surface in the  $n$ D unit cell. Thus, for the Penrose tiling, three special reflection classes can be distinguished: for  $|\sum_{i=1}^4 h_i| = m \pmod{5}$  and  $m = 0$  the class of strong main reflections is obtained, and for  $m = \pm 1, \pm 2$  the classes of weaker first- and second-order satellite reflections are obtained (see Fig. 4.6.3.18).

### 4.6.3.3.2.4. Intensity statistics

This section deals with the reciprocal-space characteristics of the 2D quasiperiodic component of the 3D structure, namely the Fourier module  $M_1^*$ . The radial structure-factor distributions of the Penrose tiling decorated with point scatterers are plotted in Figs. 4.6.3.21 and 4.6.3.22 as a function of parallel and perpendicular space. The distribution of  $|F(\mathbf{H})|$  as a function of their frequencies clearly resembles a centric distribution, as can be expected from the centrosymmetric 4D subunit cell. The shape of the distribution function depends on the radius of the limiting sphere in reciprocal space. The number of weak reflections increases to the power of four, that of strong reflections only quadratically (strong reflections always have small  $\mathbf{H}^{\perp}$  components). The radial distribution of the structure-factor amplitudes as a function of perpendicular space clearly shows three branches, corresponding to the reflection classes  $\sum_{i=1}^4 h_i = m \pmod{5}$  with  $|m| = 0$ ,  $|m| = 1$  and  $|m| = 2$  (Fig. 4.6.3.23).

The weighted reciprocal space of the Penrose tiling contains an infinite number of Bragg reflections within a limited region of the physical space. Contrary to the diffraction pattern of a periodic structure consisting of point atoms on the lattice nodes, the Bragg reflections show intensities depending on the perpendicular-space components of their diffraction vectors (Figs. 4.6.3.19, 4.6.3.20 and 4.6.3.22).

## 4. DIFFUSE SCATTERING AND RELATED TOPICS

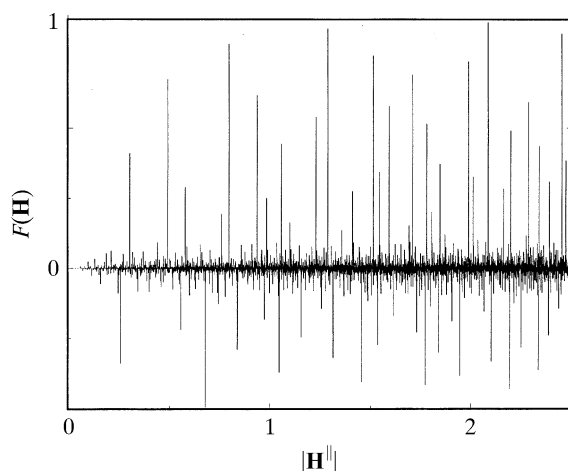


Fig. 4.6.3.21. Radial distribution function of the structure factors  $F(\mathbf{H})$  of the Penrose tiling (edge length of the Penrose unit rhombs  $a_r = 4.04 \text{ \AA}$ ) decorated with point atoms as a function of  $\mathbf{H}^{\parallel}$ . All structure factors within  $10^{-4}|F(\mathbf{0})|^2 < |F(\mathbf{H})|^2 < |F(\mathbf{0})|^2$  and  $0 \leq |\mathbf{H}^{\parallel}| \leq 2.5 \text{ \AA}^{-1}$  have been used and normalized to  $F(0000) = 1$ .

4.6.3.3.2.5. Relationships between structure factors at symmetry-related points of the Fourier image

Scaling the Penrose tiling by a factor  $\tau^{-n}$  by employing the matrix  $S^{-n}$  scales at the same time its reciprocal space by a factor  $\tau^n$ :

$$S\mathbf{H} = \begin{pmatrix} 0 & 1 & 0 & \bar{1} & 0 \\ 0 & 1 & 1 & \bar{1} & 0 \\ \bar{1} & 1 & 1 & 0 & 0 \\ \bar{1} & 0 & 1 & 0 & 0 \\ 0 & 0 & 0 & 0 & 1 \end{pmatrix}_D \begin{pmatrix} h_1 \\ h_2 \\ h_3 \\ h_4 \\ h_5 \end{pmatrix} = \begin{pmatrix} h_2 - h_4 \\ h_2 + h_3 - h_4 \\ -h_1 + h_2 + h_3 \\ -h_1 + h_3 \\ h_5 \end{pmatrix}.$$

Since this operation increases the lengths of the diffraction vectors by the factor  $\tau$  in parallel space and decreases them by the factor  $1/\tau$  in perpendicular space, the following distribution of structure-

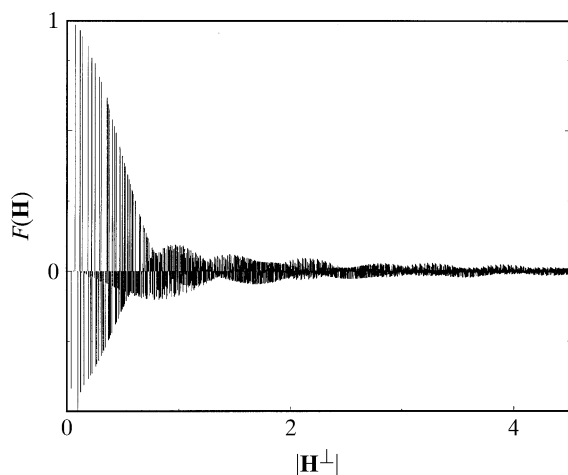
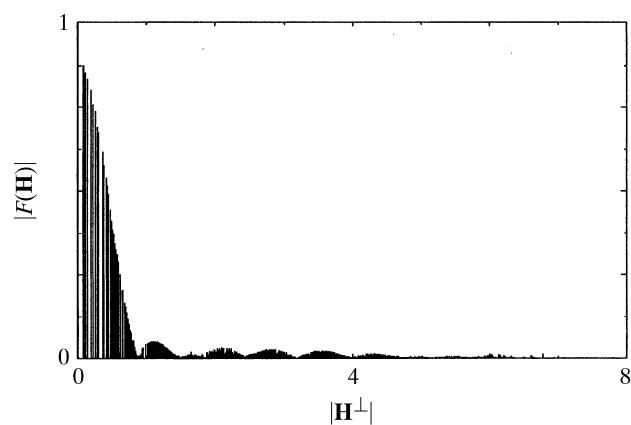
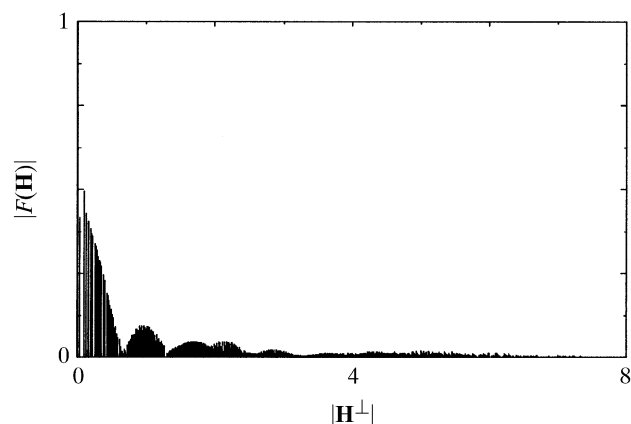


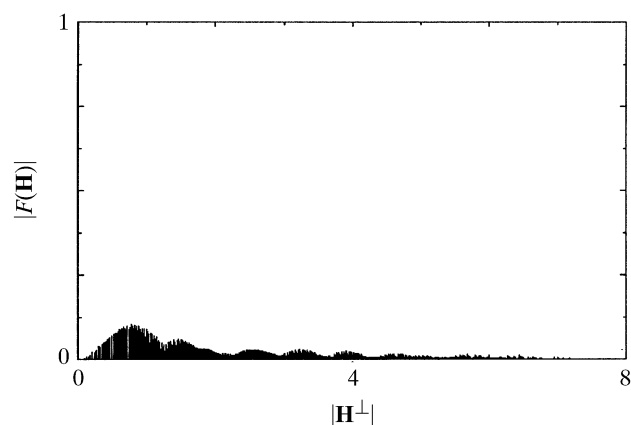
Fig. 4.6.3.22. Radial distribution function of the structure factors  $F(\mathbf{H})$  of the Penrose tiling (edge length of the Penrose unit rhombs  $a_r = 4.04 \text{ \AA}$ ) decorated with point atoms as a function of  $\mathbf{H}^{\perp}$ . All structure factors within  $10^{-4}|F(\mathbf{0})|^2 < |F(\mathbf{H})|^2 < |F(\mathbf{0})|^2$  and  $0 \leq |\mathbf{H}^{\parallel}| \leq 2.5 \text{ \AA}^{-1}$  have been used and normalized to  $F(0000) = 1$ .



(a)



(b)



(c)

Fig. 4.6.3.23. Radial distribution function of the structure-factor magnitudes  $|F(\mathbf{H})|$  of the Penrose tiling (edge length of the Penrose unit rhombs  $a_r = 4.04 \text{ \AA}$ ) decorated with point atoms as a function of  $\mathbf{H}^{\perp}$ . All structure factors within  $10^{-4}|F(\mathbf{0})|^2 < |F(\mathbf{H})|^2 < |F(\mathbf{0})|^2$  and  $0 \leq |\mathbf{H}^{\parallel}| \leq 2.5 \text{ \AA}^{-1}$  have been used and normalized to  $F(0000) = 1$ . The branches with (a)  $|\sum_{i=1}^4 h_i| = 0 \pmod{5}$ , (b)  $|\sum_{i=1}^4 h_i| = 1 \pmod{5}$  and (c)  $|\sum_{i=1}^4 h_i| = 2 \pmod{5}$  are shown.

factor magnitudes (for point atoms at rest) is obtained:

$$|F(S^n \mathbf{H})| > |F(S^{n-1} \mathbf{H})| > \dots > |F(S^1 \mathbf{H})| > |F(\mathbf{H})|,$$

$$|F(\tau^n \mathbf{H}^{\parallel})| > |F(\tau^{n-1} \mathbf{H}^{\parallel})| > \dots > |F(\tau \mathbf{H}^{\parallel})| > |F(\mathbf{H})|.$$

The scaling operations  $S^n$ ,  $n \in \mathbb{Z}$ , the roto-scaling operations  $(\Gamma(\alpha)S^2)^n$  (Fig. 4.6.3.14) and the tenfold rotation  $(\Gamma(\alpha))^n$ , where

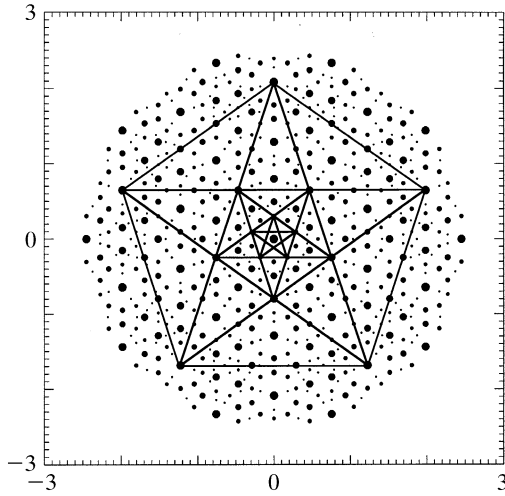


Fig. 4.6.3.24. Pentagrammatic relationships between scaling symmetry-related positive structure factors  $F(\mathbf{H})$  of the Penrose tiling (edge length  $a_r = 4.04 \text{ \AA}$ ) in parallel space. The magnitudes of the structure factors are indicated by the diameters of the filled circles.

$$(\Gamma(\alpha)S^2)^n = \begin{pmatrix} 1 & 1 & \bar{1} & \bar{1} & 0 \\ 1 & 2 & 0 & \bar{2} & 0 \\ 0 & 2 & 1 & \bar{1} & 0 \\ \bar{1} & 1 & 1 & 0 & 0 \\ 0 & 0 & 0 & 0 & 1 \end{pmatrix}_D^n,$$

connect all structure factors with diffraction vectors pointing to the nodes of an infinite series of pentagrams. The structure factors with positive signs are predominantly on the vertices of the pentagram while the ones with negative signs are arranged on circles around the vertices (Figs. 4.6.3.24 to 4.6.3.27).

#### 4.6.3.3.3. Icosahedral phases

A structure that is quasiperiodic in three dimensions and exhibits icosahedral diffraction symmetry is called an icosahedral phase. Its holohedral Laue symmetry group is  $K = m\bar{3}5$ . All reciprocal-space vectors  $\mathbf{H} = \sum_{i=1}^6 h_i \mathbf{a}_i^* \in M^*$  can be represented on a basis

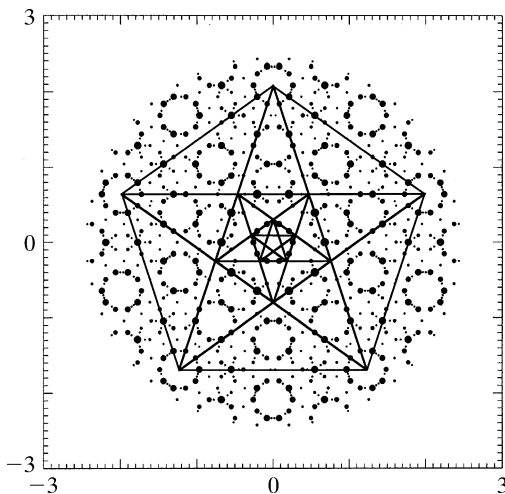


Fig. 4.6.3.25. Pentagrammatic relationships between scaling symmetry-related negative structure factors  $F(\mathbf{H})$  of the Penrose tiling (edge length  $a_r = 4.04 \text{ \AA}$ ) in parallel space. The magnitudes of the structure factors are indicated by the diameters of the filled circles.

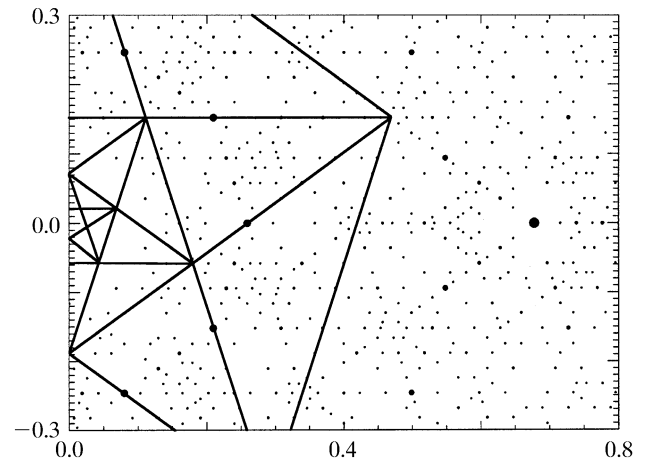
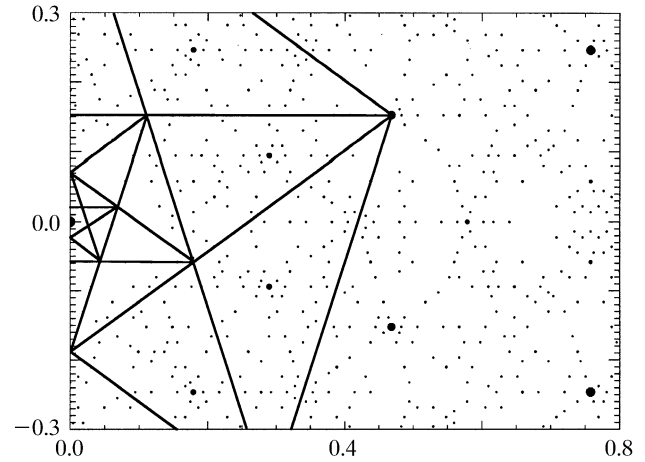


Fig. 4.6.3.26. Pentagrammatic relationships between scaling symmetry-related structure factors  $F(\mathbf{H})$  of the Penrose tiling (edge length  $a_r = 4.04 \text{ \AA}$ ) in parallel space. Enlarged sections of Figs. 4.6.3.24 (above) and 4.6.3.25 (below) are shown.

$\mathbf{a}_1^* = a^*(0, 0, 1)$ ,  $\mathbf{a}_i^* = a^*[\sin \theta \cos(2\pi i/5), \sin \theta \sin(2\pi i/5), \cos \theta]$ ,  $i = 2, \dots, 6$  where  $\sin \theta = 2/(5)^{1/2}$ ,  $\cos \theta = 1/(5)^{1/2}$  and  $\theta \simeq 63.44^\circ$ , the angle between two neighbouring fivefold axes (Fig. 4.6.3.28). This can be rewritten as

$$\begin{pmatrix} \mathbf{a}_1^* \\ \mathbf{a}_2^* \\ \mathbf{a}_3^* \\ \mathbf{a}_4^* \\ \mathbf{a}_5^* \\ \mathbf{a}_6^* \end{pmatrix} = a^* \begin{pmatrix} 0 & 0 & 1 \\ \sin \theta \cos(4\pi/5) & \sin \theta \sin(4\pi/5) & \cos \theta \\ \sin \theta \cos(6\pi/5) & \sin \theta \sin(6\pi/5) & \cos \theta \\ \sin \theta \cos(8\pi/5) & \sin \theta \sin(8\pi/5) & \cos \theta \\ \sin \theta & 0 & \cos \theta \\ \sin \theta \cos(2\pi/5) & \sin \theta \sin(2\pi/5) & \cos \theta \end{pmatrix} \begin{pmatrix} \mathbf{e}_1^V \\ \mathbf{e}_2^V \\ \mathbf{e}_3^V \end{pmatrix},$$

where  $\mathbf{e}_i^V$  are Cartesian basis vectors. Thus, from the number of independent reciprocal-basis vectors needed to index the Bragg reflections with integer numbers, the dimension of the embedding space has to be six. The vector components refer to a Cartesian coordinate system ( $V$  basis) in the physical (parallel) space.

The set  $M^* = \{\mathbf{H}^{\parallel} = \sum_{i=1}^6 h_i \mathbf{a}_i^* | h_i \in \mathbb{Z}\}$  of all diffraction vectors remains invariant under the action of the symmetry operators of the icosahedral point group  $K = m\bar{3}5$ . The symmetry-adapted matrix representations for the point-group generators, one fivefold rotation  $\alpha$ , a threefold rotation  $\beta$  and the inversion operation  $\gamma$ , can be written in the form

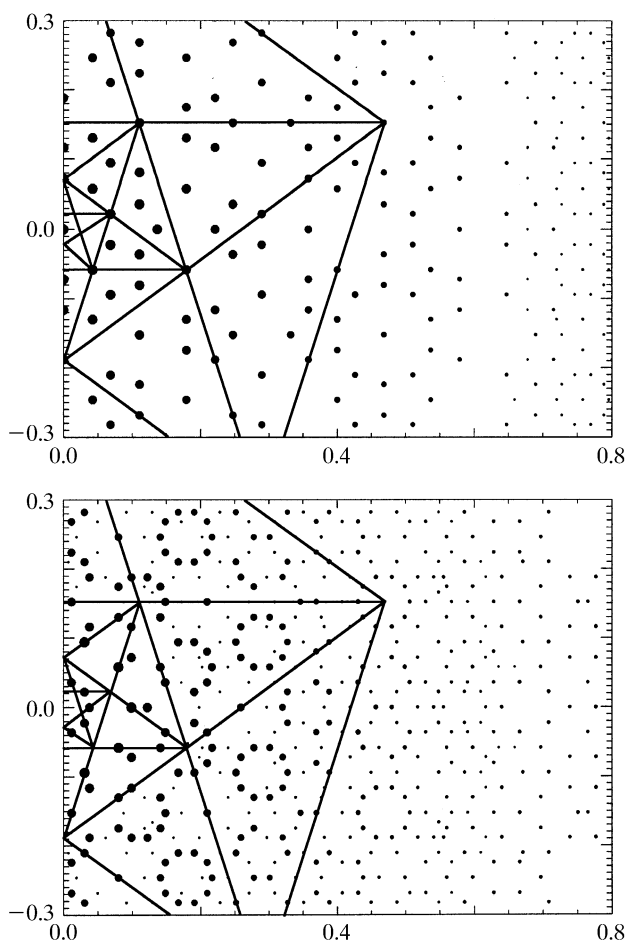


Fig. 4.6.3.27. Pentagrammatic relationships between scaling symmetry-related structure factors  $F(\mathbf{H})$  of the Penrose tiling (edge length  $a_r = 4.04 \text{ \AA}$ ) in perpendicular space. Enlarged sections of positive (above) and negative structure factors (below) are shown.

$$\Gamma(\alpha) = \begin{pmatrix} 1 & 0 & 0 & 0 & 0 & 0 \\ 0 & 0 & 0 & 0 & 0 & 1 \\ 0 & 1 & 0 & 0 & 0 & 0 \\ 0 & 0 & 1 & 0 & 0 & 0 \\ 0 & 0 & 0 & 1 & 0 & 0 \\ 0 & 0 & 0 & 0 & 1 & 0 \end{pmatrix}_D, \Gamma(\beta) = \begin{pmatrix} 0 & 1 & 0 & 0 & 0 & 0 \\ 0 & 0 & 0 & 0 & 0 & 1 \\ 0 & 0 & 0 & \bar{1} & 0 & 0 \\ 0 & 0 & 0 & 0 & \bar{1} & 0 \\ 0 & 0 & 1 & 0 & 0 & 0 \\ 1 & 0 & 0 & 0 & 0 & 0 \end{pmatrix}_D,$$

$$\Gamma(\gamma) = \begin{pmatrix} \bar{1} & 0 & 0 & 0 & 0 & 0 \\ 0 & \bar{1} & 0 & 0 & 0 & 0 \\ 0 & 0 & \bar{1} & 0 & 0 & 0 \\ 0 & 0 & 0 & \bar{1} & 0 & 0 \\ 0 & 0 & 0 & 0 & \bar{1} & 0 \\ 0 & 0 & 0 & 0 & 0 & \bar{1} \end{pmatrix}_D.$$

Block-diagonalization of these reducible symmetry matrices decomposes them into non-equivalent irreducible representations. These can be assigned to the two orthogonal subspaces forming the 6D embedding space  $\mathbf{V} = \mathbf{V}^{\parallel} \oplus \mathbf{V}^{\perp}$ , the 3D parallel (physical) subspace  $\mathbf{V}^{\parallel}$  and the perpendicular 3D subspace  $\mathbf{V}^{\perp}$ . Thus, using  $W\Gamma W^{-1} = \Gamma^{\text{red}} = \Gamma^{\parallel} \oplus \Gamma^{\perp}$ , we obtain

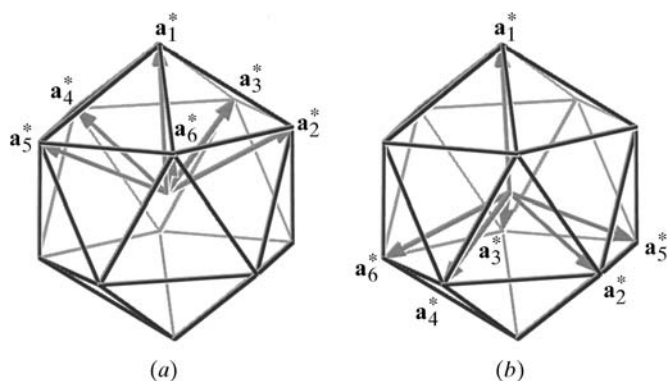


Fig. 4.6.3.28. Perspective (a) parallel- and (b) perpendicular-space views of the reciprocal basis of the 3D Penrose tiling. The six rationally independent vectors  $\mathbf{a}_i^*$  point to the edges of an icosahedron.

$$\Gamma(\alpha) = \left( \begin{array}{ccc|ccc} \cos(2\pi/5) & -\sin(2\pi/5) & 0 & 0 & 0 & 0 \\ \sin(2\pi/5) & \cos(2\pi/5) & 0 & 0 & 0 & 0 \\ 0 & 0 & 1 & 0 & 0 & 0 \\ \hline 0 & 0 & 0 & \cos(4\pi/5) & -\sin(4\pi/5) & 0 \\ 0 & 0 & 0 & \sin(4\pi/5) & \cos(4\pi/5) & 0 \\ 0 & 0 & 0 & 0 & 0 & 1 \end{array} \right)_V$$

$$= \left( \begin{array}{c|c} \Gamma^{\parallel} & 0 \\ \hline 0 & \Gamma^{\perp} \end{array} \right)_V,$$

where

$$W = a^* \begin{pmatrix} 0 & sc4 & sc6 & sc8 & s & sc2 \\ 0 & ss4 & ss6 & ss8 & 0 & ss2 \\ \hline 1 & c & c & c & c & c \\ 0 & -sc8 & -sc2 & -sc6 & -s & -sc4 \\ 0 & -ss8 & -ss2 & -ss6 & 0 & -ss4 \\ 1 & -c & -c & -c & -c & -c \end{pmatrix}_V,$$

$c = \cos \theta$ ,  $s = \sin \theta$ ,  $scn = \sin \theta \cos(n\pi/5)$ ,  $ssn = \sin \theta \sin(n\pi/5)$ . The column vectors of the matrix  $W$  give the parallel- (above the partition line) and perpendicular-space components (below the partition line) of a reciprocal basis in  $\mathbf{V}$ . Thus,  $W$  can be rewritten using the physical-space reciprocal basis defined above and an arbitrary constant  $c$ ,

$$W = \begin{pmatrix} \mathbf{a}_1^* & \mathbf{a}_2^* & \mathbf{a}_3^* & \mathbf{a}_4^* & \mathbf{a}_5^* & \mathbf{a}_6^* \\ c\mathbf{a}_1^* & -c\mathbf{a}_4^* & -c\mathbf{a}_6^* & -c\mathbf{a}_3^* & -c\mathbf{a}_5^* & -c\mathbf{a}_2^* \end{pmatrix}$$

$$= (\mathbf{d}_1^* \ \mathbf{d}_2^* \ \mathbf{d}_3^* \ \mathbf{d}_4^* \ \mathbf{d}_5^* \ \mathbf{d}_6^*),$$

yielding the reciprocal basis  $\mathbf{d}_i^*$ ,  $i = 1, \dots, 6$ , in the 6D embedding space ( $D$  space)

$$\mathbf{d}_1^* = a^* \begin{pmatrix} 0 \\ 0 \\ 1 \\ 0 \\ 0 \\ c \end{pmatrix} \text{ and } \mathbf{d}_i^* = a^* \begin{pmatrix} \sin \theta \cos(2\pi i/5) \\ \sin \theta \sin(2\pi i/5) \\ \cos \theta \\ -c \sin \theta \cos(4\pi i/5) \\ -c \sin \theta \sin(4\pi i/5) \\ -c \cos \theta \end{pmatrix}, i = 2, \dots, 6.$$

The  $6 \times 6$  symmetry matrices can each be decomposed into two  $3 \times 3$  matrices. The first one,  $\Gamma^{\parallel}$ , acts on the parallel-space component, the second one,  $\Gamma^{\perp}$ , on the perpendicular-space component. In the case of  $\Gamma(\alpha)$ , the coupling factor between a rotation in parallel and perpendicular space is 2. Thus a  $2\pi/5$

#### 4.6. RECIPROCAL-SPACE IMAGES OF APERIODIC CRYSTALS

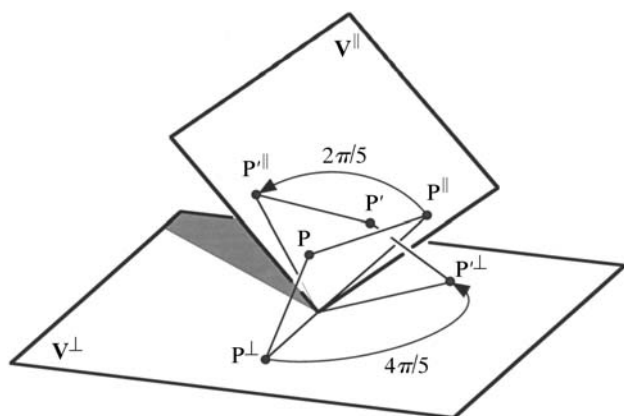


Fig. 4.6.3.29. Schematic representation of a rotation in 6D space. The point P is rotated to P'. The component rotations in parallel and perpendicular space are illustrated.

rotation in physical space is related to a  $4\pi/5$  rotation in perpendicular space (Figs. 4.6.3.28 and 4.6.3.29).

With the condition  $\mathbf{d}_i \cdot \mathbf{d}_j^* = \delta_{ij}$ , the basis in direct 6D space is obtained:

$$\mathbf{d}_1 = \frac{1}{2a^*} \begin{pmatrix} 0 \\ 0 \\ 1 \\ 0 \\ 0 \\ 1/c \end{pmatrix} \text{ and } \mathbf{d}_i = \frac{1}{2a^*} \begin{pmatrix} \sin \theta \cos(2\pi i/5) \\ \sin \theta \sin(2\pi i/5) \\ \cos \theta \\ -(1/c) \sin \theta \cos(4\pi i/5) \\ -(1/c) \sin \theta \sin(4\pi i/5) \\ -(1/c) \cos \theta \end{pmatrix}, \quad i = 2, \dots, 6.$$

The metric tensors  $G, G^*$  are of the type

$$\begin{pmatrix} A & B & B & B & B & B \\ B & A & B & -B & -B & B \\ B & B & A & B & -B & -B \\ B & -B & B & A & B & -B \\ B & -B & -B & B & A & B \\ B & B & -B & -B & B & A \end{pmatrix},$$

with  $A = (1 + c^2)a^{*2}, B = [(5)^{1/2}/5](1 - c^2)a^{*2}$  for the reciprocal space and  $A = (1 + c^2)/[4(ca^*)^2], B = [(5)^{1/2}(c^2 - 1)]/[20(ca^*)^2]$  for the direct space. For  $c = 1$  we obtain hypercubic direct and reciprocal 6D lattices.

The lattice parameters in reciprocal and direct space are  $d_i^* = a^*(2)^{1/2}$  and  $d_i = 1/[(2)^{1/2}a^*]$  with  $i = 1, \dots, 6$ , respectively. The volume of the 6D unit cell can be calculated from the metric tensor  $G$ . For  $c = 1$  it is simply  $V = [\det(G)]^{1/2} = \{1/[(2)^{1/2}a^*]\}^6$ .

The best known example of a 3D quasiperiodic structure is the canonical 3D *Penrose tiling* (see Janssen, 1986). It can be constructed from two unit tiles: a prolate and an oblate rhombohedron with equal edge lengths  $a_r$  (Fig. 4.6.3.30). Each face of the rhombohedra is a rhomb with acute angles  $\alpha_r = \arccos[1/(5)^{1/2}] \simeq 63.44^\circ$ . Their volumes are  $V_p = (4/5)a_r^3 \sin(2\pi/5), V_o = (4/5)a_r^3 \sin(\pi/5) = V_p/\tau$ , and their frequencies  $\nu_p:\nu_o = \tau:1$ . The resulting point density (number of vertices per unit volume) is  $\rho_p = (\tau + 1)/(\tau V_p + V_o) = (\tau/a_r^3) \sin(2\pi/5)$ . Ten prolate and ten oblate rhombohedra can be packed to form a rhombic triacontahedron. The icosahedral symmetry of this zonohedron is broken by the many possible decompositions into the rhombohedra. Removing one zone of the

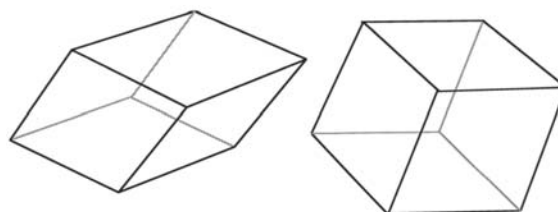


Fig. 4.6.3.30. The two unit tiles of the 3D Penrose tiling: a prolate [ $\alpha_p = \arccos(5^{-1/2}) \simeq 63.44^\circ$ ] and an oblate ( $\alpha_o = 180^\circ - \alpha_p$ ) rhombohedron with equal edge lengths  $a_r$ .

triacontahedron gives a rhomb-icosahedron consisting of five prolate and five oblate rhombohedra. Again, the singular fivefold axis of the rhomb-icosahedron is broken by the decomposition into rhombohedra. Removing one zone again gives a rhombic dodecahedron consisting of two prolate and two oblate rhombohedra. Removing the last remaining zone leads finally to a single prolate rhombohedron. Using these zonohedra as elementary clusters, a matching rule can be derived for the 3D construction of the 3D Penrose tiling (Levine & Steinhardt, 1986; Socolar & Steinhardt, 1986).

The 3D Penrose tiling can be embedded in the 6D space as shown above. The 6D hypercubic lattice is decorated on the lattice nodes with 3D triacontahedra obtained from the projection of a 6D unit cell upon the perpendicular space  $\mathbf{V}^\perp$  (Fig. 4.6.3.31). Thus the edge length of the rhombs covering the triacontahedron is equivalent to the length  $\pi^\perp(\mathbf{d}_i) = 1/2a^*$  of the perpendicular-space component of the vectors spanning the 6D hypercubic lattice  $\Sigma = \{\mathbf{r} = \sum_{i=1}^6 n_i \mathbf{d}_i | n_i \in \mathbb{Z}\}$ .

##### 4.6.3.3.3.1. Indexing

There are several indexing schemes in use. The generic one uses a set of six rationally independent reciprocal-basis vectors pointing to the corners of an icosahedron,  $\mathbf{a}_1^* = a^*(0, 0, 1), \mathbf{a}_i^* = a^*[\sin \theta \cos(2\pi i/5), \sin \theta \sin(2\pi i/5), \cos \theta], i = 2, \dots, 6, \sin \theta = 2/(5)^{1/2}, \cos \theta = 1/(5)^{1/2}$ , with  $\theta \simeq 63.44^\circ$ , the angle between two neighbouring fivefold axes (setting 1) (Fig. 4.6.3.28). In this case, the physical-space basis corresponds to a simple projection of the 6D reciprocal basis  $\mathbf{d}_i^*, i = 1, \dots, 6$ . Sometimes, the same set of six reciprocal-basis vectors is referred to a differently oriented Cartesian reference system ( $C$  basis, with

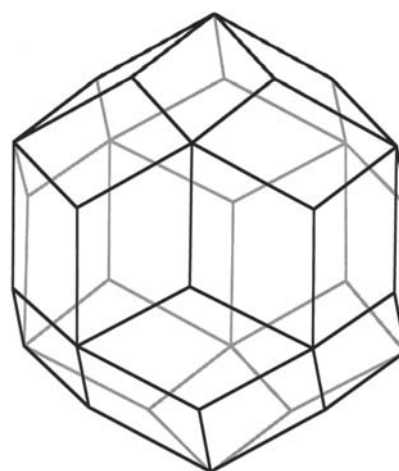


Fig. 4.6.3.31. Atomic surface of the 3D Penrose tiling in the 6D hypercubic description. The projection of the 6D hypercubic unit cell upon  $\mathbf{V}^\perp$  gives a rhombic triacontahedron.

#### 4. DIFFUSE SCATTERING AND RELATED TOPICS

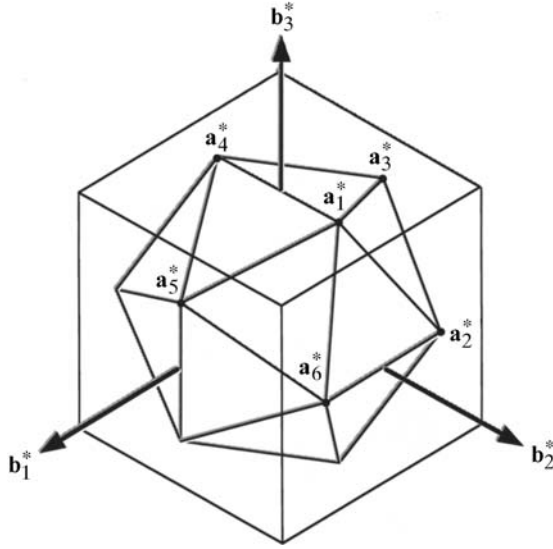


Fig. 4.6.3.32. Perspective parallel-space view of the two alternative reciprocal bases of the 3D Penrose tiling: the cubic and the icosahedral setting, represented by the bases  $\mathbf{b}_i^*$ ,  $i = 1, \dots, 3$ , and  $\mathbf{a}_i^*$ ,  $i = 1, \dots, 6$ , respectively.

basis vectors  $\mathbf{e}_i$  along the twofold axes) (Bancel *et al.*, 1985). The reciprocal basis is

$$\begin{pmatrix} \mathbf{a}_1^* \\ \mathbf{a}_2^* \\ \mathbf{a}_3^* \\ \mathbf{a}_4^* \\ \mathbf{a}_5^* \\ \mathbf{a}_6^* \end{pmatrix} = \frac{a^*}{(1 + \tau^2)^{1/2}} \begin{pmatrix} 0 & 1 & \tau \\ -1 & \tau & 0 \\ -\tau & 0 & 1 \\ 0 & -1 & \tau \\ \tau & 0 & 1 \\ 1 & \tau & 0 \end{pmatrix}_C \begin{pmatrix} \mathbf{e}_1^C \\ \mathbf{e}_2^C \\ \mathbf{e}_3^C \end{pmatrix}.$$

An alternate way of indexing is based on a 3D set of cubic reciprocal-basis vectors  $\mathbf{b}_i^*$ ,  $i = 1, \dots, 3$  (setting 2) (Fig. 4.6.3.32):

$$\begin{pmatrix} \mathbf{b}_1^* \\ \mathbf{b}_2^* \\ \mathbf{b}_3^* \end{pmatrix} = \frac{1}{2} \begin{pmatrix} 0 & \bar{1} & 0 & 0 & 0 & 1 \\ 1 & 0 & 0 & \bar{1} & 0 & 0 \\ 0 & 0 & 1 & 0 & 1 & 0 \end{pmatrix}_D \begin{pmatrix} \mathbf{a}_1^* \\ \mathbf{a}_2^* \\ \mathbf{a}_3^* \\ \mathbf{a}_4^* \\ \mathbf{a}_5^* \\ \mathbf{a}_6^* \end{pmatrix} \\ = \frac{a^*}{(1 + \tau^2)^{1/2}} \begin{pmatrix} \mathbf{e}_1^C \\ \mathbf{e}_2^C \\ \mathbf{e}_3^C \end{pmatrix}.$$

The Cartesian  $C$  basis is related to the  $V$  basis by a  $\theta/2$  rotation around  $[100]_C$ , yielding  $[001]_V$ , followed by a  $\pi/10$  rotation around  $[001]_C$ :

$$\begin{pmatrix} \mathbf{e}_1^C \\ \mathbf{e}_2^C \\ \mathbf{e}_3^C \end{pmatrix} = \begin{pmatrix} \cos(\pi/10) & \sin(\pi/10) & 0 \\ -\cos(\theta/2) \sin(\pi/10) & \cos(\theta/2) \cos(\pi/10) & \sin(\theta/2) \\ \sin(\theta/2) \sin(\pi/10) & -\sin(\theta/2) \cos(\pi/10) & \cos(\theta/2) \end{pmatrix}_V \begin{pmatrix} \mathbf{e}_1^V \\ \mathbf{e}_2^V \\ \mathbf{e}_3^V \end{pmatrix}.$$

Thus, indexing the diffraction pattern of an icosahedral phase with integer indices, one obtains for setting 1  $\mathbf{H} = \sum_{i=1}^6 h_i \mathbf{a}_i^*$ ,  $h_i \in \mathbb{Z}$ . These indices  $(h_1 h_2 h_3 h_4 h_5 h_6)$  transform into the second setting to  $(h/h' k/k' l/l')$  with the fractional cubic indices  $h_1^c = h + h'\tau$ ,  $h_2^c = k + k'\tau$ ,  $h_3^c = l + l'\tau$ . The transformation matrix is

$$\begin{pmatrix} h \\ h' \\ k \\ k' \\ l \\ l' \end{pmatrix}_C = \begin{pmatrix} 0 & \bar{1} & 0 & 0 & 0 & 1 \\ 0 & 0 & \bar{1} & 0 & 1 & 0 \\ 1 & 0 & 0 & \bar{1} & 0 & 0 \\ 0 & 1 & 0 & 0 & 0 & 1 \\ 0 & 0 & 1 & 0 & 1 & 0 \\ 1 & 0 & 0 & 1 & 0 & 0 \end{pmatrix}_D \begin{pmatrix} h_1 \\ h_2 \\ h_3 \\ h_4 \\ h_5 \\ h_6 \end{pmatrix}_D = \begin{pmatrix} h_6 - h_2 \\ h_5 - h_3 \\ h_1 - h_4 \\ h_6 + h_2 \\ h_5 + h_3 \\ h_1 + h_4 \end{pmatrix}_D.$$

##### 4.6.3.3.3.2. Diffraction symmetry

The diffraction symmetry of icosahedral phases can be described by the Laue group  $K = m\bar{3}5$ . The set of all vectors  $\mathbf{H}$  forms a Fourier module  $M^* = \{\mathbf{H}^{\parallel} = \sum_{i=1}^6 h_i \mathbf{a}_i^* | h_i \in \mathbb{Z}\}$  of rank 6 in physical space. Consequently, it can be considered as a projection from a 6D reciprocal lattice,  $M^* = \pi^{\parallel}(\Sigma^*)$ . The parallel and perpendicular reciprocal-space sections of the 3D Penrose tiling decorated with equal point scatterers on its vertices are shown in Figs. 4.6.3.33 and 4.6.3.34. The diffraction pattern in perpendicular space is the Fourier transform of the triacontahedron. All Bragg reflections within  $10^{-4}|F(\mathbf{0})|^2 < |F(\mathbf{H})|^2 < |F(\mathbf{0})|^2$  are depicted. Without intensity-truncation limit, the diffraction pattern would be densely filled with discrete Bragg reflections.

The 6D icosahedral space groups that are relevant to the description of icosahedral phases (six symmorphic and five non-symmorphic groups) are listed in Table 4.6.3.2. These space groups are a subset of all 6D icosahedral space groups fulfilling the condition that the 6D point groups they are associated with are isomorphic to the 3D point groups  $\frac{2}{m}\bar{3}5$  and 235 describing the diffraction symmetry. From 826 6D (analogues to) Bravais groups (Levitov & Rhyner, 1988), only three fulfil the condition that the projection of the 6D hypercubic lattice upon the 3D physical space is compatible with the icosahedral point groups  $\frac{2}{m}\bar{3}5$ , 235: the primitive hypercubic Bravais lattice  $P$ , the body-centred Bravais lattice  $I$  with translation  $1/2(111111)$ , and the face-centred Bravais lattice  $F$  with translations  $1/2(110000) + 14$  further cyclic permutations. Hence, the  $I$  lattice is twofold primitive (*i.e.* it contains two vertices per unit cell) and the  $F$  lattice is 16-fold primitive. The orientation of the symmetry elements in the 6D space is defined by the isomorphism of the 3D and 6D point groups. The action of the fivefold rotation, however, is different in the subspaces  $\mathbf{V}^{\parallel}$  and  $\mathbf{V}^{\perp}$ : a rotation of  $2\pi/5$  in  $\mathbf{V}^{\parallel}$  is correlated with a rotation of  $4\pi/5$  in  $\mathbf{V}^{\perp}$ . The reflection and inversion operations are equivalent in both subspaces.

##### 4.6.3.3.3.3. Structure factor

The structure factor of the icosahedral phase corresponds to the Fourier transform of the 6D unit cell,

$$F(\mathbf{H}) = \sum_{k=1}^N f_k(\mathbf{H}^{\parallel}) T_k(\mathbf{H}^{\parallel}, \mathbf{H}^{\perp}) g_k(\mathbf{H}^{\perp}) \exp(2\pi i \mathbf{H} \cdot \mathbf{r}_k),$$

with 6D diffraction vectors  $\mathbf{H} = \sum_{i=1}^6 h_i \mathbf{d}_i^*$ , parallel-space atomic scattering factor  $f_k(\mathbf{H}^{\parallel})$ , temperature factor  $T_k(\mathbf{H}^{\parallel}, \mathbf{H}^{\perp})$ , and perpendicular-space geometric form factor  $g_k(\mathbf{H}^{\perp})$ .  $T_k(\mathbf{H}^{\parallel}, \mathbf{0})$  is equivalent to the conventional Debye–Waller factor and  $T_k(\mathbf{0}, \mathbf{H}^{\perp})$  describes random fluctuations in perpendicular space. These fluctuations cause characteristic jumps of vertices (*phason flips*) in the physical space. Even random phason flips map the vertices onto positions that can still be described by physical-space vectors of the type  $\mathbf{r} = \sum_{i=1}^6 n_i \mathbf{a}_i$ . Consequently, the set  $M = \{\mathbf{r} = \sum_{i=1}^6 n_i \mathbf{a}_i | n_i \in \mathbb{Z}\}$  of all possible vectors forms a  $\mathbb{Z}$  module. The shape of the atomic surfaces corresponds to a selection rule for the positions actually occupied. The geometric form factor  $g_k(\mathbf{H}^{\perp})$  is equivalent to the Fourier transform of the *atomic surface*, *i.e.* the 3D perpendicular-space component of the 6D *hyperatoms*.

For the example of the canonical 3D Penrose tiling,  $g_k(\mathbf{H}^{\perp})$  corresponds to the Fourier transform of a triacontahedron:

## 4.6. RECIPROCAL-SPACE IMAGES OF APERIODIC CRYSTALS

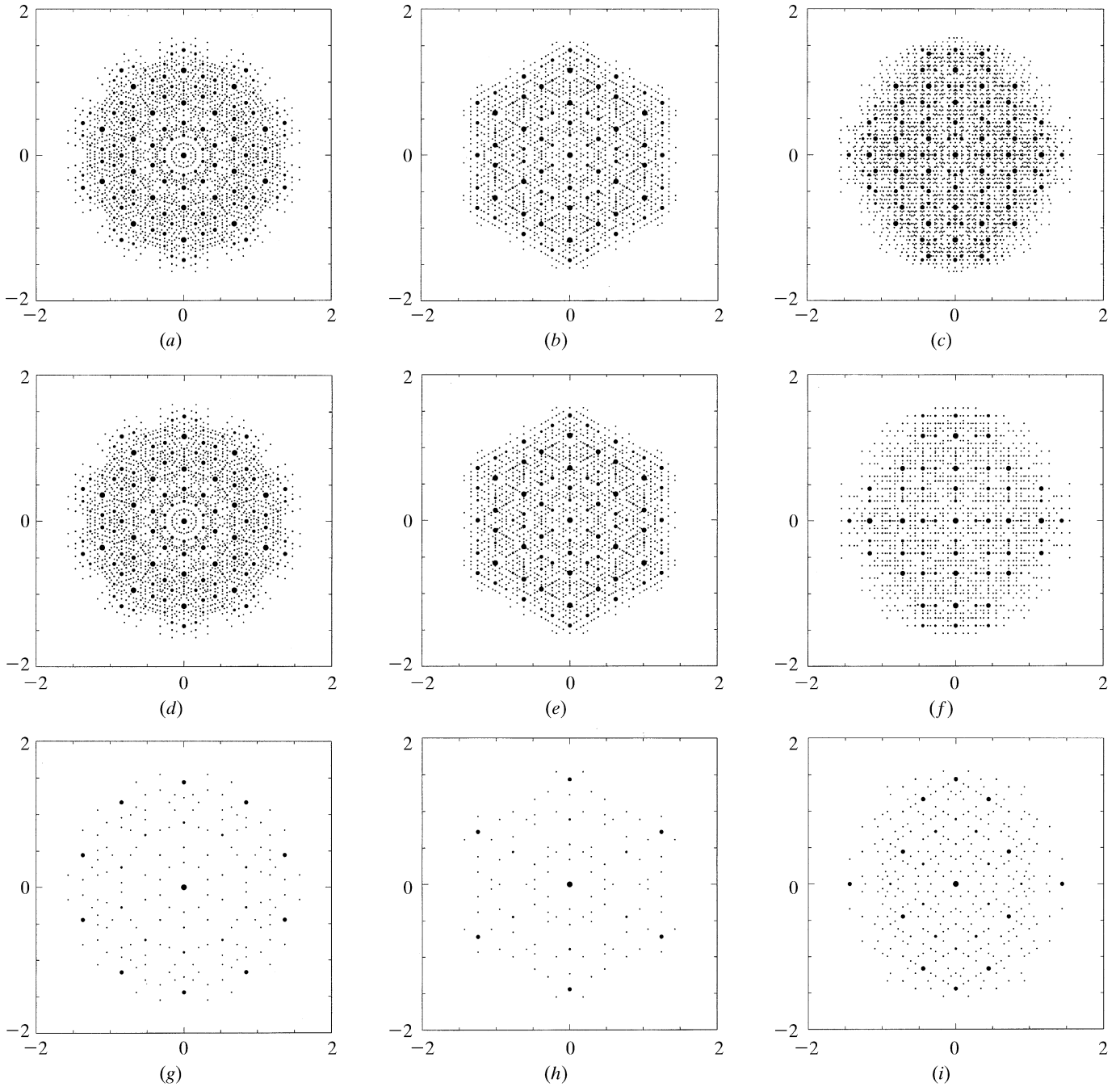


Fig. 4.6.333. Physical-space diffraction patterns of the 3D Penrose tiling decorated with point atoms (edge lengths of the Penrose unit rhombohedra  $a_r = 5.0$  Å). Sections with five-, three- and twofold symmetry are shown for the primitive 6D analogue of Bravais type  $P$  in (a, b, c), the body-centred 6D analogue to Bravais type  $I$  in (d, e, f) and the face-centred 6D analogue to Bravais type  $F$  in (g, h, i). All reflections are shown within  $10^{-4}|F(\mathbf{0})|^2 < |F(\mathbf{H})|^2 < |F(\mathbf{0})|^2$  and  $-6 \leq h_i \leq 6, i = 1, \dots, 6$ .

$$g_k(\mathbf{H}^\perp) = (1/A_{\text{UC}}^\perp) \int_{A_k} \exp(2\pi i \mathbf{H}^\perp \cdot \mathbf{r}) \, d\mathbf{r},$$

where  $A_{\text{UC}}^\perp$  is the volume of the 6D unit cell projected upon  $\mathbf{V}^\perp$  and  $A_k$  is the volume of the triacontahedron.  $A_{\text{UC}}^\perp$  and  $A_k$  are equal in the present case and amount to the volumes of ten prolate and ten oblate rhombohedra:  $A_{\text{UC}}^\perp = 8a_r^3 [\sin(2\pi/5) + \sin(\pi/5)]$ . Evaluating the integral by decomposing the triacontahedron into trigonal pyramids, each one directed from the centre of the triacontahedron to three of its corners given by the vectors  $\mathbf{e}_i, i = 1, \dots, 3$ , one obtains

$$g(\mathbf{H}^\perp) = (1/A_{\text{UC}}^\perp) \sum_R g_k(R^T \mathbf{H}^\perp),$$

with  $k = 1, \dots, 60$  running over all site-symmetry operations  $R$  of the icosahedral group,

$$g_k(\mathbf{H}^\perp) = -iV_r [A_2 A_3 A_4 \exp(iA_1) + A_1 A_3 A_5 \exp(iA_2) + A_1 A_2 A_6 \exp(iA_3) + A_4 A_5 A_6] \times (A_1 A_2 A_3 A_4 A_5 A_6)^{-1},$$

$A_j = 2\pi \mathbf{H}^\perp \cdot \mathbf{e}_j, j = 1, \dots, 3, A_4 = A_2 - A_3, A_5 = A_3 - A_1, A_6 = A_1 - A_2$  and  $V_r = \mathbf{e}_1 \cdot (\mathbf{e}_2 \times \mathbf{e}_3)$  the volume of the parallelepiped defined by the vectors  $\mathbf{e}_i, i = 1, \dots, 3$  (Yamamoto, 1992b).

## 4.6.3.3.3.4. Intensity statistics

The radial structure-factor distributions of the 3D Penrose tiling decorated with point scatterers are plotted in Fig. 4.6.3.35 as a function of parallel and perpendicular space. The distribution of  $|F(\mathbf{H})|$  as a function of their frequencies clearly resembles a centric

#### 4. DIFFUSE SCATTERING AND RELATED TOPICS

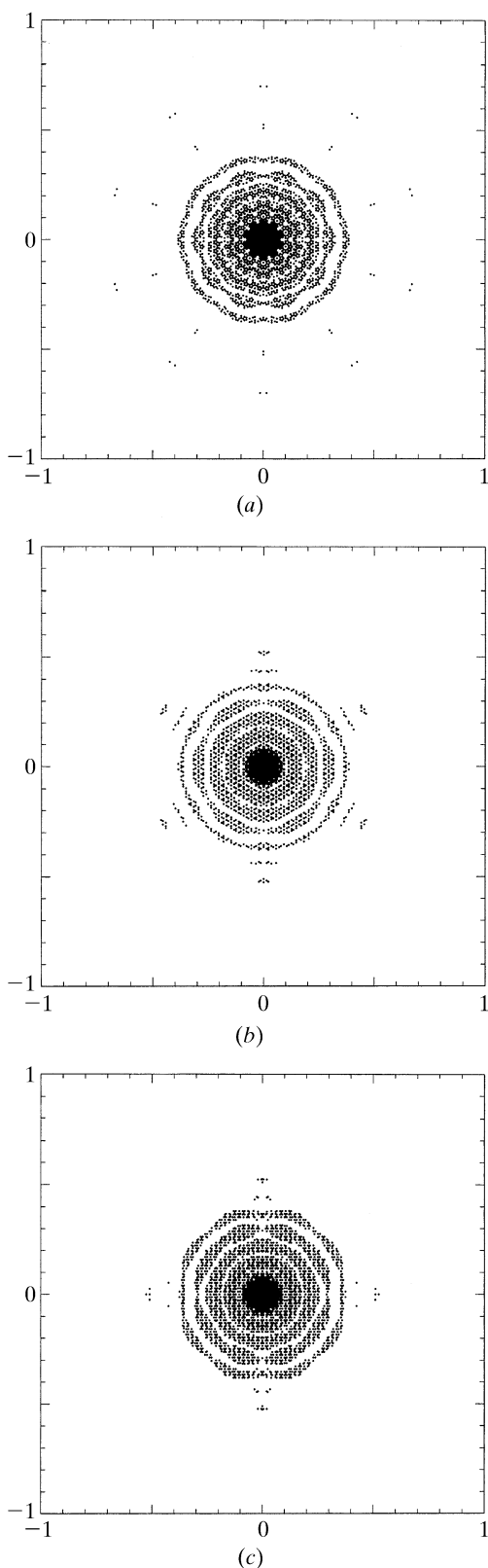


Fig. 4.6.34. Perpendicular-space diffraction patterns of the 3D Penrose tiling decorated with point atoms (edge lengths of the Penrose unit rhombohedra  $a_r = 5.0 \text{ \AA}$ ). Sections with (a) five-, (b) three- and (c) twofold symmetry are shown for the primitive 6D analogue of Bravais type  $P$ . All reflections are shown within  $10^{-4}|F(\mathbf{0})|^2 < |F(\mathbf{H})|^2 < |F(\mathbf{0})|^2$  and  $-6 \leq h_i \leq 6, i = 1, \dots, 6$ .

distribution, as can be expected from the centrosymmetric unit cell. The shape of the distribution function depends on the radius of the limiting sphere in reciprocal space. The number of weak reflections

Table 4.6.3.2. 3D point groups of order  $k$  describing the diffraction symmetry and corresponding 6D decagonal space groups with reflection conditions (see Levitov & Rhyner, 1988; Rokhsar et al., 1988)

| 3D point group        | $k$ | 5D space group         | Reflection condition   |
|-----------------------|-----|------------------------|--|
| $\frac{2}{m}\bar{3}5$ | 120 | $P\frac{2}{m}\bar{3}5$ | No condition   |
|                       |     | $P\frac{2}{n}\bar{3}5$ | $h_1h_2\bar{h}_1\bar{h}_2h_5h_6 : h_5 - h_6 = 2n$  |
|                       |     | $I\frac{2}{m}\bar{3}5$ | $h_1h_2h_3h_4h_5h_6 : \sum_{i=1}^6 h_i = 2n$   |
|                       |     | $F\frac{2}{m}\bar{3}5$ | $h_1h_2h_3h_4h_5h_6 : \sum_{i \neq j=1}^6 h_i + h_j = 2n$  |
|                       |     | $F\frac{2}{n}\bar{3}5$ | $h_1h_2h_3h_4h_5h_6 : \sum_{i \neq j=1}^6 h_i + h_j = 2n$<br>$h_1h_2\bar{h}_1\bar{h}_2h_5h_6 : h_5 - h_6 = 4n$ |
| 235                   | 60  | $P235$                 | No condition   |
|                       |     | $P235_1$               | $h_1h_2h_2h_2h_2h_2 : h_1 = 5n$  |
|                       |     | $I235$                 | $h_1h_2h_3h_4h_5h_6 : \sum_{i=1}^6 h_i = 2n$   |
|                       |     | $I235_1$               | $h_1h_2h_3h_4h_5h_6 : \sum_{i=1}^6 h_i = 2n$<br>$h_1h_2h_2h_2h_2h_2 : h_1 + 5h_2 = 10n$                        |
|                       |     | $F235$                 | $h_1h_2h_3h_4h_5h_6 : \sum_{i \neq j=1}^6 h_i + h_j = 2n$  |
|                       |     | $F235_1$               | $h_1h_2h_3h_4h_5h_6 : \sum_{i \neq j=1}^6 h_i + h_j = 2n$<br>$h_1h_2h_2h_2h_2h_2 : h_1 + 5h_2 = 10n$           |

increases as the power 6, that of strong reflections only as the power 3 (strong reflections always have small  $\mathbf{H}^\perp$  components).

The weighted reciprocal space of the 3D Penrose tiling contains an infinite number of Bragg reflections within a limited region of the physical space. Contrary to the diffraction pattern of a periodic structure consisting of point atoms on the lattice nodes, the Bragg reflections show intensities depending on the perpendicular-space components of their diffraction vectors.

##### 4.6.3.3.5. Relationships between structure factors at symmetry-related points of the Fourier image

The weighted 3D reciprocal space  $M^* = \{\mathbf{H}^\parallel = \sum_{i=1}^6 h_i \mathbf{a}_i^* | h_i \in \mathbb{Z}\}$  exhibits the icosahedral point symmetry  $K = m\bar{3}5$ . It is invariant under the action of the scaling matrix  $S^3$ :

$$S = \frac{1}{2} \begin{pmatrix} 1 & 1 & 1 & 1 & 1 & 1 \\ 1 & 1 & 1 & -1 & -1 & 1 \\ 1 & 1 & 1 & 1 & -1 & -1 \\ 1 & -1 & 1 & 1 & 1 & -1 \\ 1 & -1 & -1 & 1 & 1 & 1 \\ 1 & 1 & -1 & -1 & 1 & 1 \end{pmatrix}_D, S^3 = \begin{pmatrix} 2 & 1 & 1 & 1 & 1 & 1 \\ 1 & 2 & 1 & -1 & -1 & 1 \\ 1 & 1 & 2 & 1 & -1 & -1 \\ 1 & -1 & 1 & 2 & 1 & -1 \\ 1 & -1 & -1 & 1 & 2 & 1 \\ 1 & 1 & -1 & -1 & 1 & 2 \end{pmatrix}_D,$$

$$\begin{pmatrix} 2 & 1 & 1 & 1 & 1 & 1 \\ 1 & 2 & 1 & -1 & -1 & 1 \\ 1 & 1 & 2 & 1 & -1 & -1 \\ 1 & -1 & 1 & 2 & 1 & -1 \\ 1 & -1 & -1 & 1 & 2 & 1 \\ 1 & 1 & -1 & -1 & 1 & 2 \end{pmatrix}_D \begin{pmatrix} \mathbf{a}_1^* \\ \mathbf{a}_2^* \\ \mathbf{a}_3^* \\ \mathbf{a}_4^* \\ \mathbf{a}_5^* \\ \mathbf{a}_6^* \end{pmatrix} = \tau^3 \begin{pmatrix} \mathbf{a}_1^* \\ \mathbf{a}_2^* \\ \mathbf{a}_3^* \\ \mathbf{a}_4^* \\ \mathbf{a}_5^* \\ \mathbf{a}_6^* \end{pmatrix}.$$

The scaling transformation  $(S^{-3})^T$  leaves a primitive 6D reciprocal lattice invariant as can easily be seen from its application on the indices:

4.6. RECIPROCAL-SPACE IMAGES OF APERIODIC CRYSTALS

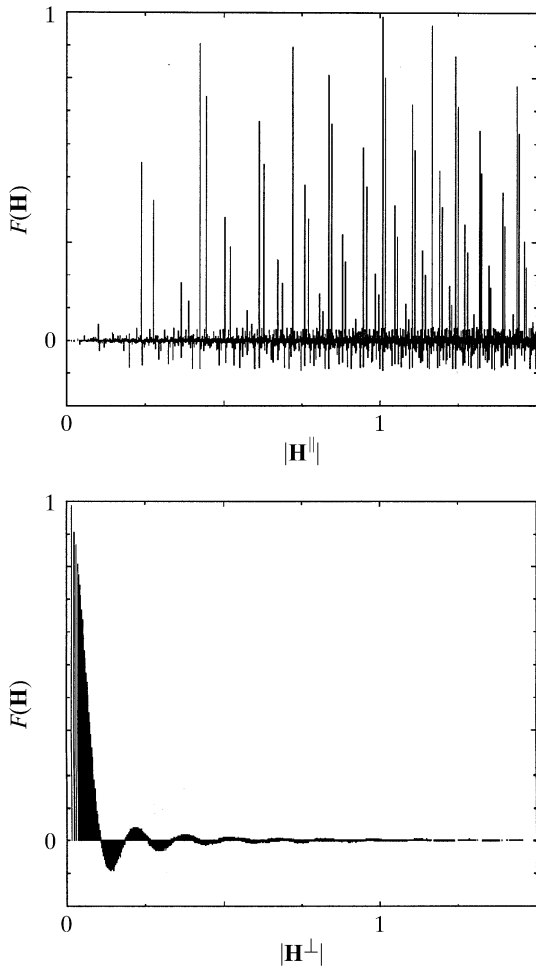


Fig. 4.6.3.35. Radial distribution function of the structure factors  $F(\mathbf{H})$  of the 3D Penrose tiling (edge lengths of the Penrose unit rhombohedra  $a_r = 5.0 \text{ \AA}$ ) decorated with point atoms as a function of  $|\mathbf{H}^{\parallel}|$  (above) and  $|\mathbf{H}^{\perp}|$  (below). All reflections are shown within  $10^{-6}|F(\mathbf{0})|^2 < |F(\mathbf{H})|^2 < |F(\mathbf{0})|^2$  and  $-6 \leq h_i \leq 6, i = 1, \dots, 6$ .

$$\begin{pmatrix} h'_1 \\ h'_2 \\ h'_3 \\ h'_4 \\ h'_5 \\ h'_6 \end{pmatrix} = \begin{pmatrix} -2 & 1 & 1 & 1 & 1 & 1 \\ 1 & -2 & 1 & -1 & -1 & 1 \\ 1 & 1 & -2 & 1 & -1 & -1 \\ 1 & -1 & 1 & -2 & 1 & -1 \\ 1 & -1 & -1 & 1 & -2 & 1 \\ 1 & 1 & -1 & -1 & 1 & -2 \end{pmatrix}_D \begin{pmatrix} h_1 \\ h_2 \\ h_3 \\ h_4 \\ h_5 \\ h_6 \end{pmatrix}.$$

The matrix  $(S^{-1})^T$  leaves  $M^* = \{\mathbf{H}^{\parallel} = \sum_{i=1}^6 h_i \mathbf{a}_i^* | h_i \in \mathbb{Z}\}$  invariant,

$$\begin{pmatrix} h'_1 \\ h'_2 \\ h'_3 \\ h'_4 \\ h'_5 \\ h'_6 \end{pmatrix} = \frac{1}{2} \begin{pmatrix} -1 & 1 & 1 & 1 & 1 & 1 \\ 1 & -1 & 1 & -1 & -1 & 1 \\ 1 & 1 & -1 & 1 & -1 & -1 \\ 1 & -1 & 1 & -1 & 1 & -1 \\ 1 & -1 & -1 & 1 & -1 & 1 \\ 1 & 1 & -1 & -1 & 1 & -1 \end{pmatrix}_D \begin{pmatrix} h_1 \\ h_2 \\ h_3 \\ h_4 \\ h_5 \\ h_6 \end{pmatrix},$$

for any  $\mathbf{H} = \sum_{i=1}^6 h_i \mathbf{d}_i^*$  with  $h_i$  all even or all odd, corresponding to a 6D face-centred hypercubic lattice. In a second case the sum  $\sum_{i=1}^6 h_i$  is even, corresponding to a 6D body-centred hypercubic lattice. Block-diagonalization of the matrix  $S$  decomposes it into two irreducible representations. With  $WSW^{-1} = S_V = S_V^{\parallel} \oplus S_V^{\perp}$  we obtain

$$S_V = \left( \begin{array}{ccc|ccc} \tau & 0 & 0 & 0 & 0 & 0 \\ 0 & \tau & 0 & 0 & 0 & 0 \\ 0 & 0 & \tau & 0 & 0 & 0 \\ \hline 0 & 0 & 0 & -1/\tau & 0 & 0 \\ 0 & 0 & 0 & 0 & -1/\tau & 0 \\ 0 & 0 & 0 & 0 & 0 & -1/\tau \end{array} \right)_V = \left( \begin{array}{c|c} S^{\parallel} & 0 \\ \hline 0 & S^{\perp} \end{array} \right)_V,$$

the scaling properties in the two 3D subspaces: scaling by a factor  $\tau$  in parallel space corresponds to a scaling by a factor  $(-\tau)^{-1}$  in perpendicular space. For the intensities of the scaled reflections analogous relationships are valid, as discussed for decagonal phases (Figs. 4.6.3.36 and 4.6.3.37, Section 4.6.3.3.2.5).

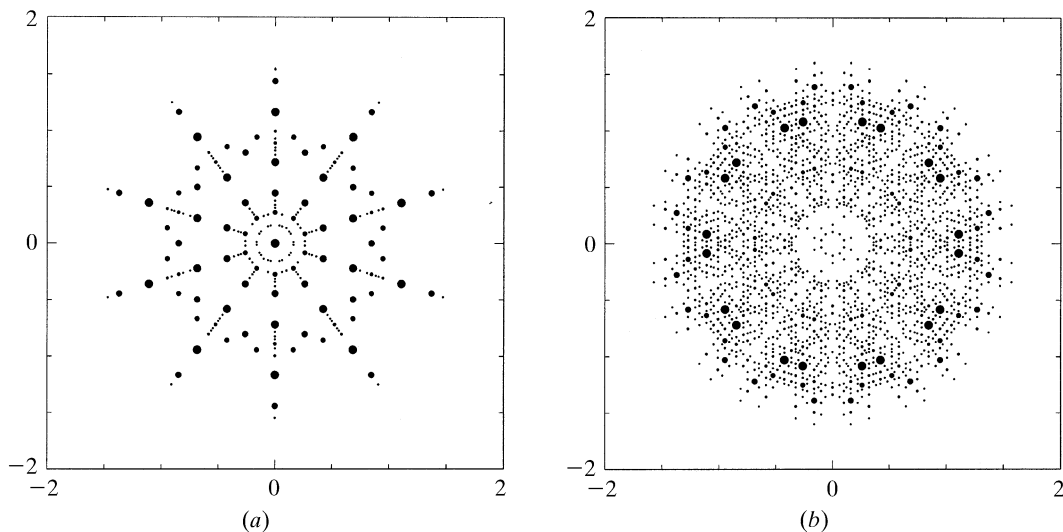


Fig. 4.6.3.36. Parallel-space distribution of (a) positive and (b) negative structure factors of the 3D Penrose tiling of the 6D  $P$  lattice type decorated with point atoms (edge lengths of the Penrose unit rhombohedra  $a_r = 5.0 \text{ \AA}$ ). The magnitudes of the structure factors are indicated by the diameters of the filled circles. All reflections are shown within  $10^{-4}|F(\mathbf{0})|^2 < |F(\mathbf{H})|^2 < |F(\mathbf{0})|^2$  and  $-6 \leq h_i \leq 6, i = 1, \dots, 6$ .

#### 4. DIFFUSE SCATTERING AND RELATED TOPICS

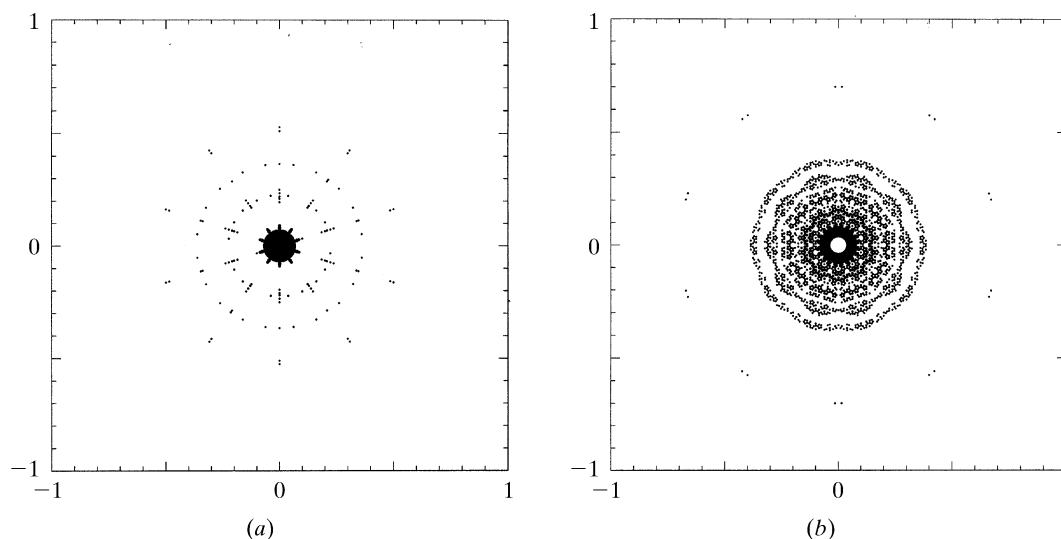


Fig. 4.6.3.37. Perpendicular-space distribution of (a) positive and (b) negative structure factors of the 3D Penrose tiling of the 6D  $P$  lattice type decorated with point atoms (edge lengths of the Penrose unit rhombohedra  $a_r = 5.0 \text{ \AA}$ ). The magnitudes of the structure factors are indicated by the diameters of the filled circles. All reflections are shown within  $10^{-4}|F(\mathbf{0})|^2 < |F(\mathbf{H})|^2 < |F(\mathbf{0})|^2$  and  $-6 \leq h_i \leq 6, i = 1, \dots, 6$ .

#### 4.6.4. Experimental aspects of the reciprocal-space analysis of aperiodic crystals

##### 4.6.4.1. Data-collection strategies

Theoretically, aperiodic crystals show an infinite number of reflections within a given diffraction angle, contrary to periodic crystals. The number of reflections to be included in a structure analysis of a *periodic* crystal may be very high (one million for virus crystals, for instance) but there is no ambiguity in the selection of reflections to be collected: all Bragg reflections within a limiting sphere in reciprocal space, usually given by  $0 \leq \sin \theta / \lambda \leq 0.7 \text{ \AA}^{-1}$ , are used. All reflections, observed and unobserved, are included to fit a reliable structure model.

However, for *aperiodic* crystals it is not possible to collect the infinite number of dense Bragg reflections within  $0 \leq \sin \theta / \lambda \leq 0.7 \text{ \AA}^{-1}$ . The number of observable reflections

within this limiting sphere depends only on the spatial and intensity resolution.

What happens if not all reflections are included in a structure analysis? How important is the contribution of reflections with large perpendicular-space components of the diffraction vector which are weak but densely distributed? These problems are illustrated using the example of the Fibonacci sequence. An infinite model structure consisting of Al atoms with isotropic thermal parameter  $B = 1 \text{ \AA}^2$ , and distances  $S = 2.5 \text{ \AA}$  and  $L = \tau S$ , was used for the calculations (Table 4.6.4.1).

It turns out that 92.6% of the total diffracted intensity of 161 322 reflections is included in the 44 strongest reflections and 99.2% in the strongest 425 reflections. It is remarkable, however, that in all the experimental data for icosahedral and decagonal quasicrystals collected so far, rarely more than 20 to 50 reflections along reciprocal-lattice lines corresponding to net planes with Fibonacci-

Table 4.6.4.1. Intensity statistics of the Fibonacci chain for a total of 161 322 reflections with  $-1000 \leq h_i \leq 1000$  and  $0 \leq \sin \theta / \lambda \leq 2 \text{ \AA}^{-1}$

In the upper line, the number of reflections in the respective interval is given; in the lower line the partial sums  $\sum I(\mathbf{H})$  of the intensities  $I(\mathbf{H})$  are given as a percentage of the total diffracted intensity. The  $F(00)$  reflection is not included in the sums.

|  | $F(\mathbf{H})/F(\mathbf{H})_{\max} \geq 0.1$ | $0.1 > F(\mathbf{H})/F(\mathbf{H})_{\max} \geq 0.01$ | $0.01 > F(\mathbf{H})/F(\mathbf{H})_{\max} \geq 0.001$ | $F(\mathbf{H})/F(\mathbf{H})_{\max} < 0.001$ |
|--|---|--|--|--|
| $0 \leq \sin \theta / \lambda \leq 0.2 \text{ \AA}^{-1}$<br>$\sum I(\mathbf{H})$   | 17<br>52.53%                                  | 148<br>2.56%   | 1505<br>0.27%  | 14 511<br>0.03%                              |
| $0.2 \leq \sin \theta / \lambda \leq 0.4 \text{ \AA}^{-1}$<br>$\sum I(\mathbf{H})$ | 11<br>27.03%                                  | 107<br>2.03%   | 1066<br>0.19%  | 14 998<br>0.02%                              |
| $0.4 \leq \sin \theta / \lambda \leq 0.6 \text{ \AA}^{-1}$<br>$\sum I(\mathbf{H})$ | 9<br>9.84%                                    | 64<br>0.96%  | 654<br>0.12%   | 15 456<br>0.01%                              |
| $0.6 \leq \sin \theta / \lambda \leq 0.8 \text{ \AA}^{-1}$<br>$\sum I(\mathbf{H})$ | 6<br>2.94%                                    | 27<br>0.34%  | 326<br>0.07%   | 15 823<br>0.01%                              |
| $0.8 \leq \sin \theta / \lambda \leq 2 \text{ \AA}^{-1}$<br>$\sum I(\mathbf{H})$   | 1<br>0.23%                                    | 35<br>0.79%  | 338<br>0.06%   | 96 720<br>0.01%                              |
| Total sum  | 44<br>92.57%                                  | 381<br>6.67%   | 3389<br>0.70%  | 157 508<br>0.06%                             |

#### 4.6. RECIPROCAL-SPACE IMAGES OF APERIODIC CRYSTALS

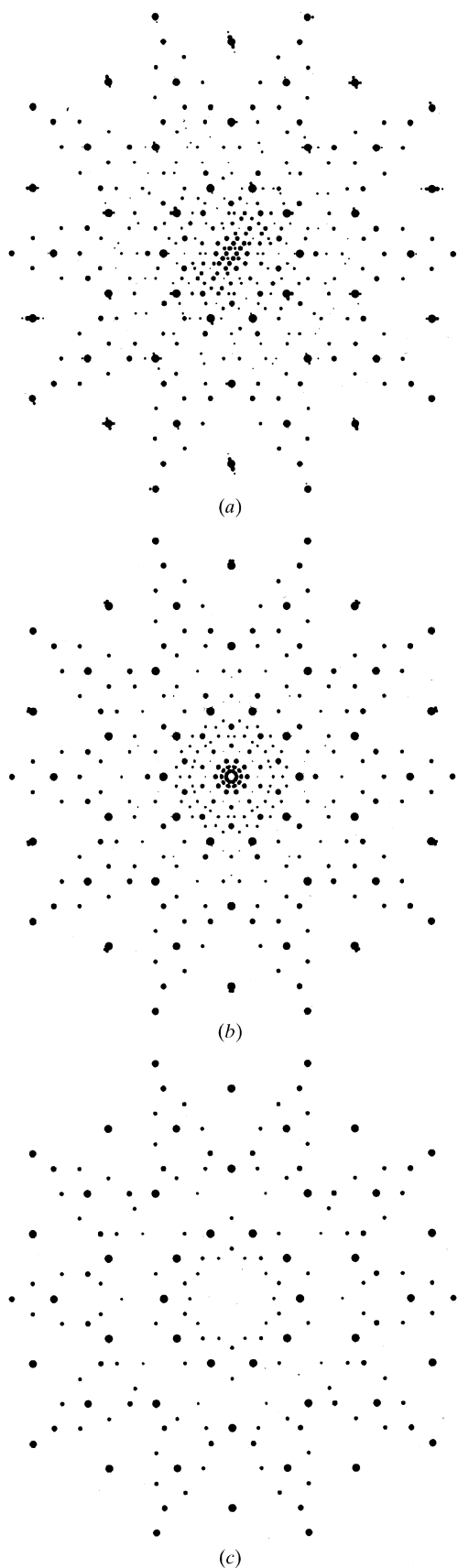


Fig. 4.6.4.1. Simulated diffraction patterns of (a) the  $\approx 52 \text{ \AA}$  single-crystal approximant of decagonal Al-Co-Ni, (b) the fivefold twinned approximant, and (c) the decagonal phase itself (Estermann *et al.*, 1994).

sequence-like distances could be observed. The consequences for structure determinations with such truncated data sets are primarily a lower resolution in perpendicular space than in physical space. This corresponds to a smearing of the hyperatoms in the perpendicular space. For the derivation of the local structure-building elements (clusters) of aperiodic crystals this is only a minor problem: the smeared hyperatoms give rise to split atoms and a biased electron-density distribution. The information on the global aperiodic structure, however, which is contained in the detailed shape of the atomic surfaces, is severely reduced when using a low-resolution diffraction data set. A combination of high-resolution electron microscopy, lattice imaging and diffraction techniques allows a good characterization of the local and global order even in these cases. For a more detailed analysis of these problems see Steurer (1995).

##### 4.6.4.2. Commensurability versus incommensurability

The question whether an aperiodic crystal is really aperiodic or rather a high-order approximant is of different importance depending on the point of view. As far as real finite crystals are considered, definitions of *periodic* and *aperiodic real crystals* and of *periodic* and *aperiodic perfect crystals* have to be given first. *Real crystals*, despite periodicity or aperiodicity, are the actual samples under investigation. Partial information about their actual structure can be obtained today by imaging methods (scanning tunnelling microscopy, atomic force microscopy, high-resolution transmission electron microscopy, . . .). Basically, the real crystal structure can be determined using full diffraction information from Bragg and diffuse scattering. In practice, however, only 'Bragg reflections' are included in a structure analysis. 'Bragg reflections' result from the integration of diffraction intensities from extended volumes around a limited number of Bragg-reflection positions ( $\mathbb{Z}$  module). This process of intensity condensation at Bragg points corresponds in direct space to an averaging process. The real crystal structure is projected upon one unit cell in direct space defined by the  $\mathbb{Z}$  module in reciprocal space. Generally, the identification of appropriate reciprocal-space metrics is not a problem in the case of crystals. It can be problematic, however, in the case of aperiodic crystals, in particular quasicrystals (see Lancon *et al.*, 1994). The metrics, and to some extent the global order in the case of quasicrystals, are fixed by assigning the reciprocal basis. The spatial resolution of a diffraction experiment defines the accuracy of the resulting metrics. The decision whether the rational number obtained for the relative length of a satellite vector indicates a commensurate or an incommensurate modulation can only be made considering temperature- and pressure-dependent chemical and physical properties of the material. The same is valid for other types of aperiodic crystals.

##### 4.6.4.3. Twinning and nanodomain structures

High-order approximants of quasicrystals often occur in orientationally twinned form or, on a smaller scale, as oriented nanodomain structures. These structures can be identified by electron microscopy, and, in certain cases, also by high-resolution X-ray diffractometry (Kalning *et al.*, 1994). If the intensity and spatial resolution is sufficient, characteristic reflection splitting and diffuse diffraction phenomena can be observed. It has been demonstrated that for the determination of the local structure (structure-building elements) it does not matter greatly whether one uses a data set for a real quasicrystal or one for a twinned approximant (Estermann *et al.*, 1994). Examples of reciprocal-space images of an approximant, a twinned approximant and the related decagonal phase are shown schematically in Fig. 4.6.4.1 and for real samples in Fig. 4.6.4.2.

#### 4. DIFFUSE SCATTERING AND RELATED TOPICS

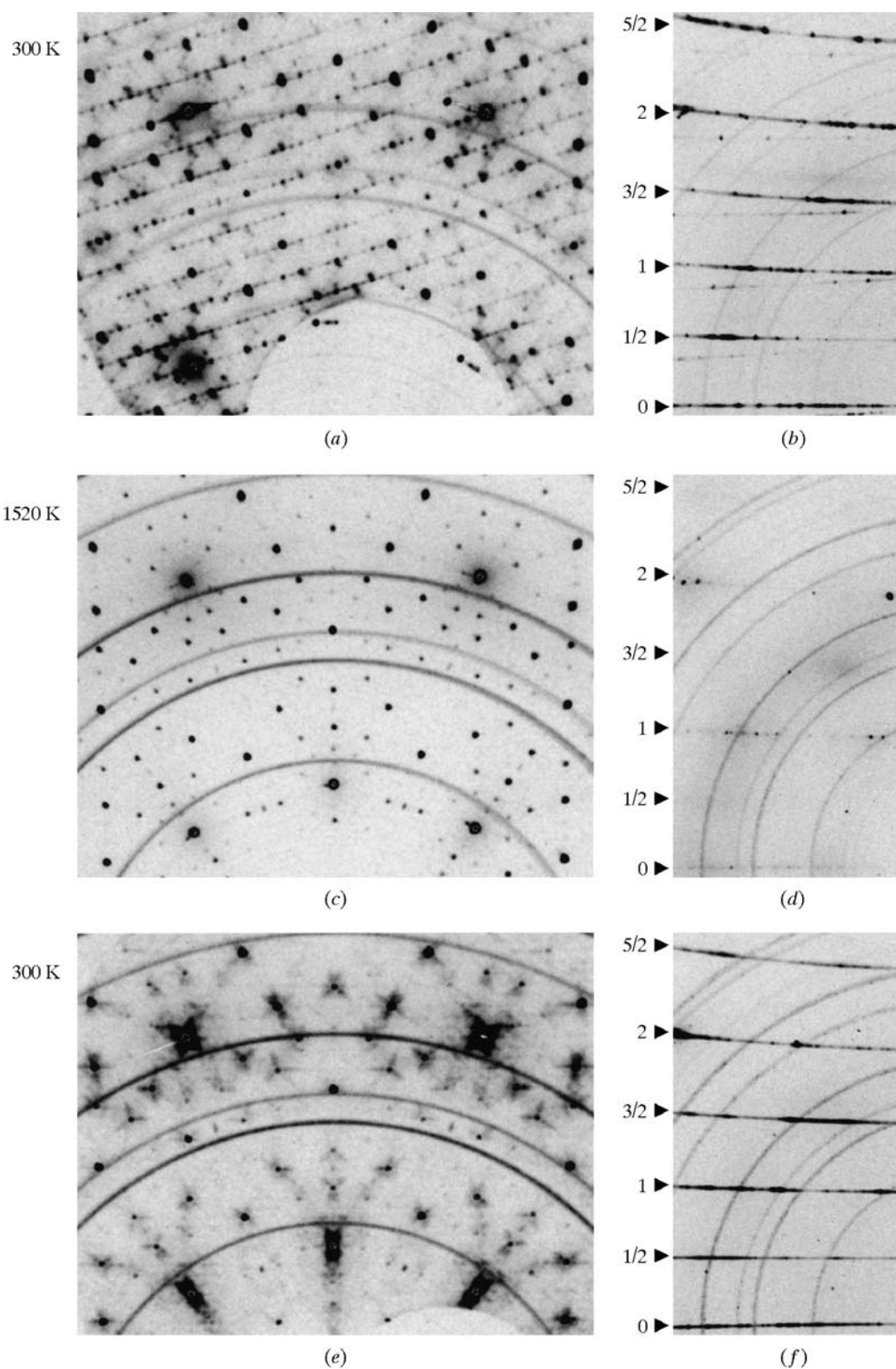


Fig. 4.6.4.2. Zero-layer X-ray diffraction patterns of decaprismatic  $\text{Al}_{73.5}\text{Co}_{21.7}\text{Ni}_{4.8}$  crystals taken parallel and perpendicular to the crystal axis on an image-plate scanner (Mar Research) at different temperatures. In (a) and (b), room-temperature (RT) diffraction patterns from a sample quenched after annealing at 1073 K are shown. Reflections from both a crystalline approximant and a decagonal phase are visible. The period along the unique direction in the decagonal phase and the corresponding period in the approximant phase is  $\approx 8 \text{ \AA}$  (b). At 1520 K, a single-phase decagonal quasicrystal is present with  $\approx 4 \text{ \AA}$  fundamental structure (c, d). In (e, f), the RT diffraction patterns of the slowly cooled sample indicate a single-phase nanodomain structure with  $\approx 8 \text{ \AA}$  periodicity along the unique direction.

## References

## 4.1

- Bilz, H. & Kress, W. (1979). *Phonon dispersion relations in insulators*. Berlin: Springer-Verlag.
- Blackman, M. (1937). *On the vibrational spectrum of a three-dimensional lattice*. *Proc. R. Soc. London Ser. A*, **159**, 416–431.
- Bloch, F. (1928). *Über die Quantenmechanik der Elektronen in Kristallgittern*. *Z. Phys.* **52**, 555–600.
- Born, M. & Huang, K. (1954). *The dynamical theory of crystal lattices*. Oxford: Clarendon Press.
- Born, M. & von Kármán, T. (1912). *Über Schwingungen in Raumgittern*. *Phys. Z.* **13**, 279–309.
- Born, M. & von Kármán, T. (1913). *Zur Theorie der spezifischen Wärme*. *Phys. Z.* **14**, 15–19.
- Boutin, H. & Yip, S. (1968). *Molecular spectroscopy with neutrons*. Cambridge, Mass.: MIT Press.
- Brockhouse, B. N. & Stewart, A. T. (1958). *Normal modes of aluminum by neutron spectrometry*. *Rev. Mod. Phys.* **30**, 236–249.
- Buyers, W. J. L., Pirie, J. D. & Smith, T. (1968). *X-ray scattering from deformable ions*. *Phys. Rev.* **165**, 999–1005.
- Chaplot, S. L., Mierzejewski, A., Pawley, G. S., Lefebvre, J. & Luty, T. (1983). *Phonon dispersion of the external and low-frequency internal vibrations in monoclinic tetracyanoethylene*. *J. Phys. C*, **16**, 625–644.
- Cochran, W. (1971). *The relation between phonon frequencies and interatomic force constants*. *Acta Cryst.* **A27**, 556–559.
- Cochran, W. (1973). *The dynamics of atoms in crystals*. London: Edward Arnold.
- Debye, P. (1912). *Zur Theorie der spezifischen Wärme*. *Ann. Phys. (Leipzig)*, **39**, 789–839.
- Dolling, C. (1974). *Dynamical properties of solids*. Vol. 1, edited by G. K. Horton & A. A. Maradudin, pp. 541–629. Amsterdam: North-Holland.
- Donovan, B. & Angress, J. F. (1971). *Lattice vibrations*. London: Chapman and Hall.
- Einstein, A. (1907). *Die Plancksche Theorie der Strahlung und die Theorie der spezifischen Wärme*. *Ann. Phys. (Leipzig)*, **22**, 180–190, 800.
- Fujii, Y., Lurie, N. A., Pynn, R. & Shirane, G. (1974). *Inelastic neutron scattering from solid <sup>36</sup>Ar*. *Phys. Rev. B*, **10**, 3647–3659.
- Harrison, W. A. (1966). *Phonons in perfect lattices*, edited by R. W. H. Stevenson, pp. 73–109. Edinburgh: Oliver & Boyd.
- Hearmon, R. F. S. (1946). *The elastic constants of anisotropic materials*. *Rev. Mod. Phys.* **18**, 409–440.
- Hearmon, R. F. S. (1956). *The elastic constants of anisotropic materials. II*. *Adv. Phys.* **5**, 323–382.
- Huntingdon, H. B. (1958). *The elastic constants of crystals*. *Solid State Phys.* **7**, 213–351.
- International Tables for Crystallography* (1999). Vol. C. *Mathematical, physical and chemical tables*, edited by A. J. C. Wilson & E. Prince. Dordrecht: Kluwer Academic Publishers.
- Kitaigorodskii, A. J. (1966). *Empilement des molécules dans un cristal, potentiel d'interaction des atomes non liés par des liaisons de valence, et calcul du mouvement des molécules*. *J. Chim. Phys.* **63**, 8–16.
- Laval, J. (1939). *Etude expérimentale de la diffusion des rayons X par les cristaux*. *Bull. Soc. Fr. Minéral.* **62**, 137–253.
- Ledermann, W. (1944). *Asymptotic formulae relating to the physical theory of crystals*. *Proc. R. Soc. London Ser. A*, **82**, 362–377.
- Olmer, P. (1948). *Dispersion des vitesses des ondes acoustiques dans l'aluminium*. *Acta Cryst.* **1**, 57–63.
- Popa, N. C. & Willis, B. T. M. (1994). *Thermal diffuse scattering in time-of-flight neutron diffractometry*. *Acta Cryst.* **A50**, 57–63.
- Raman, C. V. (1941). *The quantum theory of X-ray reflection*. *Proc. Indian Acad. Sci. Sect. A*, **14**, 317–376; *The thermal energy of crystalline solids: basic theory*. *Proc. Indian Acad. Sci. Sect. A*, **14**, 459–467.
- Schofield, P. & Willis, B. T. M. (1987). *Thermal diffuse scattering in time-of-flight neutron diffraction*. *Acta Cryst.* **A43**, 803–809.

- Schuster, S. L. & Weymouth, J. W. (1971). *Study of thermal diffuse X-ray scattering from lead single crystals*. *Phys. Rev. B*, **3**, 4143–4153.
- Squires, G. L. (1978). *Introduction to the theory of thermal neutron scattering*. Cambridge University Press.
- Vacher, R. & Boyer, L. (1972). *Brillouin scattering: a tool for the measurement of elastic and photoelastic constants*. *Phys. Rev. B*, **6**, 639–673.
- Van Hove, L. (1954). *Correlations in space and time and Born approximation scattering in systems of interacting particles*. *Phys. Rev.* **95**, 249–262.
- Venkataraman, G., Feldkamp, L. A. & Sahni, V. C. (1975). *Dynamics of perfect crystals*. Cambridge Mass.: MIT Press.
- Walker, C. B. (1956). *X-ray study of lattice vibrations in aluminum*. *Phys. Rev.* **103**, 547–557.
- Williams, D. E. (1967). *Non-bonded potential parameters derived from crystalline hydrocarbons*. *J. Chem. Phys.* **47**, 4680–4684.
- Willis, B. T. M. (1986). *Determination of the velocity of sound in crystals by time-of-flight neutron diffraction*. *Acta Cryst.* **A42**, 514–525.
- Willis, B. T. M. & Pryor, A. W. (1975). *Thermal vibrations in crystallography*. Cambridge University Press.

## 4.2

- Amorós, J. L. & Amorós, M. (1968). *Molecular crystals: their transforms and diffuse scattering*. New York: John Wiley.
- Arndt, U. W. (1986a). *X-ray position sensitive detectors*. *J. Appl. Cryst.* **19**, 145–163.
- Arndt, U. W. (1986b). *The collection of single crystal diffraction data with area detectors*. *J. Phys. (Paris) Colloq.* **47**(C5), 1–6.
- Axe, J. D. (1980). *Debye–Waller factors for incommensurate structures*. *Phys. Rev. B*, **21**, 4181–4190.
- Bardhan, P. & Cohen, J. B. (1976). *X-ray diffraction study of short-range-order structure in a disordered Au<sub>3</sub>Cu alloy*. *Acta Cryst.* **A32**, 597–614.
- Bauer, G., Seitz, E. & Just, W. (1975). *Elastic diffuse scattering of neutrons as a tool for investigation of non-magnetic point defects*. *J. Appl. Cryst.* **8**, 162–175.
- Bauer, G. S. (1979). *Diffuse elastic neutron scattering from nonmagnetic materials*. In *Treatise on materials science and technology*, Vol. 15, edited by G. Kostorz, pp. 291–336. New York: Academic Press.
- Bessière, M., Lefebvre, S. & Calvayrac, Y. (1983). *X-ray diffraction study of short-range order in a disordered Au<sub>3</sub>Cu alloy*. *Acta Cryst.* **B39**, 145–153.
- Beyeler, H. U., Pietronero, L. & Strässler, S. (1980). *Configurational model for a one-dimensional ionic conductor*. *Phys. Rev. B*, **22**, 2988–3000.
- Borie, B. & Sparks, C. J. (1971). *The interpretation of intensity distributions from disordered binary alloys*. *Acta Cryst.* **A27**, 198–201.
- Böttger, H. (1983). *Principles of the theory of lattice dynamics*. Weinheim: Physik Verlag.
- Boysen, H. (1985). *Analysis of diffuse scattering in neutron powder diagrams. Applications to glassy carbon*. *J. Appl. Cryst.* **18**, 320–325.
- Boysen, H. & Adlhart, W. (1987). *Resolution corrections in diffuse scattering experiments*. *J. Appl. Cryst.* **20**, 200–209.
- Bradley, C. J. & Cracknell, A. P. (1972). *The mathematical theory of symmetry in solids*, pp. 51–76. Oxford: Clarendon Press.
- Brämer, R. (1975). *Statistische Probleme der Theorie des Parakristalls*. *Acta Cryst.* **A31**, 551–560.
- Brämer, R. & Ruland, W. (1976). *The limitations of the paracrystalline model of disorder*. *Macromol. Chem.* **177**, 3601–3617.
- Bubeck, E. & Gerold, V. (1984). *An X-ray investigation in the small and wide angle range from G.P.I. zones in Al–Cu*. In *Microstructural characterization of materials by non-microscop-*

#### 4. DIFFUSE SCATTERING AND RELATED TOPICS

##### 4.2 (cont.)

- pical techniques, edited by N. H. Andersen, M. Eldrup, N. Hansen, R. J. Jensen, T. Leffers, H. Lilholt, O. B. Pedersen & B. N. Singh. Roskilde: Risø National Laboratory.
- Caglioti, G., Paoletti, A. & Ricci, R. (1958). *Choice of collimators for a crystal spectrometer for neutron diffraction*. *Nucl. Instrum. Methods*, **3**, 223–226.
- Cenedese, P., Bley, F. & Lefebvre, S. (1984). *Diffuse scattering in disordered ternary alloys: neutron measurements of local order in a stainless steel Fe<sub>0.56</sub>Cr<sub>0.21</sub>Ni<sub>0.23</sub>*. *Acta Cryst.* **A40**, 228–240.
- Collongues, R., Fayard, M. & Gautier, F. (1977). *Ordre et désordre dans les solides*. *J. Phys. (Paris) Colloq.* **38**(C7), Suppl.
- Comes, R. & Shirane, G. (1979). *X-ray and neutron scattering from one-dimensional conductors*. In *Highly conducting one dimensional solids*, ch. 2, edited by J. T. Devreese, R. P. Evrard & V. E. Van Doren. New York: Plenum.
- Conradi, E. & Müller, U. (1986). *Fehlordnung bei Verbindungen mit Schichtstrukturen. II. Analyse der Fehlordnung in Wismuttriiodid*. *Z. Kristallogr.* **176**, 263–269.
- Convert, P. & Forsyth, J. B. (1983). *Position-sensitive detectors of thermal neutrons*. London: Academic Press.
- Cooper, M. J. & Nathans, R. (1968). *The resolution function in neutron diffractometry. II. The resolution function of a conventional two-crystal neutron diffractometer for elastic scattering. III. Experimental determination and properties of the elastic two-crystal resolution function*. *Acta Cryst.* **A24**, 481–484 (II), 619–624 (III).
- Courville-Brenasin, J. de, Joyez, G. & Tchoubar, D. (1981). *Méthode d'ajustement automatique entre courbes expérimentale et calculée dans les diagrammes de diffraction de poudre. Cas des solides à structure lamellaire. I. Développement de la méthode*. *J. Appl. Cryst.* **14**, 17–23.
- Cowley, J. M. (1950a). *X-ray measurement of order in single crystals of Cu<sub>3</sub>Au*. *J. Appl. Phys.* **21**, 24–36.
- Cowley, J. M. (1950b). *An approximate theory of order in alloys*. *Phys. Rev.* **77**, 664–675.
- Cowley, J. M. (1976). *Diffraction by crystals with planar faults. I. General theory. II. Magnesium fluorogermanate*. *Acta Cryst.* **A32**, 83–87 (I), 88–91 (II).
- Cowley, J. M. (1981). *Diffraction physics*, 2nd ed. Amsterdam: North-Holland.
- Cowley, J. M. & Au, A. Y. (1978). *Diffraction by crystals with planar faults. III. Structure analysis using microtwins*. *Acta Cryst.* **A34**, 738–743.
- Cowley, J. M., Cohen, J. B., Salamon, M. B. & Wuensch, B. J. (1979). *Modulated structures*. *AIP Conf. Proc.* No. 53.
- Debye, B. & Menke, H. (1931). *Untersuchung der molekularen Ordnung in Flüssigkeiten mit Röntgenstrahlung*. *Ergeb. Tech. Roentgenkd.* **II**, 1–22.
- Dederichs, P. H. (1973). *The theory of diffuse X-ray scattering and its application to the study of point defects and their clusters*. *J. Phys. F*, **3**, 471–496.
- Dolling, G., Powell, B. M. & Sears, V. F. (1979). *Neutron diffraction study of the plastic phases of polycrystalline SF<sub>6</sub> and CBr<sub>4</sub>*. *Mol. Phys.* **37**, 1859–1883.
- Dorner, B. & Comes, R. (1977). *Phonons and structural phase transformation*. In *Dynamics of solids and liquids by neutron scattering*, ch. 3, edited by S. Lovesey & T. Springer. *Topics in current physics*, Vol. 3. Berlin: Springer.
- Dorner, C. & Jagodzinski, H. (1972). *Entmischung im System SnO<sub>2</sub>-TiO<sub>2</sub>*. *Krist. Tech.* **7**, 427–444.
- Dubernat, J. & Pezerat, H. (1974). *Fautes d'empilement dans les oxalates dihydratés des métaux divalents de la série magnésienne (Mg, Fe, Co, Ni, Zn, Mn)*. *J. Appl. Cryst.* **7**, 387–393.
- Edwards, O. S. & Lipson, H. (1942). *Imperfections in the structure of cobalt. I. Experimental work and proposed structure*. *Proc. R. Soc. London Ser. A*, **180**, 268–277.
- Emery, V. J. & Axe, J. D. (1978). *One-dimensional fluctuations and the chain-ordering transformation in Hg<sub>3-δ</sub>AsF<sub>6</sub>*. *Phys. Rev. Lett.* **40**, 1507–1511.
- Endres, H., Pouget, J. P. & Comes, R. (1982). *Diffuse X-ray scattering and order-disorder effects in the iodine chain compounds N,N'-diethyl-N,N'-dihydrophenazinium iodide, E<sub>2</sub>PI<sub>1.6</sub> and N,N'-dibenzyl-N,N'-dihydrophenazinium iodide, B<sub>2</sub>PI<sub>1.6</sub>*. *J. Phys. Chem. Solids*, **43**, 739–748.
- Epstein, J. & Welberry, T. R. (1983). *Least-squares analysis of diffuse scattering from substitutionally disordered crystals: application to 2,3-dichloro-6,7-dimethylantracene*. *Acta Cryst.* **A39**, 882–892.
- Epstein, J., Welberry, T. R. & Jones, R. (1982). *Analysis of the diffuse X-ray scattering from substitutionally disordered molecular crystals of monoclinic 9-bromo-10-methylantracene*. *Acta Cryst.* **A38**, 611–618.
- Fender, B. E. F. (1973). *Diffuse scattering and the study of defect solids*. In *Chemical applications of thermal neutron scattering*, ch. 11, edited by B. T. M. Willis. Oxford University Press.
- Flack, H. D. (1970). *Short-range order in crystals of anthrone and in mixed crystals of anthrone-anthraquinone*. *Philos. Trans. R. Soc. London Ser. A*, **266**, 583–591.
- Fontaine, D. de (1972). *An analysis of clustering and ordering in multicomponent solid solutions. I. Stability criteria*. *J. Phys. Chem. Solids*, **33**, 297–310.
- Fontaine, D. de (1973). *An analysis of clustering and ordering in multicomponent solid solutions. II. Fluctuations and kinetics*. *J. Phys. Chem. Solids*, **34**, 1285–1304.
- Forst, R., Jagodzinski, H., Boysen, H. & Frey, F. (1987). *Diffuse scattering and disorder in urea inclusion compounds OC(NH<sub>2</sub>)<sub>2</sub> + C<sub>n</sub>H<sub>2n+2</sub>*. *Acta Cryst.* **B43**, 187–197.
- Fourt, P. (1979). *Diffuse X-ray scattering by orientationally disordered solids*. In *The plastically crystalline state*, ch. 3, edited by J. N. Sherwood. New York: John Wiley.
- Frey, F. & Boysen, H. (1981). *Disorder in cobalt single crystals*. *Acta Cryst.* **A37**, 819–826.
- Frey, F., Jagodzinski, H. & Steger, W. (1986). *On the phase transformation zinc blende to wurtzite*. *Bull. Minéral. Crystallogr.* **109**, 117–129.
- Gehlen, P. & Cohen, J. B. (1965). *Computer simulation of the structure associated with local order in alloys*. *Phys. Rev. A*, **139**, 844–855.
- Georgopoulos, P. & Cohen, J. B. (1977). *The determination of short range order and local atomic displacements in disordered binary solid solutions*. *J. Phys. (Paris) Colloq.* **38**(C7), 191–196.
- Gerlach, P., Schärpf, O., Prandl, W. & Dorner, B. (1982). *Separation of the coherent and incoherent scattering of C<sub>2</sub>Cl<sub>6</sub> by polarization analysis*. *J. Phys. (Paris) Colloq.* **43**(C7), 151–157.
- Gerold, V. (1954). *Röntgenographische Untersuchungen über die Aushärtung einer Aluminium-Kupfer-Legierung mit Kleinwinkel-Schwenkaufnahmen*. *Z. Metallkd.* **45**, 593–607.
- Grabcev, B. (1974). *Instrumental widths and intensities in neutron crystal diffractometry*. *Acta Cryst.* **A35**, 957–961.
- Gragg, J. E., Hayakawa, M. & Cohen, J. B. (1973). *Errors in qualitative analysis of diffuse scattering from alloys*. *J. Appl. Cryst.* **6**, 59–66.
- Guinier, A. (1942). *Le mécanisme de la précipitation dans un cristal de solution solide métallique. Cas des systèmes aluminium-cuivre et aluminium-argent*. *J. Phys. Radium*, **8**, 124–136.
- Guinier, A. (1963). *X-ray diffraction in crystals, imperfect solids and amorphous bodies*. San Francisco: Freeman.
- Halla, F., Jagodzinski, H. & Ruston, W. R. (1953). *One-dimensional disorder in dodecahydrotriphenylene, C<sub>18</sub>H<sub>24</sub>*. *Acta Cryst.* **6**, 478–488.
- Harada, J., Iwata, H. & Ohshima, K. (1984). *A new method for the measurement of X-ray diffuse scattering with a combination of an energy dispersive detector and a source of white radiation*. *J. Appl. Cryst.* **17**, 1–6.
- Harburn, G., Taylor, C. A. & Welberry, T. R. (1975). *An atlas of optical transforms*. London: Bell.
- Hashimoto, S. (1974). *Correlative microdomain model for short range ordered alloy structures. I. Diffraction theory*. *Acta Cryst.* **A30**, 792–798.

## REFERENCES

## 4.2 (cont.)

- Hashimoto, S. (1981). *Correlative microdomain model for short range ordered alloy structures. II. Application to special cases.* *Acta Cryst.* **A37**, 511–516.
- Hashimoto, S. (1983). *Correlative microdomain model for short range ordered alloy structures. III. Analysis for diffuse scattering from quenched CuAu alloy.* *Acta Cryst.* **A39**, 524–530.
- Hashimoto, S. (1987). *Intensity expression for short-range order diffuse scattering with ordering energies in a ternary alloy system.* *J. Appl. Cryst.* **20**, 182–186.
- Haubold, H. G. (1975). *Measurement of diffuse X-ray scattering between reciprocal lattice points as a new experimental method in determining interstitial structures.* *J. Appl. Cryst.* **8**, 175–183.
- Hayakawa, M. & Cohen, J. B. (1975). *Experimental considerations in measurements of diffuse scattering.* *Acta Cryst.* **A31**, 635–645.
- Hendricks, S. B. & Teller, E. (1942). *X-ray interference in partially ordered layer lattices.* *J. Chem. Phys.* **10**, 147–167.
- Hohlwein, D., Hoser, A. & Prandl, W. (1986). *Orientalional disorder in cubic CsNO<sub>2</sub> by neutron powder diffraction.* *Z. Kristallogr.* **177**, 93–102.
- Hosemann, R. (1975). *Micro paracrystallites and paracrystalline superstructures.* *Macromol. Chem. Suppl.* **1**, pp. 559–577.
- Hosemann, R. & Bagchi, S. N. (1962). *Direct analysis of diffraction by matter.* Amsterdam: North-Holland.
- Iizumi, M. (1973). *Lorentz factor in single crystal neutron diffraction.* *Jpn. J. Appl. Phys.* **12**, 167–172.
- Ishii, T. (1983). *Static structure factor of Frenkel–Kontorova-systems at high temperatures. Application to K-hollandite.* *J. Phys. Soc. Jpn.* **52**, 4066–4073.
- Jagodzinski, H. (1949a,b,c). *Eindimensionale Fehlordnung und ihr Einfluß auf die Röntgeninterferenzen. I. Berechnung des Fehlordnungsgredientes aus den Röntgeninterferenzen. II. Berechnung der fehlgeordneten dichtesten Kugelpackungen mit Wechselwirkungen der Reichweite 3. III. Vergleich der Berechnungen mit experimentellen Ergebnissen.* *Acta Cryst.* **2**, 201–208 (I), 208–214 (II), 298–304 (III).
- Jagodzinski, H. (1954). *Der Symmetrieeinfluß auf den allgemeinen Lösungsansatz eindimensionaler Fehlordnungsprobleme.* *Acta Cryst.* **7**, 17–25.
- Jagodzinski, H. (1963). *On disorder phenomena in crystals.* In *Crystallography and crystal perfection*, edited by G. N. Ramachandran, pp. 177–188. London: Academic Press.
- Jagodzinski, H. (1964a). *Allgemeine Gesichtspunkte für die Deutung diffuser Interferenzen von fehlgeordneten Kristallen.* In *Advances in structure research by diffraction methods*, Vol. 1, edited by R. Brill & R. Mason, pp. 167–198. Braunschweig: Vieweg.
- Jagodzinski, H. (1964b). *Diffuse disorder scattering by crystals.* In *Advanced methods of crystallography*, edited by G. N. Ramachandran, pp. 181–219. London: Academic Press.
- Jagodzinski, H. (1968). *Fokussierende Monochromatoren für Einkristallverfahren?* *Acta Cryst.* **B24**, 19–23.
- Jagodzinski, H. (1972). *Transformation from cubic to hexagonal silicon carbide as a solid state reaction.* *Kristallografiya*, **16**, 1235–1246. [Translated into English in *Sov. Phys. Crystallogr.* **16**, 1081–1090.]
- Jagodzinski, H. (1987). *Diffuse X-ray scattering from crystals.* In *Progress in crystal growth and characterization*, edited by P. Krishna, pp. 47–102. Oxford: Pergamon Press.
- Jagodzinski, H. & Haefner, K. (1967). *On order–disorder in ionic non-stoichiometric crystals.* *Z. Kristallogr.* **125**, 188–200.
- Jagodzinski, H. & Hellner, E. (1956). *Die eindimensionale Phasenumwandlung des RhSn<sub>2</sub>.* *Z. Kristallogr.* **107**, 124–149.
- Jagodzinski, H. & Korekawa, M. (1965). *Supersatelliten im Beugungsbild des Labradorits (Ca<sub>2</sub>Na)(Si<sub>2</sub>Al)<sub>2</sub>O<sub>8</sub>.* *Naturwissenschaften*, **52**, 640–641.
- Jagodzinski, H. & Korekawa, M. (1973). *Diffuse X-ray scattering by lunar minerals.* *Geochim. Cosmochim. Acta Suppl.* **4**, **1**, 933–951.
- Jagodzinski, H. & Laves, R. (1947). *Über die Deutung der Entmischungsvorgänge in Mischkristallen unter besonderer Berücksichtigung der Systeme Aluminium–Kupfer und Aluminium–Silber.* *Z. Metallkd.* **40**, 296–305.
- Jagodzinski, H. & Penzkofer, B. (1981). *A new type of satellite in plagioclases.* *Acta Cryst.* **A37**, 754–762.
- James, R. W. (1954). *The optical principles of diffraction of X-rays*, ch. X. London: Bell.
- Janner, A. & Janssen, T. (1980). *Symmetry of incommensurate crystal phases. I. Commensurate basic structures. II. Incommensurate basic structures.* *Acta Cryst.* **A36**, 399–408 (I), 408–415 (II).
- Jefferey, J. W. (1953). *Unusual X-ray diffraction effects from a crystal of wollastonite.* *Acta Cryst.* **6**, 821–826.
- Jones, R. C. (1949). *X-ray diffraction by randomly oriented line gratings.* *Acta Cryst.* **2**, 252–257.
- Kakinoki, J. & Komura, Y. (1954). *Intensity of X-ray diffraction by a one-dimensionally disordered crystal. I. General derivation in the cases of ‘Reichweite’  $s = 0$  and  $s = 1$ .* *J. Phys. Soc. Jpn.* **9**, 169–183.
- Kakinoki, J. & Komura, Y. (1965). *Diffraction by a one-dimensionally disordered crystal. I. The intensity equation.* *Acta Cryst.* **19**, 137–147.
- Kitaigorodsky, A. I. (1984). *Mixed crystals.* Springer series in solid state science, Vol. 33, chs. 6.4, 6.5, 8.4. Berlin: Springer.
- Klug, H. P. & Alexander, L. E. (1954). *X-ray diffraction procedures.* New York: John Wiley.
- Korekawa, M. (1967). *Theorie der Satellitenreflexe.* Habilitationsschrift der Naturwissenschaftlichen Fakultät der Universität München, Germany.
- Korekawa, M. & Jagodzinski, H. (1967). *Die Satellitenreflexe des Labradorits.* *Schweiz. Mineral. Petrogr. Mitt.* **47**, 269–278.
- Krivoglaz, M. A. (1969). *Theory of X-ray and thermal neutron scattering by real crystals.* Part I. New York: Plenum.
- Kunz, C. (1979). Editor. *Synchrotron radiation – techniques and applications.* Berlin: Springer.
- Lechner, R. E. & Riekel, C. (1983). *Application of neutron scattering in chemistry.* In *Neutron scattering and muon spin rotation. Springer tracts in modern physics*, Vol. 101, edited by G. Höhler, pp. 1–84. Berlin: Springer.
- Lefebvre, J., Fouret, R. & Zeyen, C. (1984). *Structure determination of sodium nitrate near the order–disorder phase transition.* *J. Phys. (Paris)*, **45**, 1317–1327.
- Lovesey, S. W. (1984). *Theory of neutron scattering from condensed matter*, Vols. 1, 2. Oxford: Clarendon Press.
- Mardix, S. & Steinberger, I. T. (1970). *Tilt and structure transformation in ZnS.* *J. Appl. Phys.* **41**, 5339–5341.
- Martorana, A., Marigo, A., Toniolo, L. & Zenetti, R. (1986). *Stacking faults in the  $\beta$ -form of magnesium dichloride.* *Z. Kristallogr.* **176**, 1–12.
- Matsubara, E. & Georgopoulos, P. (1985). *Diffuse scattering measurements with synchrotron radiation: instrumentation and techniques.* *J. Appl. Cryst.* **18**, 377–383.
- More, M., Lefebvre, J. & Hennion, B. (1984). *Quasi-elastic coherent neutron scattering in the disordered phase of CBr<sub>4</sub>. Experimental evidence of local order and rotational dynamics of molecules.* *J. Phys. (Paris)*, **45**, 303–307.
- More, M., Lefebvre, J., Hennion, B., Powell, B. M. & Zeyen, C. (1980). *Neutron diffuse scattering in the disordered phase of CBr<sub>4</sub>. I. Experimental. Elastic and quasi-elastic coherent scattering in single crystals.* *J. Phys. C*, **13**, 2833–2846.
- Moss, S. C. (1966). *Local order in solid alloys.* In *Local atomic arrangements studied by X-ray diffraction*, ch. 3, edited by J. B. Cohen & J. E. Hilliard, pp. 95–122. New York: Gordon and Breach.
- Müller, H. (1952). *Die eindimensionale Umwandlung Zinkblende-Wurtzit und die dabei auftretenden Anomalien.* *Neues Jahrb. Mineral. Abh.* **84**, 43–76.
- Niimura, N. (1986). *Evaluation of data from 1-d PSD used in TOF method.* *J. Phys. (Paris) Colloq.* **47**(C5), Suppl., 129–136.
- Niimura, N., Ishikawa, Y., Arai, M. & Furusaka, M. (1982). *Applications of position sensitive detectors to structural analysis using pulsed neutron sources.* AIP conference proceedings, Vol. 89. *Neutron scattering*, edited by J. Faber, pp. 11–22. New York: AIP.

#### 4. DIFFUSE SCATTERING AND RELATED TOPICS

##### 4.2 (cont.)

- Ohshima, K. & Harada, J. (1986). *X-ray diffraction study of short-range ordered structure in a disordered Ag-15 at.% Mg alloy*. *Acta Cryst.* **B42**, 436–442.
- Ohshima, K., Harada, J., Morinaga, M., Georgopoulos, P. & Cohen, J. B. (1986). *Report on a round-robin study of diffuse X-ray scattering*. *J. Appl. Cryst.* **19**, 188–194.
- Ohshima, K. & Moss, S. C. (1983). *X-ray diffraction study of basal-(ab)-plane structure and diffuse scattering from silver atoms in disordered stage-2  $\text{Ag}_{0.18}\text{TiS}_2$* . *Acta Cryst.* **A39**, 298–305.
- Ohshima, K., Watanabe, D. & Harada, J. (1976). *X-ray diffraction study of short-range order diffuse scattering from disordered Cu-29.8% Pd alloy*. *Acta Cryst.* **A32**, 883–892.
- Overhauser, A. W. (1971). *Observability of charge-density waves by neutron diffraction*. *Phys. Rev. B*, **3**, 3173–3182.
- Pandey, D., Lele, S. & Krishna, P. (1980). *X-ray diffraction from one dimensionally disordered 2H-crystals undergoing solid state transformation to the 6H structure. I. The layer displacement mechanism. II. The deformation mechanism. III. Comparison with experimental observations on SiC*. *Proc. R. Soc. London Ser. A*, **369**, 435–439 (I), 451–461 (II), 463–477 (III).
- Patterson, A. L. (1959). *Fourier theory*. In *International tables for X-ray crystallography*, Vol. II, ch. 2.5. Birmingham: Kynoch Press. (Present distributor Kluwer Academic Publishers, Dordrecht.)
- Peisl, J. (1975). *Diffuse X-ray scattering from the displacement field of point defects and defect clusters*. *J. Appl. Cryst.* **8**, 143–149.
- Prandl, W. (1981). *The structure factor of orientational disordered crystals: the case of arbitrary space, site, and molecular point-group*. *Acta Cryst.* **A37**, 811–818.
- Press, W. (1973). *Analysis of orientational disordered structures. I. Method*. *Acta Cryst.* **A29**, 252–256.
- Press, W., Grimm, H. & Hüller, A. (1979). *Analysis of orientational disordered structures. IV. Correlations between orientation and position of a molecule*. *Acta Cryst.* **A35**, 881–885.
- Press, W. & Hüller, A. (1973). *Analysis of orientational disordered structures. II. Examples: Solid  $\text{CD}_4$ ,  $p\text{-D}_2$  and  $\text{ND}_4\text{Br}$* . *Acta Cryst.* **A29**, 257–263.
- Radons, W., Keller, J. & Geisel, T. (1983). *Dynamical structure factor of a 1-d harmonic liquid: comparison of different approximation methods*. *Z. Phys. B*, **50**, 289–296.
- Rietveld, H. M. (1969). *A profile refinement method for nuclear and magnetic structures*. *J. Appl. Cryst.* **2**, 65–71.
- Rosshirt, E., Frey, F., Boysen, H. & Jagodzinski, H. (1985). *Chain ordering in  $\text{E}_2\text{PI}_{1.6}$  (5,10-diethylphenazinium iodide)*. *Acta Cryst.* **B41**, 66–76.
- Sabine, T. M. & Clarke, P. J. (1977). *Powder neutron diffraction – refinement of the total pattern*. *J. Appl. Cryst.* **10**, 277–280.
- Scaringe, P. R. & Ibers, J. A. (1979). *Application of the matrix method to the calculation of diffuse scattering in linearly disordered crystals*. *Acta Cryst.* **A35**, 803–810.
- Schmatz, W. (1973). *X-ray and neutron scattering on disordered crystals*. In *Treatise on materials science and technology*, Vol. 2, ch. 3.1, edited by H. Hermans. New York: Academic Press.
- Schmatz, W. (1983). *Neutron scattering studies of lattice defects: static properties of defects*. In *Methods of experimental physics, solid state: nuclear physics*, Vol. 21, ch. 3.1, edited by J. N. Mundy, S. J. Rothman, M. J. Fluss & L. C. Smedskajew. New York: Academic Press.
- Schulz, H. (1982). *Diffuse X-ray diffraction and its application to materials research*. In *Current topics in materials science*, ch. 4, edited by E. Kaldis. Amsterdam: North-Holland.
- Schwartz, L. H. & Cohen, J. B. (1977). *Diffraction from materials*. New York: Academic Press.
- Sherwood, J. N. (1979). *The plastically crystalline state*. New York: John Wiley.
- Sparks, C. J. & Borie, B. (1966). *Methods of analysis for diffuse X-ray scattering modulated by local order and atomic displacements*. In *Atomic arrangements studied by X-ray diffraction*, ch. 1, edited by J. B. Cohen & J. E. Hilliard, pp. 5–50. New York: Gordon and Breach.
- Springer, T. (1972). *Quasielastic neutron scattering for the investigation of diffuse motions in solid and liquids*. Springer tracts in modern physics, Vol. 64. Berlin: Springer.
- Takaki, Y. & Sakurai, K. (1976). *Intensity of X-ray scattering from one-dimensionally disordered crystal having the multilayer average structure*. *Acta Cryst.* **A32**, 657–663.
- Tibbals, J. E. (1975). *The separation of displacement and substitutional disorder scattering: a correction for structure factor ratio variation*. *J. Appl. Cryst.* **8**, 111–114.
- Tucciarone, A., Lau, H. Y., Corliss, A. M., Delapalme, A. & Hastings, J. M. (1971). *Quantitative analysis of inelastic scattering in two-crystal and three-crystal spectrometry; critical scattering from  $\text{RbMnF}_3$* . *Phys. Rev. B*, **4**, 3206–3245.
- Turberfield, K. C. (1970). *Time-of-flight diffractometry*. In *Thermal neutron diffraction*, edited by B. T. M. Willis. Oxford University Press.
- Vainshtein, B. K. (1966). *Diffraction of X-rays by chain molecules*. Amsterdam: Elsevier.
- Warren, B. E. (1941). *X-ray diffraction in random layer lattices*. *Phys. Rev.* **59**, 693–699.
- Warren, B. E. (1969). *X-ray diffraction*. Reading: Addison-Wesley.
- Warren, B. E. & Gingrich, N. S. (1934). *Fourier integral analysis of X-ray powder patterns*. *Phys. Rev.* **46**, 368–372.
- Welberry, T. R. (1983). *Routine recording of diffuse scattering from disordered molecular crystals*. *J. Appl. Phys.* **16**, 192–197.
- Welberry, T. R. (1985). *Diffuse X-ray scattering and models of disorder*. *Rep. Prog. Phys.* **48**, 1543–1593.
- Welberry, T. R. & Glazer, A. M. (1985). *A comparison of Weissenberg and diffractometer methods for the measurement of diffuse scattering from disordered molecular crystals*. *Acta Cryst.* **A41**, 394–399.
- Welberry, T. R. & Siripitayananon, J. (1986). *Analysis of the diffuse scattering from disordered molecular crystals: application to 1,4-dibromo-2,5-diethyl-3,6-dimethylbenzene at 295 K*. *Acta Cryst.* **B42**, 262–272.
- Welberry, T. R. & Siripitayananon, J. (1987). *Analysis of the diffuse scattering from disordered molecular crystals: application to 1,3-dibromo-2,5-diethyl-4,6-dimethylbenzene at 295 K*. *Acta Cryst.* **B43**, 97–106.
- Welberry, T. R. & Withers, R. L. (1987). *Optical transforms of disordered systems displaying diffuse intensity loci*. *J. Appl. Cryst.* **20**, 280–288.
- Wilke, W. (1983). *General lattice factor of the ideal paracrystal*. *Acta Cryst.* **A39**, 864–867.
- Wilson, A. J. C. (1942). *Imperfections in the structure of cobalt. II. Mathematical treatment of proposed structure*. *Proc. R. Soc. London Ser. A*, **180**, 277–285.
- Wilson, A. J. C. (1949). *X-ray diffraction by random layers: ideal line profiles and determination of structure amplitudes from observed line profiles*. *Acta Cryst.* **2**, 245–251.
- Wilson, A. J. C. (1962). *X-ray optics*, 2nd ed., chs. V, VI, VIII. London: Methuen.
- Windsor, C. G. (1982). *Neutron diffraction performance in pulsed and steady sources*. In *Neutron scattering. AIP conference proceedings*, Vol. 89, edited by J. Faber, pp. 1–10. New York: AIP.
- Wolff, P. M. de (1974). *The pseudo-symmetry of modulated crystal structures*. *Acta Cryst.* **A30**, 777–785.
- Wolff, P. M. de, Janssen, T. & Janner, A. (1981). *The superspace groups for incommensurate crystal structures with a one-dimensional modulation*. *Acta Cryst.* **A37**, 625–636.
- Wong, S. F., Gillan, B. E. & Lucas, B. W. (1984). *Single crystal disorder diffuse X-ray scattering from phase II ammonium nitrate,  $\text{NH}_4\text{NO}_3$* . *Acta Cryst.* **B40**, 342–346.
- Wooster, W. A. (1962). *Diffuse X-ray reflections from crystals*, chs. IV, V. Oxford: Clarendon Press.
- Wu, T. B., Matsubara, E. & Cohen, J. B. (1983). *New procedures for qualitative studies of diffuse X-ray scattering*. *J. Appl. Cryst.* **16**, 407–414.
- Yessik, M., Werner, S. A. & Sato, H. (1973). *The dependence of the intensities of diffuse peaks on scattering angle in neutron diffraction*. *Acta Cryst.* **A29**, 372–382.

## REFERENCES

## 4.2 (cont.)

- Young, R. A. (1975). Editor. *International discussion meeting on studies of lattice distortions and local atomic arrangements by X-ray, neutron and electron diffraction*. *J. Appl. Cryst.* **8**, 79–191.
- Zernike, F. & Prins, J. A. (1927). *Die Beugung von Röntgenstrahlen in Flüssigkeiten als Effekt der Molekülanordnung*. *Z. Phys.* **41**, 184–194.
- 4.3**
- Allen, L. J., Josefsson, T. W., Lehmpfuhl, G. & Uchida, Y. (1997). *Modeling thermal diffuse scattering in electron diffraction involving higher-order Laue zones*. *Acta Cryst.* **A53**, 421–425.
- Andersson, B. (1979). *Electron diffraction study of diffuse scattering due to atomic displacements in disordered vanadium monoxide*. *Acta Cryst.* **A35**, 718–727.
- Andersson, B., Gjønnnes, J. & Taftø, J. (1974). *Interpretation of short range order scattering of electrons; application to ordering of defects in vanadium monoxide*. *Acta Cryst.* **A30**, 216–224.
- Clapp, P. C. & Moss, S. C. (1968). *Correlation functions of disordered binary alloys. II*. *Phys. Rev.* **171**, 754–763.
- Cowley, J. M. (1976a). *Diffraction by crystals with planar faults. I. General theory*. *Acta Cryst.* **A32**, 83–87.
- Cowley, J. M. (1976b). *Diffraction by crystals with planar faults. II. Magnesium fluorogermanate*. *Acta Cryst.* **A32**, 88–91.
- Cowley, J. M. (1981). *Diffraction physics*, 2nd ed. Amsterdam: North-Holland.
- Cowley, J. M. (1988). *Electron microscopy of crystals with time-dependent perturbations*. *Acta Cryst.* **A44**, 847–853.
- Cowley, J. M. (1989). *Multislice methods for surface diffraction and inelastic scattering*. In *Computer simulation of electron microscope diffraction and images*, edited by W. Krakow & M. O'Keefe, pp. 1–12. Worrendale, PA: The Minerals, Metals and Materials Society.
- Cowley, J. M. & Fields, P. M. (1979). *Dynamical theory for electron scattering from crystal defects and disorder*. *Acta Cryst.* **A35**, 28–37.
- De Meulenaere, P., Rodewald, M. & Van Tendeloo, G. (1998). *Anisotropic cluster model for the short-range order in Cu<sub>1-x</sub>-Pd<sub>x</sub>-type alloys*. *Phys. Rev. B*, **57**, 11132–11140.
- De Ridder, R., Van Tendeloo, G. & Amelinckx, S. (1976). *A cluster model for the transition from the short-range order to the long-range order state in f.c.c. based binary systems and its study by means of electron diffraction*. *Acta Cryst.* **A32**, 216–224.
- Doyle, P. A. (1969). *Dynamical calculation of thermal diffuse scattering*. *Acta Cryst.* **A25**, 569–577.
- Ferrel, R. A. (1957). *Characteristic energy loss of electrons passing through metal foils*. *Phys. Rev.* **107**, 450–462.
- Fields, P. M. & Cowley, J. M. (1978). *Computed electron microscope images of atomic defects in f.c.c. metals*. *Acta Cryst.* **A34**, 103–112.
- Fisher, P. M. J. (1969). *The development and application of an n-beam dynamic methodology in electron diffraction*. PhD thesis, University of Melbourne. [See also Cowley (1981), ch. 17.]
- Freeman, A. J. (1959). *Compton scattering of X-rays from non-spherical charge distributions*. *Phys. Rev.* **113**, 169–175.
- Freeman, A. J. (1960). *X-ray incoherent scattering functions for non-spherical charge distributions*. *Acta Cryst.* **12**, 929–936.
- Fujimoto, F. & Kainuma, Y. (1963). *Inelastic scattering of fast electrons by thin crystals*. *J. Phys. Soc. Jpn*, **18**, 1792–1804.
- Gjønnnes, J. (1962). *Inelastic interaction in dynamic electron scattering*. *J. Phys. Soc. Jpn*, **17**, Suppl. BII, 137–139.
- Gjønnnes, J. (1966). *The influence of Bragg scattering on inelastic and other forms of diffuse scattering of electrons*. *Acta Cryst.* **20**, 240–249.
- Gjønnnes, J. & Høier, R. (1971). *Structure information from anomalous absorption effects in diffuse scattering of electrons*. *Acta Cryst.* **A27**, 166–174.
- Gjønnnes, J. & Taftø, J. (1976). *Bloch wave treatment of electron channelling*. *Nucl. Instrum. Methods*, **133**, 141–148.
- Hashimoto, S. (1974). *Correlative microdomain model for short range ordered alloy structures. I. Diffraction theory*. *Acta Cryst.* **A30**, 792–798.
- Høier, R. (1973). *Multiple scattering and dynamical effects in diffuse electron scattering*. *Acta Cryst.* **A29**, 663–672.
- Honjo, G., Kodera, S. & Kitamura, N. (1964). *Diffuse streak diffraction patterns from single crystals. I. General discussion and aspects of electron diffraction diffuse streak patterns*. *J. Phys. Soc. Jpn*, **19**, 351–369.
- Howie, A. (1963). *Inelastic scattering of electrons by crystals. I. The theory of small angle inelastic scattering*. *Proc. Phys. Soc. A*, **271**, 268–287.
- Iijima, S. & Cowley, J. M. (1977). *Study of ordering using high resolution electron microscopy*. *J. Phys. (Paris)*, **38**, Suppl. C7, 21–30.
- International Tables for Crystallography* (1999). Vol. C. *Mathematical, physical and chemical tables*, edited by A. J. C. Wilson & E. Prince. Dordrecht: Kluwer Academic Publishers.
- Kainuma, Y. (1955). *The theory of Kikuchi patterns*. *Acta Cryst.* **8**, 247–257.
- Krahl, D., Pätzold, H. & Swoboda, M. (1990). *An aberration-minimized imaging energy filter of simple design*. *Proceedings of the 12th international conference on electron microscopy*, Vol. 2, pp. 60–61.
- Krivanek, O. L., Gubbens, A. J., Dellby, N. & Meyer, C. E. (1992). *Design and first applications of a post-column imaging filter*. *Micros. Microanal. Microstruct. (France)*, **3**, 187–199.
- Krivanek, O. L. & Mooney, P. E. (1993). *Applications of slow-scan CCD cameras in transmission electron microscopy*. *Ultramicroscopy*, **49**, 95–108.
- Krivoglaz, M. A. (1969). *Theory of X-ray and thermal neutron scattering by real crystals*. New York: Plenum.
- Leapman, R. D., Rez, P. & Mayers, D. F. (1980). *L and M shell generalized oscillator strength and ionization cross sections for fast electron collisions*. *J. Chem. Phys.* **72**, 1232–1243.
- Loane, R. F., Xu, P. R. & Silcox, J. (1991). *Thermal vibrations in convergent-beam electron diffraction*. *Acta Cryst.* **A47**, 267–278.
- Marks, L. D. (1985). *Image localization*. *Ultramicroscopy*, **18**, 33–38.
- Maslen, W. V. & Rossouw, C. J. (1984). *Implications of (e, 2e) scattering electron diffraction in crystals: I–II*. *Philos. Mag.* **A49**, 735–742, 743–757.
- Moliere, G. (1948). *Theory of scattering of fast charged particles: plural and multiple scattering*. *Z. Naturforsch. Teil A*, **3**, 78–97.
- Mori, M., Oikawa, T. & Harada, Y. (1990). *Development of the imaging plate for the transmission electron microscope and its characteristics*. *J. Electron Microsc. (Jpn)*, **19**, 433–436.
- Ohshima, K. & Watanabe, D. (1973). *Electron diffraction study of short-range-order diffuse scattering from disordered Cu–Pd and Cu–Pt alloys*. *Acta Cryst.* **A29**, 520–525.
- Ohtsuki, Y. H., Kitagaku, M., Waho, T. & Omura, T. (1976). *Dechannelling theory with the Fourier–Planck equation and a modified diffusion coefficient*. *Nucl. Instrum. Methods*, **132**, 149–151.
- Rez, P., Humphreys, C. J. & Whelan, M. J. (1977). *The distribution of intensity in electron diffraction patterns due to phonon scattering*. *Philos. Mag.* **35**, 81–96.
- Sauvage, M. & Parthé, E. (1974). *Prediction of diffuse intensity surfaces in short-range-ordered ternary derivative structures based on ZnS, NaCl, CsCl and other structures*. *Acta Cryst.* **A30**, 239–246.
- Taftø, J. & Lehmpfuhl, G. (1982). *Direction dependence in electron energy loss spectroscopy from single crystals*. *Ultramicroscopy*, **7**, 287–294.
- Taftø, J. & Spence, J. C. H. (1982). *Atomic site determination using channelling effect in electron induced X-ray emission*. *Ultramicroscopy*, **9**, 243–247.
- Tanaka, N. & Cowley, J. M. (1985). *High resolution electron microscopy of disordered lithium ferrites*. *Ultramicroscopy*, **17**, 365–377.
- Tanaka, N. & Cowley, J. M. (1987). *Electron microscope imaging of short range order in disordered alloys*. *Acta Cryst.* **A43**, 337–346.

## 4. DIFFUSE SCATTERING AND RELATED TOPICS

### 4.3 (cont.)

- Uyeda, R. & Nonoyama, M. (1968). *The observation of thick specimens by high voltage electron microscopy*. *Jpn. J. Appl. Phys.* **1**, 200–208.
- Van Hove, L. (1954). *Correlations in space and time and Born approximation scattering in systems of interacting particles*. *Phys. Rev.* **95**, 249–262.
- Wang, Z. L. (1995). *Elastic and inelastic scattering in electron diffraction and imaging*. New York: Plenum Press.
- Whelan, M. (1965). *Inelastic scattering of fast electrons by crystals. I. Interband excitations*. *J. Appl. Phys.* **36**, 2099–2110.
- Yoshioka, H. (1957). *Effect of inelastic waves on electron diffraction*. *J. Phys. Soc. Jpn.* **12**, 618–628.

### 4.4

- Aeppli, G. & Bruinsma, R. (1984). *Hexatic order and liquid crystal density fluctuations*. *Phys. Rev. Lett.* **53**, 2133–2136.
- Aeppli, G., Litster, J. D., Birgeneau, R. J. & Pershan, P. S. (1981). *High resolution X-ray study of the smectic A–smectic B phase transition and the smectic B phase in butyloxybenzylidene octylaniline*. *Mol. Cryst. Liq. Cryst.* **67**, 205–214.
- Aharony, A., Birgeneau, R. J., Brock, J. D. & Litster, J. D. (1986). *Multicriticality in hexatic liquid crystals*. *Phys. Rev. Lett.* **57**, 1012–1015.
- Alben, R. (1973). *Phase transitions in a fluid of biaxial particles*. *Phys. Rev. Lett.* **30**, 778–781.
- Als-Nielsen, J., Christensen, F. & Pershan, P. S. (1982). *Smectic-A order at the surface of a nematic liquid crystal: synchrotron X-ray diffraction*. *Phys. Rev. Lett.* **48**, 1107–1110.
- Als-Nielsen, J., Litster, J. D., Birgeneau, R. J., Kaplan, M., Safinya, C. R., Lindegaard, A. & Mathiesen, S. (1980). *Observation of algebraic decay of positional order in a smectic liquid crystal*. *Phys. Rev. B*, **22**, 312–320.
- Bak, P., Mukamel, D., Villain, J. & Wentowska, K. (1979). *Commensurate–incommensurate transitions in rare-gas monolayers adsorbed on graphite and in layered charge-density-wave systems*. *Phys. Rev. B*, **19**, 1610–1613.
- Barois, P., Prost, J. & Lubensky, T. C. (1985). *New critical points in frustrated smectics*. *J. Phys. (Paris)*, **46**, 391–399.
- Beaglehole, D. (1982). *Pretransition order on the surface of a nematic liquid crystal*. *Mol. Cryst. Liq. Cryst.* **89**, 319–325.
- Benattar, J. J., Doucet, J., Lambert, M. & Levelut, A. M. (1979). *Nature of the smectic F phase*. *Phys. Rev. A*, **20**, 2505–2509.
- Benattar, J. J., Levelut, A. M. & Strzelecki, L. (1978). *Etude de l'influence de la longueur moléculaire les caractéristiques des phases smectique ordonnées*. *J. Phys. (Paris)*, **39**, 1233–1240.
- Benattar, J. J., Moussa, F. & Lambert, M. (1980). *Two-dimensional order in the smectic F phase*. *J. Phys. (Paris)*, **40**, 1371–1374.
- Benattar, J. J., Moussa, F. & Lambert, M. (1983). *Two dimensional ordering in liquid crystals: the SmF and SmI phases*. *J. Chim. Phys.* **80**, 99–107.
- Benattar, J. J., Moussa, F., Lambert, M. & Germian, C. (1981). *Two kinds of two-dimensional order: the SmF and SmI phases*. *J. Phys. (Paris) Lett.* **42**, L67–L70.
- Benguigui, L. (1979). *A Landau theory of the NAC point*. *J. Phys. (Paris) Colloq.* **40**, C3-419–C3-421.
- Bensimon, D., Domany, E. & Shtrikman, S. (1983). *Optical activity of cholesteric liquid crystals in the pretransitional regime and in the blue phase*. *Phys. Rev. A*, **28**, 427–433.
- Billard, J., Dubois, J. C., Vaucher, C. & Levelut, A. M. (1981). *Structures of the two discophases of rufigallol hexa-n-octanoate*. *Mol. Cryst. Liq. Cryst.* **66**, 115–122.
- Birgeneau, R. J., Garland, C. W., Kasting, G. B. & Ocko, B. M. (1981). *Critical behavior near the nematic–smectic-A transition in butyloxybenzylidene octylaniline (4O.8)*. *Phys. Rev. A*, **24**, 2624–2634.
- Birgeneau, R. J. & Litster, J. D. (1978). *Bond orientational order model for smectic B liquid crystals*. *J. Phys. (Paris) Lett.* **39**, L399–L402.
- Blinic, R. & Levanyuk, A. P. (1986). Editors. *Modern problems in condensed matter sciences, incommensurate phases in dielectrics, 2. Materials*. Amsterdam: North-Holland.
- Brisbin, D., De Hoff, R., Lockhart, T. E. & Johnson, D. L. (1979). *Specific heat near the nematic–smectic-A tricritical point*. *Phys. Rev. Lett.* **43**, 1171–1174.
- Brock, J. D., Aharony, A., Birgeneau, R. J., Evans-Lutterodt, K. W., Litster, J. D., Horn, P. M., Stephenson, G. B. & Tajbakhsh, A. R. (1986). *Orientalional and positional order in a tilted hexatic liquid crystal phase*. *Phys. Rev. Lett.* **57**, 98–101.
- Brooks, J. D. & Taylor, G. H. (1968). In *Chemistry and physics of carbon*, Vol. 3, edited by P. L. Walker Jr, pp. 243–286. New York: Marcel Dekker.
- Bruinsma, R. & Nelson, D. R. (1981). *Bond orientational order in smectic liquid crystals*. *Phys. Rev. B*, **23**, 402–410.
- Caillé, A. (1972). *Remarques sur la diffusion des rayons X dans les smectiques*. *A. C. R. Acad. Sci. Sér. B*, **274**, 891–893.
- Carlson, J. M. & Sethna, J. P. (1987). *Theory of the ripple phase in hydrated phospholipid bilayers*. *Phys. Rev. A*, **36**, 3359–3363.
- Chan, K. K., Deutsch, M., Ocko, B. M., Pershan, P. S. & Sorensen, L. B. (1985). *Integrated X-ray scattering intensity measurement of the order parameter at the nematic to smectic-A phase transition*. *Phys. Rev. Lett.* **54**, 920–923.
- Chan, K. K., Pershan, P. S., Sorensen, L. B. & Hardouin, F. (1985). *X-ray scattering study of the smectic-A1 to smectic-A2 transition*. *Phys. Rev. Lett.* **54**, 1694–1697.
- Chan, K. K., Pershan, P. S., Sorensen, L. B. & Hardouin, F. (1986). *X-ray studies of transitions between nematic, smectic-A1, -A2, and -Ad phases*. *Phys. Rev. A*, **34**, 1420–1433.
- Chandrasekhar, S. (1982). In *Advances in liquid crystals*, Vol. 5, edited by G. H. Brown, pp. 47–78. London/New York: Academic Press.
- Chandrasekhar, S. (1983). *Liquid crystals of disk-like molecules*. *Philos. Trans. R. Soc. London Ser. A*, **309**, 93–103.
- Chandrasekhar, S., Sadashiva, B. K. & Suresh, K. A. (1977). *Liquid crystals of disk like molecules*. *Pramana*, **9**, 471–480.
- Chapman, D., Williams, R. M. & Ladbroke, B. D. (1967). *Physical studies of phospholipids. VI. Thermotropic and lyotropic mesomorphism of some 1,2-diacylphosphatidylcholines (lecithins)*. *Chem. Phys. Lipids*, **1**, 445–475.
- Chen, J. H. & Lubensky, T. C. (1976). *Landau–Ginzberg mean-field theory for the nematic to smectic-C and nematic to smectic-A phase transitions*. *Phys. Rev. A*, **14**, 1202–1207.
- Chu, K. C. & McMillan, W. L. (1977). *Unified Landau theory for the nematic, smectic A and smectic C phases of liquid crystals*. *Phys. Rev. A*, **15**, 1181–1187.
- Coates, D. & Gray, G. W. (1975). *A correlation of optical features of amorphous liquid–cholesteric liquid crystal transitions*. *Phys. Lett. A*, **51**, 335–336.
- Collett, J. (1983). PhD thesis, Harvard University, USA. Unpublished.
- Collett, J., Pershan, P. S., Sirota, E. B. & Sorensen, L. B. (1984). *Synchrotron X-ray study of the thickness dependence of the phase diagram of thin liquid-crystal films*. *Phys. Rev. Lett.* **52**, 356–359.
- Collett, J., Sorensen, L. B., Pershan, P. S. & Als-Nielsen, J. (1985). *X-ray scattering study of restacking transitions in the crystalline-B phases of heptyloxybenzylidene heptylaniline 7O.7*. *Phys. Rev. A*, **32**, 1036–1043.
- Collett, J., Sorensen, L. B., Pershan, P. S., Litster, J., Birgeneau, R. J. & Als-Nielsen, J. (1982). *Synchrotron X-ray study of novel crystalline-B phases in 7O.7*. *Phys. Rev. Lett.* **49**, 553–556.
- Crooker, P. P. (1983). *The cholesteric blue phase: a progress report*. *Mol. Cryst. Liq. Cryst.* **98**, 31–45.
- Davey, S. C., Budai, J., Goodby, J. W., Pindak, R. & Moncton, D. E. (1984). *X-ray study of the hexatic-B to smectic-A phase transition in liquid crystal films*. *Phys. Rev. Lett.* **53**, 2129–2132.
- Davidov, D., Safinya, C. R., Kaplan, M., Dana, S. S., Schaetzing, R., Birgeneau, R. J. & Litster, J. D. (1979). *High-resolution X-ray and light-scattering study of critical behavior associated with the nematic–smectic-A transition in 4-cyano-4'-octylbiphenyl*. *Phys. Rev. B*, **19**, 1657–1663.

## REFERENCES

## 4.4 (cont.)

- De Gennes, P. G. (1969a). *Conjectures sur l'état smectique*. *J. Phys. (Paris) Colloq.* **30**, C4-65–C4-71.
- De Gennes, P. G. (1969b). *Phenomenology of short-range-order effects in the isotropic phase of nematic materials*. *Phys. Lett. A*, **30**, 454–455.
- De Gennes, P. G. (1971). *Short range order effects in the isotropic phase of nematics and cholesterics*. *Mol. Cryst. Liq. Cryst.* **12**, 193–214.
- De Gennes, P. G. (1972). *An analogy between superconductors and smectics A*. *Solid State Commun.* **10**, 753–756.
- De Gennes, P. G. (1973). *Some remarks on the polymorphism of smectics*. *Mol. Cryst. Liq. Cryst.* **21**, 49–76.
- De Gennes, P. G. (1974). *The physics of liquid crystals*. Oxford: Clarendon Press.
- Demus, D., Diele, S., Klapperstück, M., Link, V. & Zschke, H. (1971). *Investigation of a smectic tetramorphous substance*. *Mol. Cryst. Liq. Cryst.* **15**, 161–169.
- Destrade, C., Gasparoux, H., Foucher, P., Tinh, N. H., Malthête, J. & Jacques, J. (1983). *Molécules discoïdes et polymorphisme mésomorphe*. *J. Chim. Phys.* **80**, 137–148.
- De Vries, H. L. (1951). *Rotary power and other optical properties of liquid crystals*. *Acta Cryst.* **4**, 219–226.
- Diele, S., Brand, P. & Sackmann, H. (1972). *X-ray diffraction and polymorphism of smectic liquid crystals. II. D and E modifications*. *Mol. Cryst. Liq. Cryst.* **17**, 163–169.
- Djurek, D., Baturic-Rubicic, J. & Franulovic, K. (1974). *Specific-heat critical exponents near the nematic–smectic-A phase transition*. *Phys. Rev. Lett.* **33**, 1126–1129.
- Doucet, J. (1979). In *Molecular physics of liquid crystals*, edited by G. W. Gray & G. R. Luckhurst, pp. 317–341. London/New York: Academic Press.
- Doucet, J. & Levelut, A. M. (1977). *X-ray study of the ordered smectic phases in some benzylideneanilines*. *J. Phys. (Paris)*, **38**, 1163–1170.
- Doucet, J., Levelut, A. M., Lambert, M., Lievert, L. & Strzelecki, L. (1975). *Nature de la phase smectique*. *J. Phys. (Paris) Colloq.* **36**, C1-13–C1-19.
- Etherington, G., Leadbetter, A. J., Wang, X. J., Gray, G. W. & Tajbakhsh, A. (1986). *Structure of the smectic D phase*. *Liq. Cryst.* **1**, 209–214.
- Faetti, S., Gatti, M., Palleschi, V. & Sluckin, T. J. (1985). *Almost critical behavior of the anchoring energy at the interface between a nematic liquid crystal and a substrate*. *Phys. Rev. Lett.* **55**, 1681–1684.
- Faetti, S. & Palleschi, V. (1984). *Nematic isotropic interface of some members of the homologous series of the 4-cyano-4'-(n-alkyl)bi-phenyl liquid crystals*. *Phys. Rev. A*, **30**, 3241–3251.
- Fan, C. P. & Stephen, M. J. (1970). *Isotropic–nematic phase transition in liquid crystals*. *Phys. Rev. Lett.* **25**, 500–503.
- Farber, A. S. (1985). PhD thesis, Brandeis University, USA. Unpublished.
- Fleming, R. M., Moncton, D. E., McWhan, D. B. & DiSalvo, F. J. (1980). In *Ordering in two dimensions. Proceedings of an International Conference held at Lake Geneva, Wisconsin*, edited by S. K. Sinha, pp. 131–134. New York: North-Holland.
- Fontell, K. (1974). In *Liquid crystals and plastic crystals*, Vol. II, edited by G. W. Gray & P. A. Winsor, pp. 80–109. Chichester, England: Ellis Horwood.
- Fontes, E., Heiney, P. A., Haseltine, J. H. & Smith, A. B. III (1986). *High resolution X-ray scattering study of the multiply reentrant polar mesogen DB9ONO<sub>2</sub>*. *J. Phys. (Paris)*, **47**, 1533–1539.
- Frank, F. C. & van der Merwe, J. H. (1949). *One-dimensional dislocations. I. Static theory*. *Proc. R. Soc. London Ser. A*, **198**, 205–216.
- Freiser, M. J. (1971). *Successive transitions in a nematic liquid*. *Mol. Cryst. Liq. Cryst.* **14**, 165–182.
- Friedel, G. (1922). *Les états mésomorphes de la matière*. *Ann. Phys. (Paris)*, **18**, 273–274.
- Gane, P. A. C. & Leadbetter, A. J. (1981). *The crystal and molecular structure of N-(4-n-octyloxybenzylidene)-4'-butylaniline (8O.4) and the crystal–smectic G transition*. *Mol. Cryst. Liq. Cryst.* **78**, 183–200.
- Gane, P. A. C. & Leadbetter, A. J. (1983). *Modulated crystal B phases and the B- to G-phase transition in two types of liquid crystalline compounds*. *J. Phys. C*, **16**, 2059–2067.
- Gane, P. A. C., Leadbetter, A. J., Wrighton, P. G., Goodby, J. W., Gray, G. W. & Tajbakhsh, A. R. (1983). *The phase behavior of bis-(4'-n-heptyloxybenzylidene)-1,4-phenylenediamine HEP-TOBPD, crystal J and K phases*. *Mol. Cryst. Liq. Cryst.* **100**, 67–74.
- Gannon, M. G. J. & Faber, T. E. (1978). *The surface tension of nematic liquid crystals*. *Philos. Mag.* **A37**, 117–135.
- Garland, C. W., Meichle, M., Ocko, B. M., Kortan, A. R., Safinya, C. R., Yu, L. J., Litster, J. D. & Birgeneau, R. J. (1983). *Critical behavior at the nematic–smectic-A transition in butyloxybenzylidene heptylaniline (4O.7)*. *Phys. Rev. A*, **27**, 3234–3240.
- Gransbergen, E. F., De Jeu, W. H. & Als-Nielsen, J. (1986). *Antiferroelectric surface layers in a liquid crystal as observed by synchrotron X-ray scattering*. *J. Phys. (Paris)*, **47**, 711–718.
- Gray, G. W. & Goodby, J. W. (1984). *Smectic liquid crystals: textures and structures*. Glasgow: Leonard Hill.
- Gray, G. W., Jones, B. & Marson, F. (1957). *Mesomorphism and chemical constitution. Part VIII. The effect of 3'-substituents on the mesomorphism of the 4'-n-alkoxydiphenyl-4-carboxylic acids and their alkyl esters*. *J. Chem. Soc.* **1**, 393–401.
- Grinstein, G. & Toner, J. (1983). *Dislocation-loop theory of the nematic–smectic A–smectic C multicritical point*. *Phys. Rev. Lett.* **51**, 2386–2389.
- Guillon, D. & Skoulios, A. (1987). *Molecular model for the R smectic DS mesophase*. *Europhys. Lett.* **3**, 79–85.
- Guillon, D., Skoulios, A. & Benattar, J. J. (1986). *Volume and X-ray diffraction study of terephthal-bis-4-n-decylaniline (TBDA)*. *J. Phys. (Paris)*, **47**, 133–138.
- Gunther, L., Imry, Y. & Lajzerowicz, J. (1980). *X-ray scattering in smectic-A liquid crystals*. *Phys. Rev. A*, **22**, 1733–1740.
- Guyot-Sionnest, P., Hsiung, H. & Shen, Y. R. (1986). *Surface polar ordering in a liquid crystal observed by optical second-harmonic generation*. *Phys. Rev. Lett.* **57**, 2963–2966.
- Halperin, B. I. & Nelson, D. R. (1978). *Theory of two-dimensional melting*. *Phys. Rev. Lett.* **41**, 121–124, 519(E).
- Hardouin, F., Levelut, A. M., Achard, M. F. & Sigaud, G. (1983). *Polymorphisme des substances mésogènes à molécules polaires. I. Physico-chimie et structure*. *J. Chim. Phys.* **80**, 53–64.
- Hardouin, F., Levelut, A. M., Benattar, J. J. & Sigaud, G. (1980). *X-ray investigations of the smectic A1–smectic A2 transition*. *Solid State Commun.* **33**, 337–340.
- Hardouin, F., Sigaud, G., Tinh, N. H. & Achard, M. F. (1981). *A fluid smectic A antiphase in a pure nitro rod-like compound*. *J. Phys. (Paris) Lett.* **42**, L63–L66.
- Hardouin, F., Tinh, N. H., Achard, M. F. & Levelut, A. M. (1982). *A new thermotropic smectic phase made of ribbons*. *J. Phys. (Paris) Lett.* **43**, L327–L331.
- Helfrich, W. (1979). *Structure of liquid crystals especially order in two dimensions*. *J. Phys. (Paris) Colloq.* **40**, C3-105–C3-114.
- Hendriks, Y., Charvolin, J. & Rawiso, M. (1986). *Uniaxial–biaxial transition in lyotropic nematic solutions: local biaxiality in the uniaxial phase*. *Phys. Rev. B*, **33**, 3534–3537.
- Hirth, J. P., Pershan, P. S., Collett, J., Sirota, E. & Sorensen, L. B. (1984). *Dislocation model for restacking phase transitions in crystalline-B liquid crystals*. *Phys. Rev. Lett.* **53**, 473–476.
- Hornreich, R. M., Luban, M. & Shtrikman, S. (1975). *Critical behavior at the onset of k-space instability on the lambda line*. *Phys. Rev. Lett.* **35**, 1678–1681.
- Hornreich, R. M. & Shtrikman, S. (1983). *Theory of light scattering in cholesteric blue phases*. *Phys. Rev. A*, **28**, 1791–1807.
- Huang, C. C. & Lien, S. C. (1981). *Nature of a nematic–smectic-A–smectic-C multicritical point*. *Phys. Rev. Lett.* **47**, 1917–1920.

#### 4. DIFFUSE SCATTERING AND RELATED TOPICS

##### 4.4 (cont.)

- Huang, C. C., Lien, S. C., Dumrongrattana, S. & Chiang, L. Y. (1984). *Calorimetric studies near the smectic-A1–smectic-A phase transition of a liquid crystal compound*. *Phys. Rev. A*, **30**, 965–967.
- Huse, D. A. (1985). *Fisher renormalization at the smectic-A1 to smectic-A2 transition in a mixture*. *Phys. Rev. Lett.* **55**, 2228.
- Kasting, G. B., Lushington, K. J. & Garland, C. W. (1980). *Critical heat capacity near the nematic–smectic-A transition in octyloxy-cyanobiphenyl in the range 1–2000 bar*. *Phys. Rev. B*, **22**, 321–331.
- Kittel, C. (1963). *Quantum theory of solids*. New York: John Wiley.
- Kosterlitz, J. M. & Thouless, D. G. (1973). *Ordering, metastability and phase transitions in two-dimensions*. *J. Phys. C*, **6**, 1181–1203.
- Landau, L. D. (1965). In *Collected papers of L. D. Landau*, edited by D. ter Haar, pp. 193–216. New York: Gordon and Breach.
- Landau, L. D. & Lifshitz, E. M. (1958). *Statistical physics*. London: Pergamon Press.
- Lawson, K. D. & Flautt, T. J. (1967). *Magnetically oriented lyotropic liquid crystalline phases*. *J. Am. Chem. Soc.* **89**, 5489–5491.
- Leadbetter, A. J., Durrant, J. L. A. & Rugman, M. (1977). *The density of 4-n-octyl-4'-cyano-biphenyl (8CB)*. *Mol. Cryst. Liq. Cryst.* **34**, 231–235.
- Leadbetter, A. J., Frost, J. C., Gaughan, J. P., Gray, G. W. & Mosley, A. (1979). *The structure of smectic A phases of compounds with cyano end groups*. *J. Phys. (Paris) Colloq.* **40**, C3-375–C3-380.
- Leadbetter, A. J., Frost, J. C., Gaughan, J. P. & Mazid, M. A. (1979). *The structure of the crystal, smectic E and smectic B forms of IBPAC*. *J. Phys. (Paris) Colloq.* **40**, C3-185–C3-192.
- Leadbetter, A. J., Frost, J. C. & Mazid, M. A. (1979). *Interlayer correlations in smectic B phases*. *J. Phys. (Paris) Lett.* **40**, L325–L329.
- Leadbetter, A. J., Gaughan, J. P., Kelley, B., Gray, G. W. & Goodby, J. J. (1979). *Characterisation and structure of some new smectic F phases*. *J. Phys. (Paris) Colloq.* **40**, C3-178–C3-184.
- Leadbetter, A. J., Mazid, M. A. & Kelly, B. A. (1979). *Structure of the smectic-B phase and the nature of the smectic-B to H transition in the N-(4-n-alkoxybenzylidene)-4'-alkylanilines*. *Phys. Rev. Lett.* **43**, 630–633.
- Leadbetter, A. J., Mazid, M. A. & Malik, K. M. A. (1980). *The crystal and molecular structure of isobutyl 4-(4'-phenylbenzylideneamino) cinnamate (IBPBAC) – and the crystal smectic E transition*. *Mol. Cryst. Liq. Cryst.* **61**, 39–60.
- Leadbetter, A. J., Mazid, M. A. & Richardson, R. M. (1980). In *Liquid crystals*, edited by S. Chandrasekhar, pp. 65–79. London: Heyden.
- Leadbetter, A. J., Richardson, R. M. & Carlile, C. J. (1976). *The nature of the smectic E phase*. *J. Phys. (Paris) Colloq.* **37**, C3-65–C3-68.
- Lee, S. D. & Meyer, R. B. (1986). *Computations of the phase equilibrium, elastic constants, and viscosities of a hard-rod nematic liquid crystal*. *J. Chem. Phys.* **84**, 3443–3448.
- Levelut, A. M. (1976). *Etude de l'ordre local lié à la rotation des molécules dans la phase smectique B*. *J. Phys. (Paris) Colloq.* **37**, C3-51–C3-54.
- Levelut, A. M. (1983). *Structures des phases mésomorphes formée de molécules discoïdes*. *J. Chim. Phys.* **80**, 149–161.
- Levelut, A. M., Doucet, J. & Lambert, M. (1974). *Etude par diffusion de rayons X de la nature des phases smectiques B et de la transition de phase solide–smectique B*. *J. Phys. (Paris)*, **35**, 773–779.
- Levelut, A. M. & Lambert, M. (1971). *Structure des cristaux liquides smectic B*. *C. R. Acad. Sci. Sér. B*, **272**, 1018–1021.
- Levelut, A. M., Tarento, R. J., Hardouin, F., Achard, M. F. & Sigaud, G. (1981). *Number of SA phases*. *Phys. Rev. A*, **24**, 2180–2186.
- Liebert, L. E. (1978). Editor. *Liquid crystals*. In *Solid state physics: advances in research and applications*, edited by H. Ehrenreich, F. Seitz & D. Turnbull, Suppl. 14. New York: Academic Press.
- Litster, J. D., Als-Nielsen, J., Birgeneau, R. J., Dana, S. S., Davidov, D., Garcia-Golding, F., Kaplan, M., Safinya, C. R. & Schaezting, R. (1979). *High resolution X-ray and light scattering studies of bilayer smectic A compounds*. *J. Phys. (Paris) Colloq.* **40**, C3-339–C3-344.
- Lubensky, T. C. (1983). *The nematic to smectic A transition: a theoretical overview*. *J. Chim. Phys.* **80**, 31–43.
- Lubensky, T. C. (1987). *Mean field theory for the biaxial nematic phase and the NNUAC critical point*. *Mol. Cryst. Liq. Cryst.* **146**, 55–69.
- Lubensky, T. C. & Ingersent, K. (1986). *Patterns in systems with competing incommensurate lengths*. Preprint.
- Luzzati, V. & Reiss-Husson, F. (1966). *Structure of the cubic phase of lipid–water systems*. *Nature (London)*, **210**, 1351–1352.
- Ma, S. K. (1976). *Modern theory of critical phenomena*. Reading, MA: Benjamin.
- McMillan, W. L. (1972). *X-ray scattering from liquid crystals. I. Cholesteryl nonanoate and myristate*. *Phys. Rev. A*, **6**, 936–947.
- McMillan, W. L. (1973a). *Measurement of smectic-A-phase order-parameter fluctuations near a second-order smectic-A–nematic-phase transition*. *Phys. Rev. A*, **7**, 1419–1422.
- McMillan, W. L. (1973b). *Measurement of smectic-A-phase order-parameter fluctuations in the nematic phase of p-n-octyloxybenzylidene-p'-toluidine*. *Phys. Rev. A*, **7**, 1673–1678.
- McMillan, W. L. (1973c). *Measurement of smectic-phase order-parameter fluctuations in the nematic phase of heptyloxybenzene*. *Phys. Rev. A*, **8**, 328–331.
- Mada, H. & Kobayashi, S. (1981). *Surface order parameter of 4-n-heptyl-4'-cyanobiphenyl*. *Mol. Cryst. Liq. Cryst.* **66**, 57–60.
- Maier, W. & Saupe, A. (1958). *Eine einfache molekulare Theorie des nematischen kristallinüssigen Zustandes*. *Z. Naturforsch. Teil A*, **13**, 564–566.
- Maier, W. & Saupe, A. (1959). *Eine einfache molekulare statistische Theorie der nematischen kristallinüssigen phase. Teil I*. *Z. Naturforsch. Teil A*, **14**, 882–889.
- Malthête, J., Liebert, L., Levelut, A. M. & Galerne, Y. (1986). *Nematic biaxe thermotrope*. *C. R. Acad. Sci.* **303**, 1073–1076.
- Martin, P. C., Parodi, O. & Pershan, P. S. (1972). *Unified hydrodynamic theory for crystals, liquid crystals, and normal fluids*. *Phys. Rev. A*, **6**, 2401–2420.
- Martinez-Miranda, L. J., Kortan, A. R. & Birgeneau, R. J. (1986). *X-ray study of fluctuations near the nematic–smectic-A–smectic-C multicritical point*. *Phys. Rev. Lett.* **56**, 2264–2267.
- Meiboom, S., Sethna, J. P., Anderson, P. W. & Brinkman, W. F. (1981). *Theory of the blue phase of cholesteric liquid crystals*. *Phys. Rev. Lett.* **46**, 1216–1219.
- Miyano, K. (1979). *Wall-induced pretransitional birefringence: a new tool to study boundary aligning forces in liquid crystals*. *Phys. Rev. Lett.* **43**, 51–54.
- Moncton, D. E. & Pindak, R. (1979). *Long-range order in two- and three-dimensional smectic-B liquid crystal films*. *Phys. Rev. Lett.* **43**, 701–704.
- Moncton, D. E., Pindak, R., Davey, S. C. & Brown, G. S. (1982). *Melting of variable thickness liquid crystal thin films: a synchrotron X-ray study*. *Phys. Rev. Lett.* **49**, 1865–1868.
- Moncton, D. E., Stephens, P. W., Birgeneau, R. J., Horn, P. M. & Brown, G. S. (1981). *Synchrotron X-ray study of the commensurate–incommensurate transition of monolayer krypton on graphite*. *Phys. Rev. Lett.* **46**, 1533–1536.
- Nelson, D. R. & Halperin, B. I. (1979). *Dislocation-mediated melting in two dimensions*. *Phys. Rev. B*, **19**, 2457–2484.
- Nelson, D. R. & Halperin, B. I. (1980). *Solid and fluid phases in smectic layers with tilted molecules*. *Phys. Rev. B*, **21**, 5312–5329.
- Nelson, D. R. & Toner, J. (1981). *Bond-orientational order, dislocation loops and melting of solids and smectic-A liquid crystals*. *Phys. Rev. B*, **24**, 363–387.
- Neto, A. M. F., Galerne, Y., Levelut, A. M. & Liebert, L. (1985). *Pseudo lamellar ordering in uniaxial and biaxial lyotropic nematics: a synchrotron X-ray diffraction experiment*. *J. Phys. (Paris) Lett.* **46**, L499–L505.
- Ocko, B. M., Birgeneau, R. J. & Litster, J. D. (1986). *Crossover to tricritical behavior at the nematic to smectic A transition: an X-ray scattering study*. *Z. Phys.* **B62**, 487–497.

## REFERENCES

## 4.4 (cont.)

- Ocko, B. M., Birgeneau, R. J., Litster, J. D. & Neubert, M. E. (1984). *Critical and tricritical behavior at the nematic to smectic-A transition*. *Phys. Rev. Lett.* **52**, 208–211.
- Ocko, B. M., Braslau, A., Pershan, P. S., Als-Nielsen, J. & Deutsch, M. (1986). *Quantized layer growth at liquid crystal surfaces*. *Phys. Rev. Lett.* **57**, 94–97.
- Ocko, B. M., Pershan, P. S., Safinya, C. R. & Chiang, L. Y. (1987). *Incommensurate smectic order at the free surface in the nematic phase of DB7NO<sub>2</sub>*. *Phys. Rev. A*, **35**, 1868–1872.
- Onsager, L. (1949). *The effects of shapes on the interaction of colloidal particles*. *Ann. NY Acad. Sci.* **51**, 627–659.
- Peierls, R. E. (1934). *Transformation temperatures*. *Helv. Phys. Acta Suppl.* **2**, 81–83.
- Pershan, P. S. (1974). *Dislocation effects in smectic-A liquid crystals*. *J. Appl. Phys.* **45**, 1590–1604.
- Pershan, P. S. (1979). *Amphiphilic molecules and liquid crystals*. *J. Phys. (Paris) Colloq.* **40**, C3-423–C3-432.
- Pershan, P. S. & Als-Nielsen, J. (1984). *X-ray reflectivity from the surface of a liquid crystal: surface structure and absolute value of critical fluctuations*. *Phys. Rev. Lett.* **52**, 759–762.
- Pershan, P. S., Braslau, A., Weiss, A. H. & Als-Nielsen, J. (1987). *Smectic layering at the free surface of liquid crystals in the nematic phase: X-ray reflectivity*. *Phys. Rev. A*, **35**, 4800–4813.
- Pershan, P. S. & Prost, J. (1975). *Dislocation and impurity effects in smectic-A liquid crystals*. *J. Appl. Phys.* **46**, 2343–2353.
- Pindak, R., Moncton, D. E., Davey, S. C. & Goodby, J. W. (1981). *X-ray observation of a stacked hexatic liquid-crystal B phase*. *Phys. Rev. Lett.* **46**, 1135–1138.
- Pokrovsky, V. L. & Talapov, A. L. (1979). *Ground state, spectrum, and phase diagram of two-dimensional incommensurate crystals*. *Phys. Rev. Lett.* **42**, 65–67.
- Prost, J. (1979). *Smectic A to smectic A phase transition*. *J. Phys. (Paris)*, **40**, 581–587.
- Prost, J. (1984). *The smectic state*. *Adv. Phys.* **33**, 1–46.
- Prost, J. & Barois, P. (1983). *Polymorphism in polar mesogens. II. Theoretical aspects*. *J. Chim. Phys.* **80**, 65–81.
- Ratna, B. R., Nagabhushana, C., Raja, V. N., Shashidhar, R. & Chandrasekhar, S. (1986). *Density, dielectric and X-ray studies of smectic A–smectic A transitions*. *Mol. Cryst. Liq. Cryst.* **138**, 245–257.
- Ratna, B. R., Shashidhar, R. & Raja, V. N. (1985). *Smectic-A phase with two collinear incommensurate density modulations*. *Phys. Rev. Lett.* **55**, 1476–1478.
- Richardson, R. M., Leadbetter, A. J. & Frost, J. C. (1978). *The structure and dynamics of the smectic B phase*. *Ann. Phys.* **3**, 177–186.
- Sadoc, J. F. & Charvolin, J. (1986). *Frustration in bilayers and topologies of liquid crystals of amphiphilic molecules*. *J. Phys. (Paris)*, **47**, 683–691.
- Safinya, C. R., Clark, N. A., Liang, K. S., Varady, W. A. & Chiang, L. Y. (1985). *Synchrotron X-ray scattering study of freely suspended discotic strands*. *Mol. Cryst. Liq. Cryst.* **123**, 205–216.
- Safinya, C. R., Liang, K. S., Varady, W. A., Clark, N. A. & Andersson, G. (1984). *Synchrotron X-ray study of the orientational ordering D<sub>2</sub>–D<sub>1</sub> structural phase transition of freely suspended discotic strands in triphenylene hexa-*n*-dodecanoate*. *Phys. Rev. Lett.* **53**, 1172–1175.
- Safinya, C. R., Roux, D., Smith, G. S., Sinha, S. K., Dimon, P., Clark, N. A. & Bellocq, A. M. (1986). *Steric interactions in a model multimembrane system: a synchrotron X-ray study*. *Phys. Rev. Lett.* **57**, 2718–2721.
- Safinya, C. R., Varady, W. A., Chiang, L. Y. & Dimon, P. (1986). *X-ray study of the nematic phase and smectic-A1 to smectic- $\bar{A}$  phase transition in heptylphenyl nitrobenzoyloxybenzoate (DB7NO<sub>2</sub>)*. *Phys. Rev. Lett.* **57**, 432–435.
- Safran, S. A. & Clark, N. A. (1987). *Editors. Physics of complex and supermolecular fluids*. New York: John Wiley.
- Shiple, C. G., Hitchcock, P. B., Mason, R. & Thomas, K. M. (1974). *Structural chemistry of 1,2-diauroyl-DL-phosphatidylethanolamine: molecular conformation and intermolecular packing of phospholipids*. *Proc. Natl Acad. Sci. USA*, **71**, 3036–3040.
- Sigaud, G., Hardouin, F., Achard, M. F. & Gasparoux, H. (1979). *Anomalous transitional behaviour in mixtures of liquid crystals: a new transition of SA–SA type?* *J. Phys. (Paris) Colloq.* **40**, C3-356–C3-359.
- Sirota, E. B., Pershan, P. S. & Deutsch, M. (1987). *Modulated crystalline-B phases in liquid crystals*. *Phys. Rev. A*, **36**, 2902–2913.
- Sirota, E. B., Pershan, P. S., Sorensen, L. B. & Collett, J. (1985). *X-ray studies of tilted hexatic phases in thin liquid-crystal films*. *Phys. Rev. Lett.* **55**, 2039–2042.
- Sirota, E. B., Pershan, P. S., Sorensen, L. B. & Collett, J. (1987). *X-ray and optical studies of the thickness dependence of the phase diagram of liquid crystal films*. *Phys. Rev. A*, **36**, 2890–2901.
- Small, D. (1967). *Phase equilibria and structure of dry and hydrated egg lecithin*. *J. Lipid Res.* **8**, 551–557.
- Smith, G. W. & Garland, Z. G. (1973). *Liquid crystalline phases in a doubly homologous series of benzylideneanilines – textures and scanning calorimetry*. *J. Chem. Phys.* **59**, 3214–3228.
- Smith, G. W., Garland, Z. G. & Curtis, R. J. (1973). *Phase transitions in mesomorphic benzylideneanilines*. *Mol. Cryst. Liq. Cryst.* **19**, 327–330.
- Solomon, L. & Litster, J. D. (1986). *Light scattering measurements in the 7S5-8OCB nematic–smectic-A–smectic-C liquid-crystal system*. *Phys. Rev. Lett.* **56**, 2268–2271.
- Sorensen, L. B. (1987). Private communication.
- Sorensen, L. B., Amador, S., Sirota, E. B., Stragler, H. & Pershan, P. S. (1987). Unpublished.
- Springer, T. (1977). In *Current physics*, Vol. 3. *Dynamics of solids and liquids by neutron scattering*, edited by S. W. Lovesey & T. Springer, pp. 255–300 (see p. 281). Berlin: Springer-Verlag.
- Sprokel, G. E. (1980). *The physics and chemistry of liquid crystal devices*. New York: Plenum.
- Stegemeyer, H. & Bergmann, K. (1981). In *Liquid crystals of one- and two-dimensional order*. *Springer Series in Chemical Physics* 11, edited by W. Helfrich & G. Heppke, pp. 161–175. Berlin/Heidelberg/New York: Springer-Verlag.
- Tardieu, A. & Billard, J. (1976). *On the structure of the 'smectic D modification'*. *J. Phys. (Paris) Colloq.* **37**, C3-79–C3-81.
- Tardieu, A. & Luzzati, V. (1970). *Polymorphism of lipids: a novel cubic phase – a cage-like network of rods with enclosed spherical micelles*. *Biochim. Biophys. Acta*, **219**, 11–17.
- Thoen, J., Marynissen, H. & Van Dael, W. (1982). *Temperature dependence of the enthalpy and the heat capacity of the liquid-crystal octylcyanobiphenyl (8CB)*. *Phys. Rev. A*, **26**, 2886–2905.
- Thoen, J., Marynissen, H. & Van Dael, W. (1984). *Nematic–smectic-A tricritical point in alkylcyanobiphenyl liquid crystals*. *Phys. Rev. Lett.* **5**, 204–207.
- Villain, J. (1980). In *Order in strongly fluctuating condensed matter system*, edited by T. Riste, pp. 221–260. New York: Plenum.
- Wang, J. & Lubensky, T. C. (1984). *Theory of the SA<sub>1</sub>–SA<sub>2</sub> phase transition in liquid crystal*. *Phys. Rev. A*, **29**, 2210–2217.
- Warren, B. E. (1968). *X-ray diffraction*. Reading, MA: Addison-Wesley.
- Winkor, M. J. & Clarke, R. (1986). *Long-period stacking transitions in intercalated graphite*. *Phys. Rev. Lett.* **56**, 2072–2075.
- Young, A. P. (1979). *Melting and the vector Coulomb gas in two dimensions*. *Phys. Rev. B*, **19**, 1855–1866.
- Young, C. Y., Pindak, R., Clark, N. A. & Meyer, R. B. (1978). *Light-scattering study of two-dimensional molecular-orientation fluctuations in a freely suspended ferroelectric liquid crystal film*. *Phys. Rev. Lett.* **40**, 773–776.
- Yu, L. J. & Saupe, A. (1980). *Observation of a biaxial nematic phase in potassium laurate–1-decanol–water mixtures*. *Phys. Rev. Lett.* **45**, 1000–1003.

## 4. DIFFUSE SCATTERING AND RELATED TOPICS

## 4.5

- Alexeev, D. G., Lipanov, A. A. & Skuratovskii, I. Y. (1992). *Patterson methods in fibre diffraction*. *Int. J. Biol. Macromol.* **14**, 139–144.
- Arnott, S. (1980). *Twenty years hard labor as a fibre diffractionist*. In *Fibre diffraction methods*, ACS Symposium Series, Vol. 141, edited by A. D. French & K. H. Gardner, pp. 1–30. Washington DC: American Chemical Society.
- Arnott, S., Chandrasekaran, R., Millane, R. P. & Park, H. (1986). *DNA–RNA hybrid secondary structures*. *J. Mol. Biol.* **188**, 631–640.
- Arnott, S. & Mitra, A. K. (1984). *X-ray diffraction analyses of glycosaminoglycans*. In *Molecular biophysics of the extracellular matrix*, edited by S. Arnott, D. A. Rees & E. R. Morris, pp. 41–67. Clifton: Humana Press.
- Arnott, S., Wilkins, M. H. F., Fuller, W. & Langridge, R. (1967). *Molecular and crystal structures of double-helical RNA III. An 11-fold molecular model and comparison of the agreement between the observed and calculated three-dimensional diffraction data for 10- and 11-fold models*. *J. Mol. Biol.* **27**, 535–548.
- Arnott, S. & Wonacott, A. J. (1966). *The refinement of the crystal and molecular structures of polymers using X-ray data and stereochemical constraints*. *Polymer*, **7**, 157–166.
- Atkins, E. D. T. (1989). *Crystal structure by X-ray diffraction*. In *Comprehensive polymer science*, Vol. 1. *Polymer characterization*, edited by G. A. Allen, pp. 613–650. Oxford: Pergamon Press.
- Barham, P. J. (1993). *Crystallization and morphology of semicrystalline polymers*. In *Materials science and technology. A comprehensive treatment*, Vol. 12. *Structure and properties of polymers*, edited by E. L. Thomas, pp. 153–212. Weinheim: VCH.
- Baskaran, S. & Millane, R. P. (1999a). *Bayesian image reconstruction from partial image and aliased spectral intensity data*. *IEEE Trans. Image Process.* **8**, 1420–1434.
- Baskaran, S. & Millane, R. P. (1999b). *Model bias in Bayesian image reconstruction from X-ray fiber diffraction data*. *J. Opt. Soc. Am. A*, **16**, 236–245.
- Biswas, A. & Blackwell, J. (1988a). *Three-dimensional structure of main-chain liquid-crystalline copolymers. 1. Cylindrically averaged intensity transforms of single chains*. *Macromolecules*, **21**, 3146–3151.
- Biswas, A. & Blackwell, J. (1988b). *Three-dimensional structure of main-chain liquid-crystalline copolymers. 2. Interchain interference effects*. *Macromolecules*, **21**, 3152–3158.
- Biswas, A. & Blackwell, J. (1988c). *Three-dimensional structure of main-chain liquid-crystalline copolymers. 3. Chain packing in the solid state*. *Macromolecules*, **21**, 3158–3164.
- Blackwell, J., Gutierrez, G. A. & Chivers, R. A. (1984). *Diffraction by aperiodic polymer chains: the structure of liquid crystalline copolyesters*. *Macromolecules*, **17**, 1219–1224.
- Blundell, D. J., Keller, A. & Kovacs, A. J. (1966). *A new self-nucleation phenomenon and its application to the growing of polymer crystals from solution*. *J. Polym. Sci. Polym. Lett. Ed.* **4**, 481–486.
- Brisse, F. (1989). *Electron diffraction of synthetic polymers: the model compound approach to polymer structure*. *J. Electron Microsc. Tech.* **11**, 272–279.
- Brisse, F., Remillard, B. & Chanzy, H. (1984). *Poly(1,4-trans-cyclohexanediyldimethylene succinate). A structural determination using X-ray and electron diffraction*. *Macromolecules*, **17**, 1980–1987.
- Brünger, A. T. (1992). *X-PLOR*. Version 3.1. New Haven: Yale University Press.
- Brünger, A. T. (1997). *Free R value: cross-validation in crystallography*. *Methods Enzymol.* **277**, 366–396.
- Cael, J. J., Winter, W. T. & Arnott, S. (1978). *Calcium chondroitin 4-sulfate: molecular conformation and organization of polysaccharide chains in a proteoglycan*. *J. Mol. Biol.* **125**, 21–42.
- Campbell Smith, P. J. & Arnott, S. (1978). *LALS: a linked-atom least-squares reciprocal-space refinement system incorporating stereochemical constraints to supplement sparse diffraction data*. *Acta Cryst.* **A34**, 3–11.
- Chandrasekaran, R. & Arnott, S. (1989). *The structures of DNA and RNA helices in oriented fibres*. In *Landolt–Bornstein numerical data and functional relationships in science and technology*, Vol. VII/1b, edited by W. Saenger, pp. 31–170. Berlin, Heidelberg: Springer-Verlag.
- Chandrasekaran, R., Radha, A. & Lee, E. J. (1994). *Structural roles of calcium ions and side chains in welan: an X-ray study*. *Carbohydr. Res.* **252**, 183–207.
- Chanzy, H., Perez, S., Miller, D. P., Paradossi, G. & Winter, W. T. (1987). *An electron diffraction study of mannan I. Crystal and molecular structure*. *Macromolecules*, **20**, 2407–2413.
- Chivers, R. A. & Blackwell, J. (1985). *Three-dimensional structure of copolymers of p-hydroxybenzoic acid and 2-hydroxy-6-naphthoic acid: a model for diffraction from a nematic structure*. *Polymer*, **26**, 997–1002.
- Clark, E. S. & Muus, I. T. (1962). *The relationship between Bragg reflections and disorder in crystalline polymers*. *Z. Kristallogr.* **117**, 108–118.
- Cochran, W., Crick, F. H. C. & Vand, V. (1952). *The structure of synthetic polypeptides. I. The transform of atoms on a helix*. *Acta Cryst.* **5**, 581–586.
- Cowley, J. M. (1961). *Diffraction intensities from bent crystals*. *Acta Cryst.* **14**, 920–927.
- Cowley, J. M. (1981). *Diffraction physics. Second revised edition*. Amsterdam: North-Holland.
- Cowley, J. M. (1988). *Imaging [and] imaging theory*. In *High-resolution transmission electron microscopy and associated techniques*, edited by P. Busek, J. M. Cowley & L. Eyring, pp. 3–57. New York: Oxford University Press.
- Crowther, R. A., DeRosier, D. J. & Klug, A. (1970). *The reconstruction of a three-dimensional structure from projections and its application to electron microscopy*. *Proc. R. Soc. London Ser. A*, **317**, 319–344.
- Daubeny, R. de P., Bunn, C. W. & Brown, C. J. (1954). *The crystal structure of polyethylene terephthalate*. *Proc. R. Soc. London Ser. A*, **226**, 531–542.
- Day, D. & Lando, J. B. (1980). *Structure determination of a poly(diacetylene) monolayer*. *Macromolecules*, **13**, 1483–1487.
- De Titta, G. T., Edmonds, J. W., Langs, D. A. & Hauptman, H. (1975). *Use of negative quartet cosine invariants as a phasing figure of merit: NQUEST*. *Acta Cryst.* **A31**, 472–479.
- Dorset, D. L. (1989). *Electron diffraction from crystalline polymers*. In *Comprehensive polymer science*, Vol. 1. *Polymer characterization*, edited by G. A. Allen, pp. 651–668. Oxford: Pergamon Press.
- Dorset, D. L. (1991a). *Is electron crystallography possible? The direct determination of organic crystal structures*. *Ultramicroscopy*, **38**, 23–40.
- Dorset, D. L. (1991b). *Electron diffraction structure analysis of polyethylene. A direct phase determination*. *Macromolecules*, **24**, 1175–1178.
- Dorset, D. L. (1991c). *Electron crystallography of linear polymers: direct structure analysis of poly( $\epsilon$ -caprolactone)*. *Proc. Natl Acad. Sci. USA*, **88**, 5499–5502.
- Dorset, D. L. (1992). *Electron crystallography of linear polymers: direct phase determination for zonal data sets*. *Macromolecules*, **25**, 4425–4430.
- Dorset, D. L. (1995a). *Comments on the validity of the direct phasing and Fourier methods in electron crystallography*. *Acta Cryst.* **A51**, 869–879.
- Dorset, D. L. (1995b). *Structural electron crystallography*. New York: Plenum.
- Dorset, D. L. (1995c). *Filling the cone – overcoming the goniometric tilt limit in electron crystallography by direct methods*. *Am. Cryst. Assoc. Abstr. Series 2*, **23**, p. 89.
- Dorset, D. L., Kopp, S., Fryer, J. R. & Tivol, W. T. (1995). *The Sayre equation in electron crystallography*. *Ultramicroscopy*, **57**, 59–89.
- Dorset, D. L. & McCourt, M. P. (1993). *Electron crystallographic analysis of a polysaccharide structure – direct phase determination and model refinement for mannan I*. *J. Struct. Biol.* **111**, 118–124.

## REFERENCES

## 4.5 (cont.)

- Dorset, D. L., McCourt, M. P., Kopp, S., Wittmann, J.-C. & Lotz, B. (1994). Direct determination of polymer crystal structures by electron crystallography – isotactic poly(1-butene), form (III). *Acta Cryst.* **B50**, 201–208.
- Doyle, P. A. & Turner, P. S. (1968). Relativistic Hartree–Fock X-ray and electron scattering factors. *Acta Cryst.* **A24**, 390–397.
- Drenth, J. (1994). *Principles of protein X-ray crystallography*. New York: Springer-Verlag.
- Finkenstadt, V. L. & Millane, R. P. (1998). Fiber diffraction patterns for general unit cells: the cylindrically projected reciprocal lattice. *Acta Cryst.* **A54**, 240–248.
- Forsyth, V. T., Mahendrasingam, A., Pigram, W. J., Greenall, R. J., Bellamy, K., Fuller, W. & Mason, S. A. (1989). Neutron fibre diffraction study of DNA hydration. *Int. J. Biol. Macromol.* **11**, 236–240.
- Franklin, R. E. (1955). Structure of tobacco mosaic virus. *Nature (London)*, **175**, 379–381.
- Franklin, R. E. & Gosling, R. G. (1953). The structure of sodium thymonucleate fibres. II. The cylindrically symmetrical Patterson function. *Acta Cryst.* **6**, 678–685.
- Franklin, R. E. & Holmes, K. C. (1958). Tobacco mosaic virus: application of the method of isomorphous replacement to the determination of the helical parameters and radial density distribution. *Acta Cryst.* **11**, 213–220.
- Franklin, R. E. & Klug, A. (1955). The splitting of layer lines in X-ray fibre diagrams of helical structures: application to tobacco mosaic virus. *Acta Cryst.* **8**, 777–780.
- Fraser, R. D. B. & MacRae, T. P. (1973). *Conformations in fibrous proteins*. New York: Academic Press.
- Fraser, R. D. B., MacRae, T. P., Miller, A. & Rowlands, R. J. (1976). Digital processing of fibre diffraction patterns. *J. Appl. Cryst.* **9**, 81–94.
- Fraser, R. D. B., Suzuki, E. & MacRae, T. P. (1984). Computer analysis of X-ray diffraction patterns. In *Structure of crystalline polymers*, edited by I. H. Hall, pp. 1–37. New York: Elsevier.
- French, A. D. & Gardner, K. H. (1980). Editors. *Fibre diffraction methods*. ACS Symposium Series, Vol. 141. Washington DC: American Chemical Society.
- Geil, P. H. (1963). *Polymer single crystals*. New York: John Wiley & Sons.
- Gilmore, C. J., Shankland, K. & Bricogne, G. (1993). Application of the maximum entropy method to powder diffraction and electron crystallography. *Proc. R. Soc. London Ser. A*, **442**, 97–111.
- Gonzalez, A., Nave, C. & Marvin, D. A. (1995). Pfl filamentous bacteriophage: refinement of a molecular model by simulated annealing using 3.3 Å resolution X-ray fiber diffraction data. *Acta Cryst.* **D51**, 792–804.
- Graaf, H. de (1989). On the calculation of small-angle diffraction patterns from distorted lattices. *Acta Cryst.* **A45**, 861–870.
- Grubb, D. T. (1993). Elastic properties of crystalline polymers. In *Materials science and technology. A comprehensive treatment*, Vol. 12. *Structure and properties of polymers*, edited by E. L. Thomas, pp. 301–356. Weinheim: VCH.
- Hall, I. H. (1984). Editor. *Structure of crystalline polymers*. New York: Elsevier.
- Hall, I. H., Neisser, J. Z. & Elder, M. (1987). A computer-based method of measuring the integrated intensities of the reflections on the X-ray diffraction photograph of an oriented crystalline polymer. *J. Appl. Cryst.* **20**, 246–255.
- Hamilton, W. C. (1965). Significance tests on the crystallographic R factor. *Acta Cryst.* **18**, 502–510.
- Hauptman, H. A. (1993). A minimal principle in X-ray crystallography: starting in a small way. *Proc. R. Soc. London Ser. A*, **442**, 3–12.
- Hendricks, S. & Teller, E. (1942). X-ray interference in partially ordered layer lattices. *J. Chem. Phys.* **10**, 147–167.
- Hirsch, P. B., Howie, A., Nicholson, P. B., Pashley, D. W. & Whelan, M. J. (1965). *Electron microscopy of thin crystals*. London: Butterworths.
- Hofmann, D., Schneider, A. I. & Blackwell, J. (1994). Molecular modelling of the structure of a wholly aromatic thermotropic copolyester. *Polymer*, **35**, 5603–5610.
- Holmes, K. C. & Barrington Leigh, J. (1974). The effect of disorientation on the intensity distribution of non-crystalline fibres. I. Theory. *Acta Cryst.* **A30**, 635–638.
- Holmes, K. C., Popp, D., Gebhard, W. & Kabsch, W. (1990). Atomic model of the actin filament. *Nature (London)*, **347**, 44–49.
- Holmes, K. C., Stubbs, G. J., Mandelkow, E. & Gallwitz, U. (1975). Structure of tobacco mosaic virus at 6.7 Å resolution. *Nature (London)*, **254**, 192–196.
- Hosemann, R. & Bagchi, S. N. (1962). *Direct analysis of diffraction by matter*. Amsterdam: North-Holland.
- Hu, H. & Dorset, D. L. (1989). Three-dimensional electron diffraction structure analysis of polyethylene. *Acta Cryst.* **B45**, 283–290.
- Hu, H. & Dorset, D. L. (1990). Crystal structure of poly( $\epsilon$ -caprolactone). *Macromolecules*, **23**, 4604–4607.
- Hudson, L., Harford, J. J., Denny, R. C. & Squire, J. M. (1997). Myosin head configuration in relaxed fish muscle: resting state myosin heads must swing axially by up to 150 Å or turn upside down to reach rigor. *J. Mol. Biol.* **273**, 440–455.
- Iannelli, P. (1994). FWR: a computer program for refining the molecular structure in the crystalline phase of polymers based on the analysis of the whole X-ray fibre diffraction patterns. *J. Appl. Cryst.* **27**, 1055–1060.
- Isoda, S., Tsuji, M., Ohara, M., Kawaguchi, A. & Katayama, K. (1983a). Structural analysis of  $\beta$ -form poly(p-xylene) starting from a high-resolution image. *Polymer*, **24**, 1155–1161.
- Isoda, S., Tsuji, M., Ohara, M., Kawaguchi, A. & Katayama, K. (1983b). Direct observation of dislocations in polymer single crystals. *Makromol. Chem. Rapid Commun.* **4**, 141–144.
- Ivanova, M. I. & Makowski, L. (1998). Iterative low-pass filtering for estimation of the background in fiber diffraction patterns. *Acta Cryst.* **A54**, 626–631.
- Klug, A., Crick, F. H. C. & Wyckoff, H. W. (1958). Diffraction from helical structures. *Acta Cryst.* **11**, 199–213.
- Kopp, S., Wittmann, J. C. & Lotz, B. (1994). Epitaxial crystallization and crystalline polymorphism of poly(1-butene): form (III) and (II). *Polymer*, **35**, 908–915.
- Lipson, H. & Cochran, W. (1966). *The determination of crystal structures*, p. 381. Ithaca: Cornell University Press.
- Liu, J. & Geil, P. H. (1993). Morphological observations of nascent poly(p-oxabenzate). *Polymer*, **34**, 1366–1374.
- Liu, J., Yuan, B.-L., Geil, P. H. & Dorset, D. L. (1997). Chain conformation and molecular packing in poly(p-oxbenzoate) single crystals at ambient temperature. *Polymer*, **38**, 6031–6047.
- Lobert, S., Heil, P. D., Namba, K. & Stubbs, G. (1987). Preliminary X-ray fibre diffraction studies of cucumber green mottle mosaic virus, watermelon strain. *J. Mol. Biol.* **196**, 935–938.
- Lobert, S. & Stubbs, G. (1990). Fibre diffraction analysis of cucumber green mottle mosaic virus using limited numbers of heavy-atom derivatives. *Acta Cryst.* **A46**, 993–997.
- Lorenz, M. & Holmes, K. C. (1993). Computer processing and analysis of X-ray fibre diffraction data. *J. Appl. Cryst.* **26**, 82–91.
- Lorenz, M., Popp, D. & Holmes, K. C. (1993). Refinement of the F-actin model against X-ray fibre diffraction data by the use of a directed mutation algorithm. *J. Mol. Biol.* **234**, 826–836.
- Lotz, B. & Wittmann, J. C. (1993). Structure of polymer single crystals. In *Materials science and technology. A comprehensive treatment*, Vol. 12. *Structure and properties of polymers*, edited by E. L. Thomas, pp. 79–154. Weinheim: VCH.
- MacGillivray, C. H. & Bruins, E. M. (1948). On the Patterson transforms of fibre diagrams. *Acta Cryst.* **1**, 156–158.
- Makowski, L. (1978). Processing of X-ray diffraction data from partially oriented specimens. *J. Appl. Cryst.* **11**, 273–283.
- Makowski, L. (1982). The use of continuous diffraction data as a phase constraint. II. Application to fibre diffraction data. *J. Appl. Cryst.* **15**, 546–557.

#### 4. DIFFUSE SCATTERING AND RELATED TOPICS

##### 4.5 (cont.)

- Makowski, L., Caspar, D. L. D. & Marvin, D. A. (1980). *Filamentous bacteriophage Pfl structure determined at 7 Å resolution by refinement of models for the  $\alpha$ -helical subunit*. *J. Mol. Biol.* **140**, 149–181.
- Mandelkern, L. (1989). *Crystallization and melting*. In *Comprehensive polymer science*, Vol. 2. *Polymer properties*, edited by C. Booth & C. Price, pp. 363–414. Oxford: Pergamon Press.
- Mandelkew, E. & Holmes, K. C. (1974). *The positions of the N-terminus and residue 68 in tobacco mosaic virus*. *J. Mol. Biol.* **87**, 265–273.
- Mandelkew, E., Stubbs, G. & Warren, S. (1981). *Structures of the helical aggregates of tobacco mosaic virus protein*. *J. Mol. Biol.* **152**, 375–386.
- Marvin, D. A., Bryan, R. K. & Nave, C. (1987). *Pfl inovirus. Electron density distribution calculated by a maximum entropy algorithm from native fiber diffraction data to 3 Å resolution and single isomorphous replacement data to 5 Å resolution*. *J. Mol. Biol.* **193**, 315–343.
- Mauritz, K. A., Baer, E. & Hopfinger, A. J. (1978). *The epitaxial crystallization of macromolecules*. *J. Polym. Sci. Macromol. Rev.* **13**, 1–61.
- Mazeau, K., Winter, W. T. & Chanzy, H. (1994). *Molecular and crystal structure of a high-temperature polymorph of chitosan from electron diffraction data*. *Macromolecules*, **27**, 7606–7612.
- Millane, R. P. (1988). *X-ray fibre diffraction*. In *Crystallographic computing 4. Techniques and new technologies*, edited by N. W. Isaacs & M. R. Taylor, pp. 169–186. Oxford University Press.
- Millane, R. P. (1989a). *R factors in X-ray fibre diffraction. I. Largest likely R factors for N overlapping terms*. *Acta Cryst. A* **45**, 258–260.
- Millane, R. P. (1989b). *R factors in X-ray fibre diffraction. II. Largest likely R factors*. *Acta Cryst. A* **45**, 573–576.
- Millane, R. P. (1989c). *Relating reflection boundaries in X-ray fibre diffraction patterns to specimen morphology and their use for intensity measurement*. *J. Macromol. Sci. Phys.* **B28**, 149–166.
- Millane, R. P. (1990a). *Intensity distributions in fibre diffraction*. *Acta Cryst. A* **46**, 552–559.
- Millane, R. P. (1990b). *Phase retrieval in crystallography and optics*. *J. Opt. Soc. Am. A*, **7**, 394–411.
- Millane, R. P. (1990c). *Polysaccharide structures: X-ray fibre diffraction studies*. In *Computer modeling of carbohydrate molecules*. ACS Symposium Series No. 430, edited by A. D. French & J. W. Brady, pp. 315–331. Washington DC: American Chemical Society.
- Millane, R. P. (1990d). *R factors in X-ray fibre diffraction. III. Asymptotic approximations to largest likely R factors*. *Acta Cryst. A* **46**, 68–72.
- Millane, R. P. (1991). *An alternative approach to helical diffraction*. *Acta Cryst. A* **47**, 449–451.
- Millane, R. P. (1992a). *Largest likely R factors for normal distributions*. *Acta Cryst. A* **48**, 649–650.
- Millane, R. P. (1992b). *R factors in X-ray fibre diffraction. IV. Analytic expressions for largest likely R factors*. *Acta Cryst. A* **48**, 209–215.
- Millane, R. P. (1993). *Image reconstruction from cylindrically averaged diffraction intensities*. In *Digital image recovery and synthesis II*, Proc. SPIE, Vol. 2029, edited by P. S. Idell, pp. 137–143. Bellingham, WA: SPIE.
- Millane, R. P. & Arnott, S. (1985). *Background removal in X-ray fibre diffraction patterns*. *J. Appl. Cryst.* **18**, 419–423.
- Millane, R. P. & Arnott, S. (1986). *Digital processing of X-ray diffraction patterns from oriented fibres*. *J. Macromol. Sci. Phys.* **B24**, 193–227.
- Millane, R. P. & Baskaran, S. (1997). *Optimal difference Fourier synthesis in fibre diffraction*. *Fiber Diffr. Rev.* **6**, 14–18.
- Millane, R. P., Byler, M. A. & Arnott, S. (1985). *Implementing constrained least squares refinement of helical polymers on a vector pipeline machine*. In *Supercomputer applications*, edited by R. W. Numrich, pp. 137–143, New York: Plenum.
- Millane, R. P., Chandrasekaran, R., Arnott, S. & Dea, I. C. M. (1988). *The molecular structure of kappa-carrageenan and comparison with iota-carrageenan*. *Carbohydr. Res.* **182**, 1–17.
- Millane, R. P. & Stroud, W. J. (1991). *Effects of disorder on fibre diffraction patterns*. *Int. J. Biol. Macromol.* **13**, 202–208.
- Millane, R. P. & Stubbs, G. (1992). *The significance of R factors in fibre diffraction*. *Polym. Prepr.* **33**(1), 321–322.
- Miller, R., DeTitta, G. T., Jones, R., Langs, D. A., Weeks, C. M. & Hauptman, H. A. (1993). *On the application of the minimal principle to solve unknown structures*. *Science*, **259**, 1430–1433.
- Namba, K., Pattanayek, R. & Stubbs, G. J. (1989). *Visualization of protein–nucleic acid interactions in a virus. Refined structure of intact tobacco mosaic virus at 2.9 Å resolution by X-ray fibre diffraction*. *J. Mol. Biol.* **208**, 307–325.
- Namba, K. & Stubbs, G. (1985). *Solving the phase problem in fibre diffraction. Application to tobacco mosaic virus at 3.6 Å resolution*. *Acta Cryst. A* **41**, 252–262.
- Namba, K. & Stubbs, G. (1987a). *Difference Fourier syntheses in fibre diffraction*. *Acta Cryst. A* **43**, 533–539.
- Namba, K. & Stubbs, G. (1987b). *Isomorphous replacement in fibre diffraction using limited numbers of heavy-atom derivatives*. *Acta Cryst. A* **43**, 64–69.
- Namba, K., Wakabayashi, K. & Mitsui, T. (1980). *X-ray structure analysis of the thin filament of crab striated muscle in the rigor state*. *J. Mol. Biol.* **138**, 1–26.
- Namba, K., Yamashita, I. & Vonderviszt, F. (1989). *Structure of the core and central channel of bacterial flagella*. *Nature (London)*, **342**, 648–654.
- Nambudripad, R., Stark, W. & Makowski, L. (1991). *Neutron diffraction studies of the structure of filamentous bacteriophage Pfl*. *J. Mol. Biol.* **220**, 359–379.
- Park, H., Arnott, S., Chandrasekaran, R., Millane, R. P. & Campagnari, F. (1987). *Structure of the  $\alpha$ -form of poly-(dA)-poly(dT) and related polynucleotide duplexes*. *J. Mol. Biol.* **197**, 513–523.
- Perez, S. & Chanzy, H. (1989). *Electron crystallography of linear polysaccharides*. *J. Electron Microsc. Tech.* **11**, 280–285.
- Rickert, S. E., Lando, J. B., Hopfinger, A. J. & Baer, E. (1979). *Epitaxial polymerization of (SN)<sub>x</sub> I. Structure and morphology of single crystals on alkali halide substrates*. *Macromolecules*, **12**, 1053–1057.
- Rybnikar, F., Liu, J. & Geil, P. H. (1994). *Thin film melt-polymerized single crystals of poly(p-oxybenzoate)*. *Makromol. Chem. Phys.* **195**, 81–104.
- Sayre, D. (1952). *The squaring method: a new method for phase determination*. *Acta Cryst.* **5**, 60–65.
- Schneider, A. I., Blackwell, J., Pielartzik, H. & Karbach, A. (1991). *Structure analysis of copoly(ester carbonate)*. *Macromolecules*, **24**, 5676–5682.
- Shotton, M. W., Denny, R. C. & Forsyth, V. T. (1998). *CCP13 software development*. *Fiber Diffr. Rev.* **7**, 40–44.
- Sim, G. A. (1960). *A note on the heavy atom method*. *Acta Cryst.* **13**, 511–512.
- Squire, J. M., Al-Khayat, H. A. & Yagi, N. (1993). *Muscle thin-filament structure and regulation. Actin sub-domain movements and the tropomyosin shift modelled from low-angle X-ray diffraction*. *J. Chem. Soc. Faraday Trans.* **89**, 2717–2726.
- Squire, J., Cantino, M., Chew, M., Denny, R., Harford, J., Hudson, L. & Luther, P. (1998). *Myosin rod-packing schemes in vertebrate muscle thick filaments*. *J. Struct. Biol.* **122**, 128–138.
- Squire, J. M. & Vibert, P. J. (1987). *Editors. Fibrous protein structure*. London: Academic Press.
- Stanley, E. (1986). *'Peakiness' test functions*. *Acta Cryst. A* **42**, 297–299.
- Stark, W., Glucksman, M. J. & Makowski, L. (1988). *Conformation of the coat protein of filamentous bacteriophage Pfl determined by neutron diffraction from magnetically oriented gels of specifically deuterated virions*. *J. Mol. Biol.* **199**, 171–182.
- Storks, K. H. (1938). *An electron diffraction examination of some linear high polymers*. *J. Am. Chem. Soc.* **60**, 1753–1761.
- Stroud, W. J. & Millane, R. P. (1995a). *Analysis of disorder in biopolymer fibres*. *Acta Cryst. A* **51**, 790–800.

## REFERENCES

## 4.5 (cont.)

- Stroud, W. J. & Millane, R. P. (1995b). *Diffraction by disordered polycrystalline fibres*. *Acta Cryst.* **A51**, 771–790.
- Stroud, W. J. & Millane, R. P. (1996a). *Cylindrically averaged diffraction by distorted lattices*. *Proc. R. Soc. London*, **452**, 151–173.
- Stroud, W. J. & Millane, R. P. (1996b). *Diffraction by polycrystalline fibres with correlated disorder*. *Acta Cryst.* **A52**, 812–829.
- Stubbs, G. (1987). *The Patterson function in fibre diffraction*. In *Patterson and Pattersons*, edited by J. P. Glusker, B. K. Patterson & M. Rossi, pp. 548–557. Oxford University Press.
- Stubbs, G. (1989). *The probability distributions of X-ray intensities in fibre diffraction: largest likely values for fibre diffraction R factors*. *Acta Cryst.* **A45**, 254–258.
- Stubbs, G. (1999). *Developments in fiber diffraction*. *Curr. Opin. Struct. Biol.* **9**, 615–619.
- Stubbs, G., Warren, S. & Holmes, K. (1977). *Structure of RNA and RNA binding site in tobacco mosaic virus from a 4 Å map calculated from X-ray fibre diagrams*. *Nature (London)*, **267**, 216–221.
- Stubbs, G. J. (1974). *The effect of disorientation on the intensity distribution of non-crystalline fibres. II. Applications*. *Acta Cryst.* **A30**, 639–645.
- Stubbs, G. J. & Diamond, R. (1975). *The phase problem for cylindrically averaged diffraction patterns. Solution by isomorphous replacement and application to tobacco mosaic virus*. *Acta Cryst.* **A31**, 709–718.
- Stubbs, G. J. & Makowski, L. (1982). *Coordinated use of isomorphous replacement and layer-line splitting in the phasing of fibre diffraction data*. *Acta Cryst.* **A38**, 417–425.
- Tadokoro, H. (1979). *Structure of crystalline polymers*. New York: Wiley.
- Tanaka, S. & Naya, S. (1969). *Theory of X-ray scattering by disordered polymer crystals*. *J. Phys. Soc. Jpn*, **26**, 982–993.
- Tatarinova, L. I. & Vainshtein, B. K. (1962). *Issledovanie poli- $\gamma$ -metil-L-glutamata v  $\alpha$ -forme metodom difraktsii elektronov. (Electron diffraction study of poly- $\gamma$ -methyl-L-glutamate in the  $\alpha$ -form.)* *Visokomol. Soed.* **4**, 261–269. (In Russian.)
- Tirion, M., ben Avraham, D., Lorenz, M. & Holmes, K. C. (1995). *Normal modes as refinement parameters for the F-actin model*. *Biophys. J.* **68**, 5–12.
- Tsujii, M. (1989). *Electron microscopy*. In *Comprehensive polymer science*, Vol. 1. *Polymer characterization*, edited by G. A. Allen, pp. 785–866. Oxford: Pergamon Press.
- Vainshtein, B. K. (1964). *Structure analysis by electron diffraction*. Oxford: Pergamon Press.
- Vainshtein, B. K. (1966). *Diffraction of X-rays by chain molecules*. Amsterdam: Elsevier.
- Vainshtein, B. K. & Tatarinova, L. I. (1967). *The  $\beta$ -form of poly- $\gamma$ -methyl-L-glutamate*. *Sov. Phys. Crystallogr.* **11**, 494–498.
- Vibert, P. J. (1987). *Fibre diffraction methods*. In *Fibrous protein structure*, edited by J. M. Squire & P. J. Vibert, pp. 23–45. New York: Academic Press.
- Wang, H., Culver, J. N. & Stubbs, G. (1997). *Structure of ribgrass mosaic virus at 2.9 Å resolution: evolution and taxonomy of tobamoviruses*. *J. Mol. Biol.* **269**, 769–779.
- Wang, H. & Stubbs, G. (1993). *Molecular dynamics refinement against fibre diffraction data*. *Acta Cryst.* **A49**, 504–513.
- Wang, H. & Stubbs, G. J. (1994). *Structure determination of cucumber green mottle mosaic virus by X-ray fibre diffraction. Significance for the evolution of tobamoviruses*. *J. Mol. Biol.* **239**, 371–384.
- Welberry, T. R., Miller, G. H. & Carroll, C. E. (1980). *Paracrystals and growth-disorder models*. *Acta Cryst.* **A36**, 921–929.
- Welsh, L. C., Symmons, M. F. & Marvin, D. A. (2000). *The molecular structure and structural transition of the  $\alpha$ -helical capsid in filamentous bacteriophage Pf1*. *Acta Cryst.* **D56**, 137–150.
- Welsh, L. C., Symmons, M. F., Sturtevant, J. M., Marvin, D. A. & Perham, R. N. (1998). *Structure of the capsid of Pf3 filamentous phage determined from X-ray fiber diffraction data at 3.1 Å resolution*. *J. Mol. Biol.* **283**, 155–177.
- Wilson, A. J. C. (1950). *Largest likely values for the reliability index*. *Acta Cryst.* **3**, 397–399.
- Wittmann, J. C. & Lotz, B. (1985). *Polymer decoration: the orientation of polymer folds as revealed by the crystallization of polymer vapor*. *J. Polym. Sci. Polym. Phys. Ed.* **23**, 205–226.
- Wittmann, J. C. & Lotz, B. (1990). *Epitaxial crystallization of polymers on organic and polymeric substrates*. *Prog. Polym. Sci.* **15**, 909–948.
- Wunderlich, B. (1973). *Macromolecular physics*, Vol. 1. *Crystal structure, morphology, defects*. New York: Academic Press.
- Yamashita, I., Hasegawa, K., Suzuki, H., Vonderviszt, F., Mimori-Kiyosue, Y. & Namba, K. (1998). *Structure and switching of bacterial flagellar filaments studied by X-ray fiber diffraction*. *Nature Struct. Biol.* **5**, 125–132.
- Zugenmaier, P. & Sarko, A. (1980). *The variable virtual bond*. In *Fibre diffraction methods*, ACS Symposium Series Vol. 141, edited by A. D. French & K. H. Gardner, pp. 225–237. Washington DC: American Chemical Society.

## 4.6

- Axel, F. & Gratias, D. (1995). *Beyond quasicrystals*. Les Ulis: Les Editions de Physique and Berlin: Springer-Verlag.
- Bancel, P. A., Heiney, P. A., Stephens, P. W., Goldman, A. I. & Horn, P. M. (1985). *Structure of rapidly quenched Al-Mn*. *Phys. Rev. Lett.* **54**, 2422–2425.
- Böhm, H. (1977). *Eine erweiterte Theorie der Satellitenreflexe und die Bestimmung der modulierten Struktur des Natriumnitrits*. Habilitation thesis, University of Munster.
- Cummins, H. Z. (1990). *Experimental studies of structurally incommensurate crystal phases*. *Phys. Rep.* **185**, 211–409.
- Dehlinger, U. (1927). *Über die Verbreiterung der Debyelinien bei kaltbearbeiteten Metallen*. *Z. Kristallogr.* **65**, 615–631.
- Dräger, J. & Mermin, N. D. (1996). *Superspace groups without the embedding: the link between superspace and Fourier-space crystallography*. *Phys. Rev. Lett.* **76**, 1489–1492.
- Estermann, M., Haibach, T. & Steurer, W. (1994). *Quasicrystal versus twinned approximant: a quantitative analysis with decagonal Al<sub>70</sub>Co<sub>15</sub>Ni<sub>15</sub>*. *Philos. Mag. Lett.* **70**, 379–384.
- Goldman, A. I. & Kelton, K. F. (1993). *Quasicrystals and crystalline approximants*. *Rev. Mod. Phys.* **65**, 213–230.
- Gouyet, J. F. (1996). *Physics and fractal structures*. Paris: Masson and Berlin: Springer-Verlag.
- Hausdorff, F. (1919). *Dimension und äusseres Mass*. *Math. Ann.* **79**, 157–179.
- Hermann, C. (1949). *Kristallographie in Räumen beliebiger Dimensionszahl. I. Die Symmetrioperationen*. *Acta Cryst.* **2**, 139–145.
- Ishihara, K. N. & Yamamoto, A. (1988). *Penrose patterns and related structures. I. Superstructure and generalized Penrose patterns*. *Acta Cryst.* **A44**, 508–516.
- Janner, A. (1992). *Decagrammatic symmetry of decagonal Al<sub>78</sub>Mn<sub>22</sub> quasicrystal*. *Acta Cryst.* **A48**, 884–901.
- Janner, A. & Janssen, T. (1979). *Superspace groups*. *Physica A*, **99**, 47–76.
- Janner, A. & Janssen, T. (1980a). *Symmetry of incommensurate crystal phases. I. Commensurate basic structures*. *Acta Cryst.* **A36**, 399–408.
- Janner, A. & Janssen, T. (1980b). *Symmetry of incommensurate crystal phases. II. Incommensurate basic structures*. *Acta Cryst.* **A36**, 408–415.
- Janner, A., Janssen, T. & de Wolff, P. M. (1983a). *Bravais classes for incommensurate crystal phases*. *Acta Cryst.* **A39**, 658–666.
- Janner, A., Janssen, T. & de Wolff, P. M. (1983b). *Determination of the Bravais class for a number of incommensurate crystals*. *Acta Cryst.* **A39**, 671–678.
- Janot, Chr. (1994). *Quasicrystals. A primer*. Oxford: Clarendon Press.

## 4.6 (cont.)

- Janssen, T. (1986). *Crystallography of quasicrystals*. *Acta Cryst.* **A42**, 261–271.
- Janssen, T. (1988). *Aperiodic crystals: a contradictio in terminis?* *Phys. Rep.* **168**, 55–113.
- Janssen, T. (1995). *From quasiperiodic to more complex systems*. In *Beyond quasicrystals*, edited by F. Axel & D. Gratias, pp. 75–140. Les Ulis: Les Éditions de Physique and Berlin: Springer-Verlag.
- Janssen, T., Janner, A., Looijenga-Vos, A. & de Wolff, P. M. (1999). *Incommensurate and commensurate modulated crystal structures*. In *International tables for crystallography*, Vol. C, edited by A. J. C. Wilson and E. Prince, ch. 9.8. Dordrecht: Kluwer Academic Publishers.
- Jaric, M. V. (1986). *Diffraction from quasicrystals: geometric structure factor*. *Phys. Rev. B*, **34**, 4685–4698.
- Kalning, M., Kek, S., Burandt, B., Press, W. & Steurer, W. (1994). *Examination of a multiple twinned periodic approximant of the decagonal phase Al<sub>70</sub>Co<sub>15</sub>Ni<sub>15</sub>*. *J. Phys. Condens. Matter*, **6**, 6177–6187.
- Kato, K. (1990). *Strukturverfeinerung des Kompositkristalls im mehrdimensionalen Raum*. *Acta Cryst.* **B46**, 39–44.
- Kelton, K. F. (1995). *Quasicrystals and related structures*. In *Intermetallic compounds. Principles and practice*, Vol. 1, edited by J. H. Westbrook & R. L. Fleischer, pp. 453–491. Chichester: John Wiley & Sons.
- Korekawa, M. (1967). *Theorie der Satellitenreflexe*. Habilitation thesis, University of Munich.
- Lancon, F., Billard, L., Burkov, S. & DeBoissieu, M. (1994). *On choosing a proper basis for determining structures of quasicrystals*. *J. Phys. I France*, **4**, 283–301.
- Levine, D. & Steinhardt, P. J. (1986). *Quasicrystals. I. Definition and structure*. *Phys. Rev. B*, **34**, 596–616.
- Levitov, L. S. & Rhyner, J. (1988). *Crystallography of quasicrystals; application to icosahedral symmetry*. *J. Phys. France*, **49**, 1835–1849.
- Luck, J. M., Godréche, C., Janner, A. & Janssen, T. (1993). *The nature of the atomic surfaces of quasiperiodic self-similar structures*. *J. Phys. A Math. Gen.* **26**, 1951–1999.
- Paciorek, W. A. & Chapuis, G. (1994). *Generalized Bessel functions in incommensurate structure analysis*. *Acta Cryst.* **A50**, 194–203.
- Pavlovitch, A. & Kleman, M. (1987). *Generalized 2D Penrose tilings: structural properties*. *J. Phys. A Math. Gen.* **20**, 687–702.
- Penrose, R. (1974). *The role of aesthetics in pure and applied mathematical research*. *Bull. Math. Appl.* **10**, 266–271.
- Penrose, R. (1979). *Pentaplexity. A class of non-periodic tilings of the plane*. *Math. Intell.* **2**, 32–37.
- Petricek, V., Maly, K. & Cisarova, I. (1991). *The computing system 'JANA'*. In *Methods of structural analysis of modulated structures and quasicrystals*, edited by J. M. Pérez-Mato, F. J. Zuniga & G. Madriaga, pp. 262–267. Singapore: World Scientific.
- Petricek, V., Maly, K., Coppens, P., Bu, X., Cisarova, I. & Frost-Jensen, A. (1991). *The description and analysis of composite crystals*. *Acta Cryst.* **A47**, 210–216.
- Rabson, D. A., Mermin, N. D., Rokhsar, D. S. & Wright, D. C. (1991). *The space groups of axial crystals and quasicrystals*. *Rev. Mod. Phys.* **63**, 699–733.
- Rokhsar, D. S., Wright, D. C. & Mermin, N. D. (1988). *Scale equivalence of quasicrystallographic space groups*. *Phys. Rev. B*, **37**, 8145–8149.
- Senechal, M. (1995). *Quasicrystals and geometry*. Cambridge University Press.
- Shechtman, D., Blech, I., Gratias, D. & Cahn, J. W. (1984). *Metallic phase with long-range orientational order and no translational symmetry*. *Phys. Rev. Lett.* **53**, 1951–1953.
- Smaalen, S. van (1991). *Symmetry of composite crystals*. *Phys. Rev. B*, **43**, 11330–11341.
- Smaalen, S. van (1992). *Superspace description of incommensurate intergrowth compounds and the application to inorganic misfit layer compounds*. *Mater. Sci. Forum*, **100 & 101**, 173–222.
- Smaalen, S. van (1995). *Incommensurate crystal structures*. *Crystallogr. Rev.* **4**, 79–202.
- Socolar, J. E. S. & Steinhardt, P. J. (1986). *Quasicrystals. II. Unit-cell configurations*. *Phys. Rev. B*, **34**, 617–647.
- Steurer, W. (1990). *The structure of quasicrystals*. *Z. Kristallogr.* **190**, 179–234.
- Steurer, W. (1995). *Experimental aspects of the structure analysis of aperiodic materials*. In *Beyond quasicrystals*, edited by F. Axel & D. Gratias, pp. 203–228. Les Ulis: Les Éditions de Physique and Berlin: Springer-Verlag.
- Steurer, W. (1996). *The structure of quasicrystals*. In *Physical metallurgy*, Vol. I, edited by R. W. Cahn & P. Haasen, pp. 371–411. Amsterdam: Elsevier.
- Willis, B. T. M. & Pryor, A. W. (1975). *Thermal vibrations in crystallography*. Cambridge University Press.
- Wolff, P. M. de (1974). *The pseudo-symmetry of modulated crystal structures*. *Acta Cryst.* **A30**, 777–785.
- Wolff, P. M. de (1977). *Symmetry operations for displacively modulated structures*. *Acta Cryst.* **A33**, 493–497.
- Wolff, P. M. de (1984). *Dualistic interpretation of the symmetry of incommensurate structures*. *Acta Cryst.* **A40**, 34–42.
- Wolff, P. M. de, Janssen, T. & Janner, A. (1981). *The superspace groups for incommensurate crystal structures with a one-dimensional modulation*. *Acta Cryst.* **A37**, 625–636.
- Yamamoto, A. (1982). *Structure factor of modulated crystal structures*. *Acta Cryst.* **A38**, 87–92.
- Yamamoto, A. (1992a). *Unified setting and symbols of superspace groups for composite crystals*. *Acta Cryst.* **A48**, 476–483.
- Yamamoto, A. (1992b). *Ideal structure of icosahedral Al–Cu–Li quasicrystals*. *Phys. Rev. B*, **45**, 5217–5227.
- Zobetz, E. (1993). *One-dimensional quasilattices: fractally shaped atomic surfaces and homometry*. *Acta Cryst.* **A49**, 667–676.